

The out-flowing behavior of particles at the discharge end of rotary kilns

Dissertation

zur Erlangung des Akademischen Grades

Doktoringenieur

(Dr.-Ing.)

von: M.Sc. Shi, Yi Chun

geb.: am 04. Juni 1980

in: Nanjing / V.R.China

genehmigt durch die Fakultät für Verfahrens- und Systemtechnik
der Otto-von-Guericke-Universität Magdeburg.

Gutachter: Prof. Dr.-Ing. habil. Eckehard Specht
Prof. Dr.-techn. Peter Walzel

Danksagung

Die Dissertation berichtet meiner Forschungstätigkeit im Institut für Strömungs- und Thermodynamik an der Otto-von-Guericke-Universität Magdeburg, Deutschland in den Jahren 2006 bis 2009.

Mein besonderer Dank gilt meinem Betreuer Herrn Prof. Dr.-Ing habil. Eckehard Specht für die fachlichen Anregungen, die Diskussionsbereitschaft und seine jederzeit freundliche Unterstützung von Arbeiten und Leben.

Ebenfalls bedanken möchte ich mich bei Herrn Prof. Dr. techn. Peter Walzel Universität Dortmund für die fachliche Unterstützung und die Bereitschaft zur Übernahme des Zweitgutachten.

Mein herzlicher Dank gilt allen Kollegen des Institut für Strömungs- und Thermodynamik sowie die Mitarbeit von der Werkstatt für die Hilfsbereitschaft und Unterstützung, die einen wesentlichen Anteil am Gelingen dieser Arbeit hatte.

Außerdem bedanke ich die finanzielle Förderung von Sachsen-Anhalt und Prof. Dr.-Ing habil. Eckehard Specht.

Schriftliche Erklärung

Ich erkläre hiermit, dass ich die vorliegende Arbeit ohne unzulässige Hilfe Dritter und ohne Benutzung anderer als der angegebenen Hilfsmittel angefertigt habe. Die aus fremden Quellen direkt oder indirekt übernommenen Gedanken sind als solche kenntlich gemacht.

Insbesondere habe ich nicht die Hilfe einer kommerziellen Promotionsberatung in Anspruch genommen. Dritte haben von mir weder unmittelbar noch mittelbar geldwerte Leistungen für Arbeiten erhalten, die im Zusammenhang mit dem Inhalt der vorgelegten Dissertation stehen.

Die Arbeit wurde bisher weder im Inland noch im Ausland in gleicher oder ähnlicher Form als Dissertation eingereicht und ist als Ganzes auch noch nicht veröffentlicht.

Shi, Yi Chun

Magdeburg, Mai 2009

Contents

Kurzfassung	6
Abstract	8
1. Industrial background	11
1.1 Rotary kiln	11
1.2 Cement production process	11
1.2.1. Raw materials	11
1.2.2. Process description	12
2. Emphasis of this work	15
3. The filling degree of solid bed at the kiln discharge end	17
3.1 Introduction	17
3.2. Experimental.....	21
3.2.1 Rotary kilns	21
3.2.2 Determination of the dynamic angle of repose of the solid bed in the kiln.....	21
3.2.3 Experimental parameters and materials.....	22
3.2.4 Measuring method	24
3.3 Results and discussion	25
3.3.1 Dimensionless description.....	25
3.4 Correlation with the end depth of the solid bed.....	26
3.5 Correlation with the end filling degree.....	28
3.6 Influence of the materials	29
3.7 Equations for $Bd-F_0$ correlation.....	29
3.8 Transfer to industrial kilns	30

4. The radial out-flowing of particles	32
4.1 Introduction	32
4.2 Experimental.....	35
4.2.1 Experimental kilns, parameters and materials.....	35
4.2.2 Setup and method	35
4.3 Determination of the radial out-flowing distribution	36
4.4 Determination of the downstream velocity v_{sd}	37
4.5 Qualitative analysis of the mean velocity v_{sd}	39
4.5.1 Influence of the mass flow.....	39
4.5.2 Influence of the rotational speed	40
4.6 Quantitative study to predict radial downstream velocity v_{sd}	41
4.6.1 Normalization of the surface downstream velocity	41
4.6.2 The velocity fluctuation of the out-flowing particles at discharge end.	43
5. The axial out-flowing of particles	45
5.1 Introduction	45
5.2 Experimental.....	47
5.2.1 Experimental kilns, parameters and materials.....	47
5.2.2 Setup and method	47
5.3 Determination of the distribution of the axial out-flowing particles.....	47
5.4 Determination of the axial velocity	48
5.5 Qualitative study of the axial out-flowing velocity v_{sa}	49
5.5.1 Influence of the mass flow.....	49
5.5.2 Influence of the rotational speed	49
5.6 Quantitative study to predict axial discharge velocity v_{sa}	50

5.6.1 Conservation of mass	50
5.6.2 Axial discharge velocity	51
5.6.3 Fluctuation of axial discharging velocity	52
6. Conclusions	54
Nomenclature	56
Reference	59
Figures abstract	61
Appendix	98

Kurzfassung

Drehrohöfen werden häufig in der chemischen, Zement- und Metallindustrie verwendet. Die Partikelbewegung in Drehrohröfen ist besonders für die Wärmerübertragung vom Gas zum Material, sowie für die Prozesskontrolle wichtig. Obwohl die Partikelbewegung in Drehrohöfen durch andere Autoren experimentell und theoretisch untersucht worden ist, ist das Ausflussverhalten der Partikel noch nicht bestimmt. Doch dieses Verhalten ist für industrielle Produktionsprozesse auch von besonderer Bedeutung.

Die Schüttguttiefe an der Auslassöffnung des Ofens wird für verschiedene Massenströme, Drehzahlen, Neigungswinkel und drei Versuchsmaterialien mit zwei Drehrohröfen untersucht. Die Öfen besitzen Abmessungen von $0,4m(\text{ID}) * 5m(\text{L})$ sowie $0,25m(\text{ID}) * 6,7m(\text{L})$. Die Tiefe des Schüttgutes kann um ein Vielfaches größer als die materialspezifischen Partikeldurchmesser sein. Alle Parameter nach Saemans Model [29] werden in eine neue dimensionlose 'Bed depth number' (Bd) implementiert. Der Füllungsgrad des Schüttgutes an der Auslassöffnung kann mit $F_0 = 1.75 * Bd^{0.5}$ ($\beta = 1^\circ - 4^\circ$) berechnet werden. Die untersuchten Bereiche der 'Bed depth number' (Bd) sind für alle industriellen Drehrohöfen gültig. Die Tiefe des Stoffbettes am Auslass ist ebenso zur Beschreibung des Ausflussverhaltens in radialer und axialer Richtung notwendig.

Des Weiteren wurde die radiale Partikelgeschwindigkeit an der Auslassöffnung mit einer Gitterbox gemessen. Als Versuchsmaterialien wurden Sand, Glaskugeln und Klinker verwendet. Die Partikelverteilung in radialer Richtung konnte sehr gut mit der 'Normalverteilung' angepasst werden. Die radiale Geschwindigkeit der Partikel kann durch diese Verteilung berechnet werden. Es wurde festgestellt, dass der Füllungsgrad an der Auslassöffnung die Partikelgeschwindigkeit beeinflusst. Mit Hilfe der 'Bed depth number', wird die Berechnungsgleichung für die radiale Geschwindigkeit aus der

Literatur erweitert. Entsprechend der Partikelverteilung ist die Geschwindigkeitsschwankung von Klinker an der Auslassöffnung am größten und die der Glaskugeln am niedrigsten.

Die Ausflussgeschwindigkeit der Partikel in axialer Richtung wurde ebenfalls untersucht. Die entsprechende Verteilung lässt sich auch sehr gut mit der 'Normalverteilung' anpassen. Auf Grundlage der theoretischen Massenbilanz sowie der Ergebnisse der Schüttguttiefe an der Auslassöffnung, wird die axiale Geschwindigkeit experimentell und theoretisch verglichen. Es stellt sich heraus, dass aus der gesamten Schüttguttiefe eine aktive Schicht wird. Die totale Querschnittsfläche des Stoffbettes an der Auslassöffnung kann zur Berechnung der axialen Partikelgeschwindigkeit verwendet werden.

Schlüsselwörter: Drehrohfen ,Ausfluss, Auslassöffnung, Füllungsgrad, radiale Ausfluss Geschwindigkeit, axiale Geschwindigkeit.

Abstract

Rotary kilns are often used in cement, metallurgy and chemical industries. The particle movement in the kiln is specially significant for the heat transfer from hot gas to the materials as well as process control. Although the particle movement inside kilns has been experimentally and theoretically studied by a lot of authors, the flowing behavior of particles at kiln discharge end is still not researched. Furthermore, this behavior is concerned by industries in the production process.

The solid bed depth at the discharge end of rotary kilns was investigated for different mass flow rates, rotational speeds, inclination angles and materials using two kilns with size $0.4m(\text{ID}) * 5m(\text{L})$ and $0.25m(\text{ID}) * 6.7m(\text{L})$, respectively. The depth could be more times higher than the particle diameter in dependence on the materials. All parameters according to Saeman's model [29] were combined in a newly developed dimensionless 'Bed depth number' designated as ' Bd '. The filling degree of solid bed at the discharge can be correlated with $F_0 = 1.75 * Bd^{0.5}$ (for inclination angle between $1^\circ - 4^\circ$). The range of the researched *Bed depth number* (Bd) is suitable for all industrial kilns. The variation of the end bed depth is also necessary for the discharge behavior in radial and axial direction.

Still with the two kilns, the radial downstream velocity at the discharge end was measured with a grid box. Sand, glass beads and clinker were used as experimental materials. The particles distributions in radial direction had the best agreement with the normal distributions. The velocity is calculated according to the distribution. The end filling degree was found to influence the velocity. Based on the 'Bed depth number', the velocity equation in literature was extended, including all influencing parameters. According to the distribution, the velocity fluctuation of clinker at discharge end is the highest and glass beads is the lowest.

The discharge velocity in the axial direction was also experimentally investigated. The axial discharge distribution had best fit with the normal distribution. Based on the mass balance and the results of the bed depth at discharge end, the velocities from experiments and calculation are compared. It is found that the end bed depth becomes totally active layer. The whole cross section area of the solid bed can be used to calculate the axial velocity.

Keywords: Rotary kiln, Out-flowing, discharge end, filling degree, radial downstream velocity, axial velocity,

1. Industrial background

1.1 Rotary kiln

Rotary kilns are important equipments used in the chemical, metallurgical industries as well as waste treatment, where they are operated for the continuous process of mixing, heating, incineration, pyrolysis and drying. The basic components of a rotary kiln are the steel shell made from rolled mild steel plate, the refractory material to insulate the steel shell from the high temperatures inside the kiln, a selected burner according to designed process, supporting tyres and rollers, driving motor and driving gears. An industrial kiln can be up to 6m internal diameter and more than 100 meter long. Usually it is operated at 1-5rpm rotational speed, 1°- 4° inclination angle and mass flow up to 12,000 t/d. The products quality is strongly influenced by material property and mixing, combustion temperature, and operational parameters of kilns, i.e. mass flow, rotational speed and cylinder inclination angle. Materials frequently produced using rotary kilns include cement, lime, refractories and metakaolin. A typical rotary kiln with 6.2m internal diameter and 98m length in a clinker production line is shown in Fig.1.

1.2 Cement production process

1.2.1. Raw materials

The main raw materials used in the cement manufacturing process are limestone, sand, shale, clay, and iron ore. The main material, limestone, is usually mined on site while the other minor materials may be mined either on site or in nearby quarries. Another source of raw materials is industrial by-products. The use of by-product materials to replace natural raw materials is a key element in achieving sustainable development.

1.2.2. Process description

Fig.2 [LEHIGH, Heidelbergcement Group] presents a detailed flow chart of cement production process with devices in each step starting from obtaining the mining of raw materials until produced cements distributed in silos. In general, the basic production process could be described as:

(1). Preparation of the raw materials

Mining of limestone requires the use of drilling and blasting techniques. Blasting produces materials in a wide range of sizes from approximately 1.5 meters in diameter to small particles less than a few millimeters in diameter. Materials are loaded into trucks for transportation to the crushing plant. Through a series of crushers and screens, the limestone is reduced to a size less than 10 mm and stored until required. Depending on size, the minor materials (sand, shale, clay, and iron ore) may or may not be crushed before being stored in separate areas until required.

(2). Raw grinding.

In the wet process, each raw material is proportioned to meet a desired chemical composition and fed into a rotating ball mill with water. The raw materials are ground to a size where the majority of the materials are less than 75 microns. Materials exiting the mill are called "slurry" and have flow ability characteristics. This slurry is pumped to blending tanks and homogenized to ensure the chemical composition of the slurry is correct. Following the homogenization process, the slurry is stored in tanks until required.

In the dry process, each raw material is proportioned to meet a desired chemical composition and fed to either a rotating ball mill or vertical roller mill. The raw materials are dried with waste process gases and ground to a size where the majority of the materials

are less than 75 microns. The dry materials are called "kiln feed". The kiln feed is pneumatically blended to ensure the chemical composition of the kiln feed is also well homogenized and then stored in silos until required.

(3) Burning of the raw material mixture to give cement clinker.

Whether the process is wet or dry, the same chemical reactions take place. Basic chemical reactions are: evaporating all moisture, calcinating the limestone to produce free calcium oxide, and reacting the calcium oxide with the minor materials (sand, shale, clay, and iron). This results in a final black, granular product known as "clinker".

In the wet process, the slurry is fed to a rotary kiln, which can be from 3.0 m to 5.0 m in diameter and from 120.0 m to 165.0 m in length. The rotary kiln is made of steel and lined with special refractory materials to protect it from the high process temperatures. Process temperatures can reach as high as 1450°C during the clinker making process.

In the dry process, kiln feed is fed to a preheater tower which can be as high as 150.0 meters and is heated to 800°C. Material from the preheater tower is discharged to a rotary kiln, which can have the same diameter as a wet process kiln, but the length is much shorter at approximately 45.0 m. The rotary kiln is fired with an intense flame produced by burning coal, coke, oil, gas or waste fuels. Near the flame, in the sintering or clinkering zone of the rotary kiln with a gas temperature of 1800°C-2000°C, the temperature of the material being burnt reaches 1350°C-1500°C, which is necessary for the formation of clinker.

The rotary kiln discharges the red-hot clinker under the intense flame into a clinker cooler. The clinker cooler recovers heat from the clinker and returns the heat to the heating and reaction system thus reducing fuel consumption and improving energy efficiency. Clinker leaving the clinker cooler is at a temperature below 100°C in order to being

handled on standard conveying equipment.

(4). Mixing and grinding of the cement components

The cooled black clinker is stored on site in silos until needed for cement production. Clinker, gypsum, and other process additions are ground together in ball mills to form the final cement products. Fineness of the final products, amount of gypsum added, and the amount of process additions added are all varied to develop a desired performance in each of the final cement product.

2. Emphasis of this work

The study of the particle movement is very important for the heat transfer from hot gas to the material as well as process control. Some modes of the solid flow inside the kilns have been deeply investigated by many authors. However, it is found that the behavior of the solid flow at the kiln discharge end shows great difference. Meanwhile, this behavior is demanded in the industrial applications. Fig.3 presents a real image of particles discharging from rotary kiln with extreme high temperature. Because of the discharge behavior, particles fall on with the radial and axial velocity, which lead to the radial and axial displacement of the discharging. This displacement has great impact on the next production process. As shown an example in Fig.4, the cooling equipment is used to receive the out-flowing clinker from the rotary kiln and cool hot clinker on the moving lanes from 1300 °C to 100 °C as soon as possible. Only at such low temperature, the clinker can be transported and further processed. Therefore, the discharging behavior at the kiln end is one of the significant influence on the cooling efficiency. However, the discharge end behavior of particles has never been studied.

In this work, the experimental and theoretical investigations of the particle flow behavior at the kiln discharge end have been reported. The emphasis of this work are,

- 1). To observe the solid flow at the kiln discharge end. The variation of the bed depth needs to be investigated under different parameters. To predict the end bed depth with different materials.
- 2). To measure the surface downstream velocity of particles at the discharge end for different conditions. Combine the models from literature and our studies, to predict the radial downstream velocity at the discharge end. And to obtain information about the velocity fluctuation of particles discharging in radial direction.

3). To measure the axial discharge velocity of particles at the discharge end for different conditions. Based on the experimental results, to theoretically predict the axial velocity of particles at the discharge end. To find out the velocity fluctuation of particles discharging in the axial direction.

Two rotary kilns in the pilot plant and three kinds of materials are employed to investigate the out-flowing behavior at the kiln discharge end. All investigated results must be transferable to industrial kilns.

3. The filling degree of solid bed at the kiln discharge end

3.1 Introduction

Solid bed depth or filling degree in the rotary kiln is always a very important parameter to study the solid transport as well as the heat transfer from gas to material. The local filling degree inside kilns changes with the operational conditions. Likewise, the filling degree of solid bed at the discharge end also changes according to the operations. However, the solid bed conditions at discharge end have never been reported. This work is not only a complementarity of study of the bed depth profile from feed end to the discharge end, but also is necessary to obtain the information of the radial and axial discharge velocities, which will be discussed in the *Chapter4* and *Chapter5*, respectively. This chapter reports the experiments to measure the end depth, experimental results as well as the influence of the variables on the end filling degree. An empirical equation is also given to predict the end filling degree.

Sullivan et al. [33] firstly carried out experimental work on the solid axial transport and hold-up in kilns in the manufacture of Portland cement clinker. A model for steady state transport of granular solid through kiln drum which was slowly rotated and lightly loaded was first developed by Saeman [29]. His model is often used to calculate a local depth change h shown in **Fig.5**. This figure also depicts the solid depth change from feeding end till discharge end of the cylinder. The differential equation to solve the solid depth variation along the cylinder is given in Eq. (1),

$$\frac{dh}{dx} = \frac{0.75 \cdot \tan\theta}{\pi \cdot n} \cdot \frac{\dot{M}}{\rho_s} \cdot [R^2 - (h-R)^2]^{-3/2} - \frac{\tan\beta}{\cos\theta} \quad (1)$$

where \dot{M} is the mass flow; n is the rotation speed; R is the internal radius of cylinder;

3. The filling degree of solid bed at the kiln discharge end

β is the inclination angle; ρ_s is the solid bulk density and θ is the dynamic angle of repose. To solve this differential equation an initial condition or boundary condition are needed. Saeman set $h=0$ at the discharge end ($x=0$) of the kiln as the initial condition to numerically solve his equation. From the mathematical point of view, the function can be successfully solved. The bed depth profile can be obtained along the cylinder. But this assumption means no out-flowing of particles at discharge end.

Hogg et al. [13] continued to study axial transport of dry particles through horizontal rotary drums of both constricted-end and open-end based on the model of Saeman[29]. He firstly mentioned particles out-flowing at discharge end. In their studies, the differential equation was built up with the change of filling angle,

$$\frac{d\varepsilon}{dx} = \frac{3 \cdot \dot{M} \cdot \tan \theta}{4 \cdot \mu \cdot \rho_s \cdot \pi \cdot n \cdot R^4 \cdot \sin^4 \varepsilon}, \quad (2)$$

where ε is the half of the filling angle and μ is the fraction of time spent in bed to total time. For a dynamic angle of repose of 38° and a bulk density of 1.46g/cm^3 , the value $\mu = 0.51$ is recommended. The simple initial condition for open discharge end $\varepsilon=0$ at $x=0$ was used, which is similar to $h=0$ at $x=0$. For this case he got the analytical solution

$$\sin 4\varepsilon - 8 \sin 2\varepsilon + 12\varepsilon = \frac{24\dot{M} \cdot x \cdot \tan \theta}{\mu \cdot \rho_s \cdot \pi \cdot n \cdot R^4}. \quad (3)$$

For practical application the filling degree is more suitable which can be calculated from the filling angle

$$F = \frac{2\varepsilon - \sin(2\varepsilon)}{2\pi}. \quad (4)$$

3. The filling degree of solid bed at the kiln discharge end

Taking this advantage, the filling degree was approximated using the term $\sin 4\varepsilon - 8\sin 2\varepsilon + 12\varepsilon$ from Eq.(3) with

$$F \approx 0.0735 \cdot (\sin 4\varepsilon - 8 \sin 2\varepsilon + 12\varepsilon)^{0.64}, \quad (5)$$

which is valid in the range of $0.04 \leq F \leq 0.40$. The filling degree changes with the axial position then results in

$$F = 0.56 \left(\frac{\dot{M} \cdot x \cdot \tan \theta}{\mu \cdot \rho_s \cdot \pi \cdot n \cdot R^4} \right)^{0.64}. \quad (6)$$

For a rotary kiln with central overflow discharge end, the equation

$$F = F_0 \cdot \left[1 + \frac{0.406 \cdot \tan \theta \cdot \dot{M} \cdot x}{\mu \cdot \rho_s \cdot \pi \cdot n \cdot R^4 \cdot F_0^{1.56}} \right]^{0.64} \quad (7)$$

was recommended, which is based on the Eq.(6). Here F_0 is the filling degree at the discharge end. Based on experiments this filling degree was correlated with the mass flow rate

$$F_0 = \left[1 + \left(\frac{\dot{M}}{3.65} \right)^{1/4} \right] \cdot F_{\min}. \quad (8)$$

Here F_{\min} is the minimum filling degree at the discharge given by the geometry

$$F_{\min} = \frac{\varepsilon_d - 0.5 \sin(2\varepsilon_d)}{\pi}, \quad (9)$$

where ε_d is the filling angle at the overflow given as

$$\varepsilon_d = \arccos(R_d / R) \quad (10)$$

with R_d as the radius of the overflow discharge hole. In this case, only the mass flow rate in all operational variables is considered to influence the end condition.

Afacan and Masliyah [2] studied flow of granular solid in a horizontal drum with and without lifters and end constrictions. Their experiments results were compared with equations from different authors [1,12,29].. Based on the numerical solution of Saeman's equation they estimated the solid end depth as twice of particle diameter $h_0 = 2d_p$ in the drum without end constriction.

Recently Spurling [32] carried out experimental and theoretical studies on axial bed depth profile and the hold-up of solids based on the theory of Saeman's model in cylinders with different types of dams and without dam. He solved the equation with $h_0 = d_p$ for kilns without a discharge dam. For kilns with discharge dam $h_0 = d_p + h_{dam}$ was applied.

On the other hand for a cylinder without dam, Spurling gave an alternative boundary condition to solve the Eq.(1). Physically the highest slope of solid bed at a boundary axial position x_{bc} near the discharge end cannot be greater than the angle of repose of the granular solids considering the inclination of the cylinder,

$$\frac{dh}{dx} \leq \tan(\theta - \beta) \quad (11)$$

Combining Eq.(1) and Eq.(11), we get

$$\tan(\theta - \beta) = \frac{0.75 \cdot \tan \theta}{\pi \cdot n} \cdot \frac{\dot{M}}{\rho_s} \cdot [R^2 - (h_{bc} - R)^2]^{-3/2} - \frac{\tan \beta}{\cos \theta} \quad (12)$$

From Eq.(12) the depth h_{bc} is shown in **Fig.6**. Assuming a constant gradient between x_{bc} and the discharge end, we get the axial position from Eq.(13)

$$x_{bc} = \frac{h_{bc}}{\tan(\theta - \beta)}. \quad (13)$$

Thus, the value for the boundary condition (x_{bc}, h_{bc}) was derived. However, with this boundary condition the solid depth at $x=0$ is still calculated as zero.

According to the literatures, all authors assumed a fixed value for bed depth at discharge end or inadequately considered the influence of parameters on the end depth. However, similar as the other local depth inside the kiln, the end depth also varies with the operational conditions of rotary kilns. Therefore, the bed depth at the discharge end must be experimentally investigated in details.

3.2. Experimental

3.2.1 Rotary kilns

Two laboratory kilns were used to carry out the experiments. Kiln1 had an internal diameter of 400mm and the length of 5m, as shown in **Fig.7**. The discharge end of the kiln1 was designed with a conical dam and a 90mm extension of the length. Although the extension is relatively short, the diameter of 350mm was applied for the calculation and analysis. The inclination angle of the kiln can be adjusted at 1°, 2°, 3°, 4° and 5° for measurements.

Kiln2¹ had an uniform internal diameter of 0.25m without installation of a dam at discharge end, see **Fig.8**. This kiln can be inclined at 1° and 2° to perform the experiments.

3.2.2 Determination of the dynamic angle of repose of the solid bed in the kiln.

The image shown in **Fig.9** represents the scene of particles flowing out of the kiln at

¹ In the text and figures of the dissertation, all descriptions are valid in kiln1, if not mentioned in kiln2.

discharge end. A thread was hanged at the center of outlet cross section plane as a reference center line. In transverse view, the solid bed always keeps a fixed angle during the rotation of cylinder. A center line is found on the surface of solid bed and is extended to the end of cylinder. Following the bed center line at kiln discharge end an intersection point O could be marked on the edge of the wall. The exact position of point O also refers to Fig.9. The horizontal distance from point O to the center line of the kiln cylinder is designated as value KBC , which can be easily measured. The measurements with three materials in kiln1 and only glass beads in kiln2 are carried out. For accuracy, measurements were carried out many times. With known radius of cylinder R and measured KBC value, the dynamic angle of repose θ can be obtained

$$\theta = \arcsin\left(\frac{KBC}{R}\right). \quad (14)$$

As a consequence, the angle of clinker and quartz sand is 31° and 32° in kiln1, respectively. Remarkably, it was found that glass beads had different dynamic angle of repose, which are 21° in kiln1 and 28° in kiln2. The variation of the angle could be caused by the change of the diameter of kilns. This is also mentioned by Liu et al.[19]. The other reason could be raised by the friction difference of the wall material. Both lab kilns have different inner refractory materials, which contact solids. Kiln2 has obviously rough inner wall surface than kiln1. The rough surface of wall is much easier to pull up the solid bed to a higher position, i.e. a greater dynamic angle of repose.

3.2.3 Experimental parameters and materials

In order to find out the end depth of solid bed, a wide range of mass flow, rotational speed and kiln inclination angle have been chosen according to the capability of both rotary kilns and other equipments. Rotational speed and inclination angle chosen in

3. The filling degree of solid bed at the kiln discharge end

experiments were identical with practical industrial situations. An overview of experimental parameters is listed in **Table 1**. Detailed parameters can be seen in Appendix A3.1-A3.3.

Table 1. Overview of experimental parameters

Parameters	Kiln1	Kiln2
Mass flow [kg/h]	45-440	25-90
Rotational speed [rpm]	1-8	3.5
Kiln inclination angle [°]	1, 2, 3, 4, 5	1, 2

More than 100 measurements have been performed in both rotary kilns with different kinds of materials. Particles' images are shown in **Fig.10**. Not only the dynamic angle of repose, but also bulk density and particle size distribution were measured. The bulk density of three materials is similar. Clinker has the biggest particle size and widest size distribution than other materials. Although the mean particle diameter of glass beads is bigger than that of sand, its size distribution is smaller than sand. The accurate measurement of the particle property is important for the later investigation of the end condition of bed, radial and axial velocity fluctuation, discussed in *Chapter3.5*, *Chapter4.6.2* and *Chapter5.6.3*, respectively. All measured physical properties of three materials are listed in **Table2**. Glass bead was employed in both kilns. Quartz sand and clinker were only used in the kiln1.

Materials	Quartz sand	Clinker	Glass bead
Diameter distribution [mm]	0.1 - 0.4	1 - 12	0.4-0.84
Mean diameter d_p [mm]	0.25	4.5	0.72
Bulk density ρ_s [kg/m ³]	1570	1410	1560
Dynamic angle of repose θ [°]	32 (in kiln1)	31 (in kiln1)	21 (in kiln1) 28 (in kiln2)

Table 2. Physical property of experimental materials

3.2.4 Measuring method

All experiments and measurements were carried out under steady state of solid flow, i.e. $\dot{M}_{out} = \dot{M}_{in}$. No gas flow passed through the cylinder and a heating process did not exist. The solid depth at discharge end is so small that accurate and direct measurement were too difficult. An easy and relatively accurate way was to measure the bed surface width which could be done with normal measuring tools. A photo of the measuring area at the kiln discharge end is shown in **Fig.11**. Then the solid end depth was calculated with Eq.(15)

$$h_0 = R - \sqrt{R^2 - \left(\frac{L_0}{2}\right)^2} . \quad (15)$$

At discharge end, the kiln wall was scaled by grids, which can help to recognise the width of out-flowing solid bed. In order to reflect the real operational situation the measurements were carried out always under dynamic conditions. The bed surface width was measured under keeping the rotation of the kiln. Solids out-flowing is not stopped. Due to the sensitive fluctuation of the bed surface width at discharge end during rotation,

measurements were performed 4-5 times. The mean value was recorded finally.

3.3 Results and discussion

3.3.1 Dimensionless description

In the practical operation of rotary kilns, the end depth of solid bed must be greater than zero as long as there is a solid flow out of the rotary kiln. Furthermore, the end depth is also not a fixed value because it must depend on the different conditions. We know that the parameters influencing the end depth are same as those influencing the solid depth profile inside the kilns. Saeman's model [29] has been proved applicable in lightly loaded kilns by a lot of researchers [2,12,13,20,32]. From Eq.(1), it can be seen that *a*). the operational parameters: mass flow, rotational speed and cylinder inclination angle; *b*). the kiln geometry: radius of kiln; *c*). the particle properties: particle size, bulk density and dynamic angle of repose, determine the solid bed depth $h(x)$ in axial direction

$$h(x) = f(\dot{M}, n, \beta, R, d_p, \rho_s, \theta). \quad (16)$$

Considering the dimension of these parameters Eq. (1) can be rewritten in the form of Eq.(65)

$$\frac{dh}{dx} = Bd \cdot \left[1 - \left(1 - \frac{h}{R}\right)^2\right]^{-3/2} - B, \quad (17)$$

with

$$B = \frac{\tan \beta}{\cos \theta} \quad (18)$$

and

$$Bd = \frac{3}{4} \cdot \frac{\dot{M} \cdot \tan \theta}{\pi \cdot n \cdot \rho_s \cdot R^3} \quad (19)$$

All expressions dh/dx , Bd , h/R and B are dimensionless. Each unit has a great advantage to transfer the deduced results into any other application. B contains the both angles of kiln inclination and solid repose so that it is named as the 'Angle constant'. Bd includes mass flow, rotational speed, kiln diameters, and particle properties. It dominates the bed depth change in kilns so that it is designated here as *Bed depth number*. Meanwhile, Bd can be physically interpreted as the ratio of two velocities

$$Bd = 1.5\pi \tan \theta \cdot \frac{v_{sa}}{v_k}, \quad (20)$$

where

$$v_{sa} = \frac{\dot{M}}{\rho_s \cdot \pi \cdot R^2} \quad (21)$$

is the axial velocity of the solid in a fully filled kiln and

$$v_k = 2\pi nR \quad (22)$$

is the tangential velocity of the cylinder, which is also the maximum tangential velocity of the solid near the internal wall. Therefore, the formulation in Eq.(20) can be also interpreted as the ratio of inertial force to the centrifugal force for a certain material.

3.4 Correlation with the end depth of the solid bed

Some authors assumed $h_0 = d_p$ [20,32] or $h_0 = 2d_p$ [2] as the initial conditions, as explained in the beginning. To the purpose of comparison, the solid end depth from our measurements is scaled by the particle diameter as h_0/d_p . This also represents the number of particles heaped at mid-chord of the kiln discharge end (at the position of the line

\overline{EF} in Fig.5). **Fig.12** shows the variation of the number of clinker particles with respect to Bd in kiln1. The data were measured in the range of mass flows between 45-440kg/h and rotational speeds between 1.5rpm-7rpm, and were sorted by the inclination angle. It can be seen that all data lie closely together. The inclination angle at 1°-4° didn't strongly influence the correlation between h_0/d_p and Bd , however at 5° h_0/d_p was a little bit smaller. The bed depth of clinker varies in the range about 0.6-2 particles diameter depending on Bd . For small Bd the end depth was found to be smaller than one particle diameter. This results is caused by relatively bigger particle size, the fluctuation of the mean size diameter of clinker at kiln end and the conversion from bed surface width to the bed depth. In this case, the out-flowing of only one particle at the mid-chord length of the solid bed occurs. This results in a very low bulk density of the particle flow. However, the bulk density of the material in the kiln is used in the 'Bed depth number'. Therefore, the average value of the bed height can be smaller than one particle diameter. This problem can always occur for the particles with big size.

The end depth of glass beads was measured in both kilns, see **Fig.13**. In kiln1 the mass flow and rotational speed were adjusted between 60kg/h-400kg/h and 1.5rpm-2rpm, respectively. The ratio h_0/d_p sorted by inclination angles increases with Bd as before. An influence of the inclination can not be seen in the range between 1°-4° in kiln1. Only for 5° the values are again a little bit smaller. In the kiln2 measurements were performed at inclination 1° and 2°, mass flows between 25kg/h-185kg/h and a rotational speed of 3.5rpm. The values depend on Bd with the same tendency. However, the values are significantly lower than those measured in kiln1. For the glass beads the end depth is 3-8 times larger than the particle diameter. This is caused by its smaller particle diameter.

The sand has the smallest size (see **Table2**) among the three materials. The end

depth of the sand was measured at mass flows between 100kg/h-250kg/h and rotational speeds between 1rpm-8rpm at 3° inclination angle in kiln1. The values are shown in **Fig.14**. In this case the end depth was found to be 10-25 particles.

The initial condition was often assumed to be one or two particle diameters, as explained in the beginning. This assumption is not suitable for very fine materials and especially not for industrial big kilns, where the ratio of the kiln diameter to the particle diameter is much larger than in the laboratory kilns. As a consequence, also for clinker, the end depth must be much higher than the particle diameter in industrial kilns.

3.5 Correlation with the end filling degree

The end depth is not a proper parameter for the initial condition because it depends on the particle size and on the kiln diameter. Therefore, the filling degree will be used as a parameter. The filling degree is a commonly used parameter for rotary kilns. It can be easily calculated directly from the measured surface bed width L_0 and the kiln radius R

$$\varepsilon_0 = \arcsin\left(\frac{L_0}{R}\right), \quad (23)$$

$$F_0 = \frac{2\varepsilon_0 - \sin(2\varepsilon_0)}{2\pi}. \quad (24)$$

The filling degree was correlated with the *Bed depth number* (Bd) using the inclination angle as the parameter as before. The results for clinker are shown in **Fig.15**. It is obvious that the values can be fitted with only one curve for $\beta=1^\circ-4^\circ$. At 5° inclination the values are a little bit lower designated with the dashed line.

Fig.16 shows the results for glass beads. All values can be fitted with the same curve as before. For 5° inclination the values are again a little bit smaller. The measured values

in both kilns can be fitted with this curve. As a consequence, the influence of the kiln radius can be described with this *Bed depth number (Bd)*.

3.6 Influence of the materials

The influence of the material on the end filling degree has not yet been investigated in details. Therefore, the values of the filling degree associated to three materials are compared. **Fig.17** presents the values at $\beta=1^\circ$ for clinker in kiln1 and glass beads in both kilns where they had a small deviation of the dynamic angle of repose because of a different wall friction. **Fig.18** presents the values at $\beta=3^\circ$ for all three materials in kiln1. **Fig.19** shows the values at $\beta=4^\circ$ for clinker and glass beads in kiln1. It is obvious that for all cases the values can be fitted with the same curve in each figure. Consequently, the influence of the materials can be described also with the *Bed depth number (Bd)*.

According to Eq.(17) the bed depth in the kiln is not only influenced by *Bd* but also by *B* which was named as the 'Angle constant', see Eq.(18). To check if *B* influences the end filling degree, the values of *B* are given in the Fig.17, Fig.18 and Fig.19. These values vary between 0.019-0.082. They are mainly influenced by $\tan\beta$. Because the dynamic angle of repose lies in the range between 21° (Glass beads) and 32° (Sand), the cosines of this angle changes only between 0.93-0.85. As could be seen before in the figures, the inclination angle has no influence for values lower than 4° . Therefore, also *B* has no influence on the end filling degree.

3.7 Equations for *Bd-F₀* correlation

All values of the end filling degree for the three materials are finally presented together in **Fig.20**. For the inclination 1° - 4° , the values can be correlated with the power function

$$F_0 = 1.75 \cdot Bd^{0.5} \quad (\beta = 1^\circ-4^\circ). \quad \text{in [\%]} \quad (25)$$

The deviation of the fitting curve is within $\pm 10\%$. At 5° inclination angle another fitting function

$$F_0 = 1.86 \cdot Bd^{0.58} \quad (\beta = 5^\circ) \quad \text{in [\%]} \quad (26)$$

is recommended.

Why the values for 5° inclination are significantly lower than those for $1^\circ-4^\circ$ can not be clearly explained. Tests with inclination at 4.5° or large than 5° with our kilns are not possible. However, kiln inclinations higher than 4° have no tight industrial relevance.

3.8 Transfer to industrial kilns

Both equations are derived from our experimental conditions in the laboratory. However, some parameters are not comparable with industrial situations, such as mass flow and kiln size. One purpose of the dimensional description was to transfer the results into industrial applications. Therefore we have to prove the availability of the range of Bd which has been used in the laboratory conditions. For example, in cement industry the typical range of the mass flow for rotary kilns is generally $1000t/d-4000t/d$ (up to $12000t/d$) with kiln diameter of $3-4m$ (up to $6m$). Rotational speed varies between $2rpm-4rpm$. The values of Bd for clinker lie therewith in the range of about $0.008-0.1$. For rotary kilns in ceramic industry typical value of mass flow is $26t/d$. The kiln diameter is between $0.5-1.5m$. Rotational speed varies between $2-3rpm$. The values of Bd lie in the range of $0.004-0.08$. In metallurgical industry for reduction treatment or recovery process, the mass flow of the metal oxide is about $30t/d$ in the rotary kilns. The typical kiln diameter and the rotational speed are $0.44m$ and $2-3rpm$, respectively. The corresponding value of Bd is about $0.08-0.1$. The range of Bd investigated in our laboratory conditions coincide with the industrial applications. For kiln at $1^\circ-4^\circ$ Eq.(25)

3. The filling degree of solid bed at the kiln discharge end

can be applied for industrial kilns

4. The radial out-flowing of particles

4.1 Introduction

The velocity of the particles in the cascading layer of the moving bed in rotary kilns is a measure for the quality of the mixing and the heat transfer. The particles are lifted up with the rotating wall as a fixed bed vortex. During this time period they have no relative velocity to the wall and to each other. Only when the particles slip down on the solid bed surface in a thin layer (named cascading layer or active layer), they are transported in the axial direction. Due to this moving mode, at discharge end particles flow downstream on the bed surface and flow out of the kiln in the radial direction, see **Fig.21**. The surface downstream velocity of particles v_{sd} (shown in **Fig.21**) in inside kiln has been researched by other authors. However, the particle surface downstream velocity at the kiln discharge end has never been attached importance. But it is demanded in the industrial applications, as described in *Chapter 2*. Because of the special conditions at the kiln end as described in *Chapter 3*, this velocity must be also different. In this chapter, the downstream velocity from literatures is firstly reviewed. Our measurements for the downstream velocity of the particles at kiln end and the discussion are afterwards reported.

Elperin et al. [9] studied the flow of granular materials in a partially filled rotary cylinder using the boundary layer approach. A model for the flow in the active layer was developed. A simple analytical solution for the velocity distribution $v_{sd}(\varphi)$ in the layer was derived

$$v_{sd}(\varphi) = \left[\frac{\omega}{\eta^{3/2}} \cdot \sqrt{\frac{L}{8g}} \cdot (1 - \varphi^2) \right]^{3/5} . \quad (27)$$

Here with the dimensionless distance along the flow direction in x'-y' coordination

system(see Fig.21)

$$\varphi = 2 x' / L_{bw} . \quad (28)$$

Here L_{bw} is the bed surface width, ω is the angular velocity of kiln, g is the gravity acceleration and η is a parameter which accounts for the stress between the active layer and passive layer interface. It is an fitting parameter and quite difficult to transfer into the practical calculation. Besides η , only the rotational speed with the power 0.6 and the bed width, which is coupled to the filling degree, influence the velocity in this model.

Alexander et al. [3] examined the particle motion on the bed surface at a fixed filling degree for different rotational speeds and drum diameters. With the approach of dimensional analysis a simple downstream velocity equation was developed

$$v_{sd} = k_1 \cdot R \cdot n^{2/3} \cdot \left(\frac{g}{d_p} \right)^{1/6} , \quad (29)$$

where R is the radius of the kiln; n is the rotational speed and d_p is the particle size. The dimensionless value k_1 is used as a fitting parameter to match this calculated velocities with measured ones. The surface velocity is therewith proportional to R , $n^{2/3}$ and $(d_p)^{-1/6}$. In comparison with the results of Elperin et al. [9], only the influence of the rotational speed with a power of 0.6 and 0.67 is similar.

Mellmann et al. [23] developed a mathematical model based on the force and mass balance to investigate the transverse solid motion in the kilns. A differential equation was given to predict the boundary line of the active layer. Therewith the thickness of the active layer and the downstream velocity in the layer can be calculated. Experimental results of 14 different materials have a good agreement with the theoretical calculations.

The advantage of this model is that no fitting parameter is needed. Liu et al. [18] introduced some simplifying assumptions that an analytical solution for the active layer thickness and mean downstream velocity could be derived. This solution is obtained with in the following:

$$v_{sd} = \omega \cdot R \cdot \frac{1 - (\delta_{\max} + \cos \varepsilon)^2}{2 \cdot \delta_{\max}}, \quad (30)$$

where ε is the half filling degree R is the radius of the kilns and δ_{\max} is the dimensionless active layer depth at the mid-chord length of the solid bed,

$$\delta_{\max} = \frac{t}{R} = \frac{-\xi_0}{\tan \theta} + \frac{1}{k \cdot \sin^2(\theta)} \ln \frac{2 + k\xi_0 \sin(2\theta)}{2} + \frac{d_p}{D}. \quad (31)$$

Here t is the local thickness of the active layer, θ is the dynamic angle of repose of particles, d_p is the particle diameter and D is kiln diameter. ξ_0 and k are expressed as

$$\xi_0 = -\sqrt{\sin^2(\varepsilon) - 2(1 + \cos \varepsilon) \frac{d_p}{D}} \quad (32)$$

$$k = \frac{\tan \theta - \tan(\gamma_A + \theta)}{\sin \varepsilon}, \quad (33)$$

with

$$\gamma_A = 0.32 \cdot \theta \cdot (1 + F) + 1800 \cdot Fr \sqrt{\frac{d_p}{D}}, \quad (34)$$

the filling degree

$$F = \frac{2\varepsilon - \sin(2\varepsilon)}{2\pi} \quad (35)$$

and Fr is the Froude number

$$Fr = \omega^2 R / g = 4\pi^2 n^2 R / g . \quad (36)$$

In this model rotational speed, kiln size, particle size and filling degree are involved to calculate the mean velocity in the active layer. The influence of the kiln radius and rotational speed on the mean velocity is presented in **Fig.22** and **Fig.23**, respectively. It can be seen that the velocity increases nearly linearly with the radius, increases with rotational speed approximately with the power 0.5 to 0.7 and decreases slightly with the particle diameter. These results match well with those reported by Alexander et al.[3]. However, the velocity is also influenced by the filling degree which is furthermore depend on the mass flow and on the rotational speed.

4.2 Experimental

4.2.1 Experimental kilns, parameters and materials

The same kilns and materials are employed for these experiments, which have been introduced in *Chapter 3.2.1.* and *Chapter 3.2.3.*, respectively.

4.2.2 Setup and method

Solid bed moving behavior has been experimentally investigated with many different types of optic technologies, such as video camera and digital camera [3,23,31], particle tracking velocimetry (PTV) [14,25], MRI (Magnetic resonance imaging) [22], PEPT (Positron Emission Particle Tracking) [7, 26, 32]. But at the discharge end the length of the bed is extreme short and the thickness of the bed is sometimes only a few particle diameters, also see Fig.11. Therefore, another method was used based on the out-flow behavior. As can be seen in Fig.9, the out-flowing particles follows the law of free falling. A grid box with the dimension of 48cm (length) x 25cm (width) x

29cm(height) is employed, see **Fig.24**. The box is divided into 24 grids by 23 metal plates. Each grid is about 2cm wide. The front panel of the box is transparent for the measurements.

After the solid transport in the kiln comes into the steady state, the kiln rotation and feed are stopped. The grid box is placed horizontally under the kiln discharge end. see **Fig.25**. A pendulum is hanged in front of the vertical centre of the discharge end as a reference line. The box centre corresponds to the hanged thread. A small container is temporarily held above the grid box to receive the out-flowing particles before restarting the rotation. This can avoid the short fluctuation of the solid flow during immediate restarting. After the particle flow is stable again in several minutes, the container is moved away. Particles flow out and are distributed in the grid box. The solid amount in each grid and corresponding radial positions are recorded.

This measurement is performed more than 100 times with three materials in two kilns. Experimental parameters are also presented in **Table1**.

4.3 Determination of the radial out-flowing distribution

The particles amounts in each grid referring to total received particles in y (%) and corresponding radial position x/R are recorded. The experimental values are found to have the best fit with the normal function. The normal function can be described as

$$y = y_{\max} \cdot \exp\left[-\left(\frac{x/R - b}{c}\right)^2\right]. \quad (37)$$

As fitting results the values y_{\max} , b , c are derived based on the experimental data. y_{\max} is the peak value of the distribution in %. b refers to the dimensionless displacement of the distribution in x -axis. c reflects the deviation of the distribution. The range of the particle

distribution over the box length also indicates the downstream velocity fluctuation of the out-flowing particles, which will be discussed in the later chapter. All measured data and fitted normal distributions in the radial direction for three materials are presented in *Appendix A1.1-A1.3*.

4.4 Determination of the downstream velocity v_{sd}

Through experiments and data analysis with computer software, the fitting results b can be used to obtain the experimental radial offset L_r

$$L_r = b \cdot R. \quad (38)$$

In *Chapter 3.2.2*, the distance KBC is measured. It is useful to calculate not only the dynamic angle of repose, but also here the actual projecting distance L_{out} from the discharge end of the kiln, also see Fig.21

$$L_{out} = KBC - L_r. \quad (39)$$

With known experimental values of L_{out} , the mean surface out-flowing velocity v_{sd} could be obtained based on the Newton's free falling theory. The radial flowing velocity v_{sd} can be decomposed into two velocity vectors, vertical v_{sv} and horizontal v_{sh} , respectively, see Fig.21. They are influenced by the dynamic angle of repose θ , which we have practically measured for each experimental material,

$$v_{sh} = v_{sd} \cdot \cos \theta \quad (40)$$

$$v_{sv} = v_{sd} \cdot \sin \theta \quad (41)$$

The velocity vector v_{sv} is vertical to the ground so that it is used to calculate the falling

time t of the particles at a certain falling height H

$$H = v_{sv} \cdot t + 0.5 \cdot g \cdot t^2 . \quad (42)$$

Then, the falling time t is obtained

$$t = \frac{-v_{sv} + \sqrt{v_{sv}^2 + 2gH}}{g} . \quad (43)$$

Another velocity vector v_{sh} is horizontal to the ground. It contributes to the horizontal projecting distance L_{out} with the known falling time

$$L_{out} = v_{sh} \cdot t . \quad (44)$$

The experimental values of L_{out} have been derived so that the horizontal velocity is obtained as

$$v_{sh} = L_{out} / t . \quad (45)$$

Insert Eq.(43) into Eq.(45), we have

$$v_{sh} = \frac{L_{out}}{\frac{-v_{sv} + \sqrt{v_{sv}^2 + 2gH}}{g}} . \quad (46)$$

v_{sh} , v_{sv} and L_{out} in Eq.(46) could be displaced by Eq.(40), Eq.(41), Eq.(38) and Eq.(39)

$$v_{sd} \cdot \cos \theta = \frac{KBC - b \cdot R}{\frac{-(v_{sd} \cdot \sin \theta) + \sqrt{(v_{sd} \cdot \sin \theta)^2 + 2gH}}{g}} . \quad (47)$$

Consequently, the experimental value of v_{sd} is derived as

$$v_{sd} = \frac{KBC - bR}{\cos \theta} \cdot \sqrt{\frac{g}{2H - 2 \tan \theta (KBC - bR)}} \quad (48)$$

At the right side of Eq.(48) the parameters are all known from the experimental measurements. Thus, the mean downstream velocity v_{sd} at the kiln discharge end is experimentally obtained.

4.5 Qualitative analysis of the mean velocity v_{sd}

The measured particle distribution in grid box, fitting results as well as accordingly derived velocity v_{sd} are firstly qualitatively discussed in this section. The influence of the mass flow and the rotational speed is presented.

4.5.1 Influence of the mass flow

Fig.26 shows the mass distribution in the grid box for sand as material for 3rpm and 3° inclination. Here x is the distance in the radial horizontal direction, R the kiln radius and original point 0 is crossed at the centre line of the kiln and the radial horizontal distance. Parameter is the mass flow rate. The measured solid amount in each grid is fitted with the normal distribution for each different mass flow rates. It can be seen that the distributions were shifted to the left direction with increasing the mass flow. **Fig.27** shows the measured sand amount and fitting distribution as before but for 5rpm. In **Fig.28** and **Fig.29** measuring results and corresponding fitting distributions are shown for clinker and glass beads, respectively. The displacement is still shifted in all cases to the left with increasing mass flow.

The displacement L_{out} (see Fig.21) results from the mean downstream velocity of the out-flowing particles. The calculated mean velocity values in dependence on the mass flow are shown in **Fig.30** for glass beads and clinker. The mean velocity tends to

increase linearly with the mass flow. The velocity is also influenced by the particle properties. In **Fig.31** the velocity for sand is presented for 3rpm and 5rpm at 3°, respectively. Higher mass flow still leads to higher downstream velocity. Furthermore, for the same material the rotational speed shows influence on the velocity. This is discussed in the following.

4.5.2 Influence of the rotational speed

In the **Fig.32** and **Fig.33** the mass distributions are shown with the rotational speed as the parameter for clinker and sand, respectively. They are at the same mass flow of 250kg/h and the same inclination angle of 3°. It can be seen that the distributions are shifted to the right with increasing rotational speed. Accordingly, the calculated mean velocities from the distributions are depicted in **Fig.34**. The velocity decreases with the increase of the rotational speed. How the various parameters influence the outlet velocity will be analysed in the following.

Alexander et al.[3] found that the radial downstream velocity is proportional to $n^{2/3}$, see Eq.(29). Likewise, based on the model of Mellman [23], Liu et al. [18] also found that the velocity increases with the rotational speed, see Fig.23. However these results and conclusion are valid for a fixed filling degree. If the rotational speed increases and filling degree is not maintained, according to our experiments the results have a big conflict with the above authors. In industries the variation of the filling degree with changing the operational parameters are more practical. In the following, the quantitative influence of each parameter with various filling degree will be discussed in order to predict the downstream velocity.

4.6 Quantitative study to predict radial downstream velocity v_{sd}

In Elperin's model [9], the mean velocity can be calculated with a simple equation, but η is a parameter which is different to determine for different material. Mellman's [23] model is developed based on the physical and geometric structure of particle flow in the rolling motion in transverse view. The bed depth has great influence on the calculation of the velocity. We applied also our experimental parameters and measuring results in Liu's [18] velocity equations. At first, the filling degree of bed at discharge end is quite low. For a bulk material with different particle size, especially for clinker in our measurements the bed depth was found smaller than the mean particle size, see Fig.12. In this case, the calculation with Liu's equation is not possible, because the minimal bed depth should be a particle diameter. In other case, the quite low filling degree of bed at discharge end doesn't match the rolling mode assumption in the model.

However, Alexander et al. [3] employed dimensional analysis to derive the downstream velocity of particles. The method is not based on the geometric or physical model of the particle flow, but those governing variables. All of the variables believed to be important in the process of particle flow are listed. Then the variables are organized into non-dimensional quantities. This model is found to be valid also for the case of out-flowing particles. The influence of each parameter must be in the chapter qualitatively determined.

4.6.1 Normalization of the surface downstream velocity

The downstream velocity was measured by Alexander et al. [3]. As already explained with Eq.(29) in the introduction, the influence of the involved parameters matches with the mathematical model given by Liu et al. [18]. Therewith the velocity

increases with the rotational speed. This seems to be contrary to the results of this study. However, they all kept the filling degree always constant in their experiments and they used only glass beads as material. The influence of the filling degree was not subject of their research. But the filling degree changes with the rotational speed for a constant mass flow. To prove if the constant k_I in Eq.(29) depends on other parameters the dimensionless velocity

$$v_{sd}^* = \frac{v_{sd}}{R \cdot n^{2/3} \cdot (g / d_p)^{1/6}} \quad (49)$$

is introduced according to Eq.(29).

Fig.35 shows this mean velocity in dependence on the bed depth number for the three researched materials at an inclination angle of 3° . It is obvious that this dimensionless velocity can be approximated with the bed depth number by a straight line. In **Fig.36** all determined dimensionless velocities for the material glass beads are depicted. Parameters are the kiln radius and the inclination angle. All values can be fitted with the same line as before. At least, in **Fig.37** all measurements for the material clinker are summarized. Also in this case the dimensionless velocity depends linearly on the bed depth number. As a consequence, based on our results and the results of Alexander, the mean outlet velocity can be described with the simple dimensionless function

$$v_{sd}^* = 50 \cdot Bd \quad (50)$$

With Eq.(19) and Eq.(50), the velocity can be finally calculated using

$$v_{sd} = \frac{37.5}{\pi} \cdot R^{-2} \cdot n^{-1/3} \cdot \rho_s^{-1} \cdot \dot{M} \cdot \left(\frac{g}{d_p} \right)^{1/6} \cdot \tan \theta \quad (51)$$

The fluctuation of the outlet velocity will be explained in the next chapter.

4.6.2 The velocity fluctuation of the out-flowing particles at discharge end.

The formation of the distribution indicates that the out-flowing particles have different velocities at discharge end. In Eq.(37) the value c is the parameter for the distributed width. In **Fig.38** the values of velocity are measured for three materials. It can be seen that that clinker has the largest and glass beads has the lowest values. It means that clinker has the widest distribution and therewith the highest fluctuation. To analyze the fluctuation a maximum and a minimum velocity are introduced. In order to reduce the experimental error and set a criteria for all measurements, both velocities are defined at that extreme left position and right position, which derived with 10% of the peak values of the distribution, see **Fig.39**. At the furthest falling position, particles have the maximal velocity v_{sd_max} . These particles are found flowing out correspondingly from the lower edge of the solid bed at kiln end. Similarly, at the closest falling position of the distribution particles has the minimal velocity v_{sd_min} . These particles flow out correspondingly from the upper edge of the solid bed at kiln end. With the same theory and method discussed in *Section 3.2.*, both maximal and minimal velocity can be also derived. The results of the v_{sd_max} and v_{sd_min} are presented in **Fig.40**, **Fig.41** and **Fig.42** for three materials with the variation of Bd . The values of the mean velocity v_{sd} are fitted by a line. They show a very good linear correlation with Bd for each material. Above the values of the mean velocity are the maximal velocity. Below the values of the mean velocity are the minimal velocity.

Similar with the mean velocity, the maximal velocity and minimal velocity increases with the increase with Bd for three materials. However, it is obvious that sand and clinker have relatively bigger velocity deviation at the discharge end than glass beads. This could be caused by the particle size distribution of the bulk material. According to

4. The radial out-flowing of particles

our measurements clinker has the higher size deviation to the mean size than other two particles.

5. The axial out-flowing of particles

5.1 Introduction

Similar with the downstream velocity of the out-flowing particles, the axial out-flowing velocity of particles from rotary kiln is still unknown and is demanded by industries. As shown in **Fig.43**, due to the axial velocity v_{sa} , particles are discharged from the kiln end to a certain axial displacement L_a . In this chapter, relevant research of other authors are firstly summarized. Subsequently, our studies of the axial discharging behavior of the particles are reported.

Perron and Bui [27] propose a semi-experimental model to predict the axial transport velocity of the granular particles in the inclined kilns. All geometrical and physical parameters that can affect the axial velocity are listed. With these parameters the dimensional analysis were employed to derive the mean axial velocity equation,

$$v_{sa} = \xi \cdot R \cdot \beta \cdot n \frac{\varepsilon + 2 \tan \frac{\varepsilon}{2}}{(1 - \cos \frac{\varepsilon}{2})^3 \cdot (\cos \theta + 2 \cot \frac{\varepsilon}{4} \cdot \sin \theta)}, \quad (52)$$

where R is the internal radius cylinder; β the inclination angle; n the rotational speed; ε is the filling angle, θ is the dynamic angle of repose. ξ is an unknown empirical constant. In order to get ξ , Perron et al. experimentally measured the bed depth h at different axial positions along the cylinder. The corresponding local cross section area of the bed could be calculated

$$A_x = \frac{1}{2} R^2 (\varepsilon - \sin \varepsilon), \quad (53)$$

where

$$\varepsilon = 2 \arccos\left(\frac{R-h}{R}\right). \quad (54)$$

Accordingly, the local axial velocity $v_{a,x}$ is known from the experiments

$$v_{a,x} = \frac{\dot{V}}{A_x}. \quad (55)$$

For a constant volume flow rate the local axial velocity of the solid bed is influenced by the bed depth. With the axial velocity derived from Eq.(55), the local ξ can be obtained at each corresponding axial position. Over the whole length of the cylinder, ξ is the arithmetic mean of all local values. It is recommended as 0.10115. Hatzilyberis et al. [11] performed their own experiments to investigate the axial velocity. The total hold-up of solid in the cylinder is measured at different operational conditions. The mean axial velocity is calculated with

$$v_{sa} = \frac{L \cdot m}{\dot{M}}, \quad (56)$$

where L is the length of the cylinder, m is the total hold-up of the solid in the cylinder, \dot{M} is the mass flow. The experimental values are compared with the theoretical prediction of the mean axial velocity from Perron et al.[27]. The deviation between the measurements and calculations is within $\pm 15\%$. Das Gupta et al. [6] developed a model for the axial transport of solids for a horizontal rotating cylinder. This model is based on the theory of the single particle trajectory model of Saeman [29]. For a continuously operated horizontal rotary cylinder the bed depth increases in longitudinal direction from discharge end to the feed end. The average axial velocity is found to be proportional to the local slope of the bed depth dh/dx and the rotational speed.

5.2 Experimental

5.2.1 Experimental kilns, parameters and materials

Experimental kilns and materials are exactly the same as that of the radial out-flowing velocity measurement, introduced in *chapter 4.2.1*. Detailed experimental parameters can be see in *Appendix A3.1-A3.3* for the three materials.

5.2.2 Setup and method

The grid box is still used to receive the discharged particles in the axial direction. The experimental setup is similar as that of the measurement of the radial out-flowing particles. Box was put under the kiln end. Only the grid box was horizontally turned by 90° . The length direction of the box is parallel to axial direction of the kiln, as shown in **Fig.44**. The kiln discharge end aims to the middle of the grid box, which is also the zero point of the axial direction, see Fig.43. The experimental method are the same as that of the radial out-flowing, introduced in *Chapter 4.2.2*.

5.3 Determination of the distribution of the axial out-flowing particles

The measured particles amounts in each grid referring to total received particles as y (%) and corresponding dimensionless axial position as x/R are recorded. The values are also found to have the best fit with the normal function. The normal function is described in Eq.(37). The meanings of the values y_{max} , b , c is also the same, but for the distributions of the axial out-flowing particles. All measured data and fitted normal distributions in the axial direction for three materials are presented in *Appendix A2.1-A2.3*.

5.4 Determination of the axial velocity

For an inclined cylinder, the axial transport velocity v_{sa} is always parallel to the cylinder length, as shown in **Fig.43**. This velocity can be decomposed into two velocity vectors, $v_{sa,h}$ and $v_{sa,v}$.

$$v_{sa,h} = v_{sa} \cdot \cos \beta \quad (57)$$

and

$$v_{sa,v} = v_{sa} \cdot \sin \beta . \quad (58)$$

The horizontal component contributes to the horizontal displacement L_a . This displacement is proportional to the falling time according to the Newton's law of free falling

$$L_a = v_{sa,h} \cdot t \quad (59)$$

The falling time t in Eq. (59) depends on the falling height H and the vertical component of the velocity $v_{sa,v}$,

$$H = v_{sa,v} \cdot t + 0.5gt^2 \quad (60)$$

which gives

$$t = \frac{\sqrt{v_{sa,v}^2 + 2gH} - v_{sa,v}}{g} \quad (61)$$

Consequently, the axial velocity can be derived as

$$v_{sa} = \frac{L_a}{\cos \beta} \sqrt{\frac{g}{2H - 2L_a \tan \beta}} \quad (62)$$

where L_a is derived from the fitting result

$$L_a = b \cdot R . \quad (63)$$

5.5 Qualitative study of the axial out-flowing velocity v_{sa}

5.5.1 Influence of the mass flow

Fig.45 shows the mass distribution of glass beads in the grid box at 2rpm and 3° inclination with the mass flow rates as the parameter. The points are the measured particle mass in the grids related to the total mass. All measured points are fitted with the normal distribution for each case. The normal distribution will be discussed later. It can be seen that the distributions are shifted to the left with increasing mass flow, i.e. higher mass flow rates cause higher axial discharge velocities. **Fig.46** shows the measured mass distribution as before however for clinker at 1.5rpm and 5° inclination. The distributions are shifted again to the left with increasing mass flow.

The horizontal displacement L_a from the kiln discharge end to the peak of the distributions is caused by the mean axial out-flowing velocity. This mean axial velocity v_{sa} was calculated from Eq.(62) and are shown in **Fig.47** in dependence on the mass flow. The velocity increases with the mass flow rate.

5.5.2 Influence of the rotational speed

In **Fig.48** the mass distributions of clinker are compared with different rotational speed as the parameter at 250kg/h and 3° inclination. It can be seen that the distributions are shifted to the left with increasing rotational speed. The mean velocity (from peak position of the distribution) is depicted in **Fig.49** for the case in Fig.48. The velocity increases with the rotational speed. This is caused by the fact that the solid bed depth, i.e.

the cross section area of bed at the kiln end decreases with increasing the rotational speed.

5.6 Quantitative study to predict axial discharge velocity v_{sa}

5.6.1 Conservation of mass

During the steady state of the kiln operation the volume flow rate of solid bed \dot{V} keeps constant. And feeding mass flow rate is always equal to the discharging rate. Based on the mass conservation of solid transport in the axial direction, the axial discharge velocity can be calculated as

$$v_{sa} = \frac{\dot{V}}{A_0} = \frac{\dot{M}}{\rho_s \cdot A_0} \quad (64)$$

where A_0 is the cross section area of the 'moving bed' in axial direction. This 'moving bed' determines the axial transport velocity. The cross section of solid bed inside kilns is divided into two layers for the rolling mode motion [4,5,12,14,16], see Fig.21,. The upper layer is called 'active layer' or 'cascading layer'. Underneath exists a passive layer where is no relative motion of the particles to the wall. It is found that the axial transport of the particles takes place only during the downstream flow of particles in the active layer. The active layer profile in transverse view has been researched by Mellman et.al [23]. Then Liu et.al [18] recommended the analytical solution for the active layer profile inside kiln. However, at kiln discharge end the bed depth is extreme low. The flow behavior has shown difference with the flow inside kilns. This 'moving bed' at kiln end is still unknown and must be firstly determined.

In **Fig.50** the theoretical values of the axial discharge velocity are compared with the experimental values of the axial discharge velocity for the three materials. The

theoretical values are calculated with the total bed depth at kiln discharge end, which has been measured in Chapter 1. The red line is the function $y=x$, which is only used as a reference line to compare the values in x-axis and y-axis. We did not find that the theoretical values were obviously smaller than that of the experimental values. All values scatter around the reference line. This indicates that the total bed cross section area at kiln discharge end becomes the 'moving bed'. Otherwise the measured outlet velocities have to be significantly higher as the calculated velocities. Therefore, the total cross section area of the bed at discharge end was used to predict the axial velocity. The end cross section area of the bed can be expressed with the kiln internal radius R and the end filling degree F_0 , which has been investigated in Chapter 1,

$$A_0 = \pi \cdot R^2 \cdot F_0 \quad . \quad (65)$$

5.6.2 Axial discharge velocity

The axial discharge velocity can be calculated using the mass conservation Eq.(64). With the discharge filling degree from Eq.(25) and the bed transverse area from Eq.(65) and we get,

$$v_{sa}^* = \frac{v_{sa} \cdot \rho_s \cdot \pi \cdot R^2}{\dot{M}} = 57 \cdot \frac{1}{Bd^{0.5}} \quad . \quad (66)$$

In this dimensionless form the discharge velocity is related to an axial superficial velocity, that means the volume flow is divided by the empty area of the kiln. The scaled experimental values v_{sa}^* for the three materials are presented in **Fig.51** independence of the bed depth number. The velocity decreases with the increase of the bed depth number. The curve shows the theoretical values of the scaled axial velocity according to Eq.(66). The theoretical prediction has very good agreement with the experimental values. This

also proves that the total bed depth, instead of a partially bed depth, at the discharge end contributes to the axial discharge velocity.

Inserting Eq.(19) for the bed depth number in the previous equation results finally for the outflow velocity as

$$v_{sa} = 66 \cdot \left(\frac{\dot{M} \cdot n}{\pi \cdot R \cdot \rho_s \cdot \tan \theta} \right)^{0.5} \quad (67)$$

All influencing variables act with the power of 1/2. The axial outflow velocity can be interpreted as the square root from the product of the axial superficial velocity with the angular velocity.

5.6.3 Fluctuation of axial discharging velocity

The measured particle mass distribution in the grid box are found to be a normal function in Eq.(37). The width of the distribution means that the outlet velocity must have a fluctuation. According to **Fig.43**, the mass on the left side is caused by a higher velocity than the mean velocity, the mass on the right side by a lower one. According to the fitting results of the particle distribution in the grid box, the value c is the measure for the width of the distribution. In **Fig.52** these values are given for the three materials. It can be seen that clinker has relatively higher values than glass bead and sand. That means that clinker has the widest distribution and therewith the highest fluctuation. To analyze the fluctuation a maximum and a minimum velocity are introduced. Both velocity are defined at the left and right position of the distribution, where the mass has 10% of the maximum value (referring to Fig.39 (b), for axial discharge velocity $v_{sa,max}$ at x_1/R , $v_{sa,min}$ at x_2/R) . In **Fig.53**, **Fig.54** and **Fig.55** the measured maximum, minimum

and mean velocities are shown for the three materials glass beads, sand, and clinker in dependence on the parameters in Eq.(67). The corresponding fitting curve is also given in the figures. It is obvious that clinker has a relatively larger axial velocity fluctuation at the discharge end than sand and glass beads. This could be caused by the particle size distribution of the bulk material. Clinker has the widest particle size distribution of all materials.

6. Conclusions

The out-flowing behavior of particles at kiln discharge end were studied. The end filling degree, the radial downstream velocity and axial discharge velocity of particles were concentrated. Two kilns and three experimental materials were used for experimental measurements. Investigated parameters are: (1). mass flow rate; (2). rotational speed; (3). inclination angle; (4). filling degree; (5). particle property and (6). kiln diameter. Consequently, it can be concluded that:

- (i). The end depth of the out-flowing material in rotary kilns depends on the mass flow, kiln diameter, rotational speed, angle of repose of the material and the inclination angle lower than 5° . It changes from one to several particle diameters. The influence of all these parameters can be described using only one dimensionless number, the so called *Bed depth number* (Bd). This number was derived from Saeman's model for the axial profile of the bed depth. The end bed depth for different kiln diameters can be described using the end filling degree by the correlation $F_0 = 1.75 \cdot Bd^{0.5}$. The accuracy of this equation to the experimental values are within $\pm 10\%$. The range of the investigated *Bed depth number* covers the range of all processes in industrial rotary kilns.
- (ii). The downstream velocity v_{sd} in rotary kilns at the discharge end is proportional to the mass flow. The downstream velocity decreases with kiln radius with the power of 2 and the rotational speed with the power of 1/3. The influence of the material is characterized by the angle of repose, the bulk density and the mean particle size. The larger the angle of repose or the lower the particle size and bulk density is, the higher is the downstream velocity. However, the influence of the particle size is with the power 1/6 relatively low. The downstream velocity can be described with the bed depth number (Bd) $v_{sd}^* = 50 \cdot Bd$. The advantage of

such a dimensionless description is that the results from laboratory kilns can be transferred to large industrial kilns. The range of the researched bed depth number covers the values of industrial kilns. The fluctuation of the radial downstream velocity seems to depend on the particle size distribution. Clinker with the largest particle size distribution showed the highest fluctuation.

- (iii). The axial outlet velocity at the discharge end of rotary kilns increases with the mass flow and the rotational speed. It decreases with the kiln radius, the bulk density of the material and the tangent of its angle of repose. All parameters act with the power of $1/2$. Thus, the discharge velocity can be interpreted as the square root of the product of the axial superficial velocity (volume flow divided by the empty kiln area) and the angular velocity of the material. The fluctuation of the discharge velocity seems to depend on the particle size distribution. Clinker with the largest particle size distribution showed relatively higher velocity fluctuation than sand and glass beads. The discharge velocity is the axial volume flow divided by the total cross section area at the discharge end. It has been proved that the total cross section area of the bed becomes the active layer. No passive layer exists at kiln discharge end any more.

Nomenclature

A_x	Cross section area of the solid bed at the local axial position x [m ²]
A_0	Cross section area of the solid bed at discharge end [m ²]
B	defined in Eq.(18) [-]
Bd	Bed depth number, in Eq.(19) [-]
b	The dimensionless position of the distribution in x-axis (x/R) or L_r/R [-]
c	The width of the distribution [-]
d_p	Diameter of one particle [m] or [mm]
F	Filling degree [%]
F_0	Filling degree at the discharge end [%]
Fr	Froude number [-]
g	Gravity acceleration [m ² /s]
H	Falling height of solids from kiln [m]
h	Solid depth in the cylinder [m]
h_0	Solid depth at the discharge of a cylinder [m]
h_{dam}	height of the dam at discharge end [m]
h_{bc}	Solid depth solved with boundary condition [m]
k_1	Constant in Eq.(29)
KBC	The horizontal distance from kiln center to the end center of the bed, in Fig.9
L_{bw}	Solid bed surface width [m]
L_c	Cylinder length [m]

Nomenclature

L_0	Solid surface bed width at cylinder end [m]
L_{out}	Out-flow distance of particles in radial direction [m]
L_r	Radial displacement from the kiln center to the solid distribution center [m]
\dot{M}	Flow rate of solids [kg/s]
n	Rotational speed [rpm]
R	Radius of cylinder. [m]
t	Falling time of particles [s] / the local thickness of the active layer [m]
v_k	Tangential velocity of cylinder with radius R[m/s]
v_{sa}	The solid bed velocity in axial direction [m/s]
$v_{sa,h}$	The horizontal vector of the surface downstream velocity [m/s]
$v_{sa,v}$	The vertical vector of the surface downstream velocity [m/s]
$v_{sa,x}$	The local solid bed velocity in axial direction [m/s]
v_{sd}	Solid surface downstream velocity [m/s]
v_{sh}	Horizontal component of v_{sd} [m/s]
v_{sv}	Vertical component of v_{sd} [m/s]
x	Distance from discharge end ; axial distance of the kiln [m]; radial distance [m]
x_{bc}	Axial position in cylinder of the boundary condition [m]
y	Solid amount in grid box [%]
z	Residence time of solid [s]
β	Inclination angle of kiln [rad.]/[°]
γ_A	Defined in Eq. (34) [-]

Nomenclature

δ_{max}	Dimensionless maximal depth of the active layer [-]
ε	Half filling angle [rad.]
ε_0	Half filling angle at the discharge end [rad.]
η	A parameter which accounts for the stress between the active layer and passive layer interface. [-]
θ	Dynamic angle of repose [rad.]
μ	Fraction of time spent locked in bed to total time, in Eq.(2) [-]
ρ_s	Bulk density of solids [kg/m ³]
ξ	Constant in Eq.(52) [-]
ξ_0	Defined in Eq.(32) [-]
ω	Angular velocity [rad./s]

Reference

1. Abhouzeid, A.Z.M., Fuerstenau, D.W., 1980. A study of the hold-up in rotary drums with discharge end constrictions. *Powder Technology* 25, 21-29.
2. Afacan, A., Masliyah, J.H. 1990. Solids hold-up in Rotary drums. *Powder Technology* 61, 179-184.
3. Alexander, A., Shinbrot, T., Muzzio, F., 2002. Scaling surface velocity in rotating cylinders as a function of vessel radius, rotational rate, and particle size. *Power Technology* 126 174-190.
4. Ashish V. Orpe, D. V. Khakhar. 2001. Scaling relations for granular flow in quasi-two dimensional rotating cylinders. *Physical review E* 64, 031302.
5. Boateng, A. A. and Barr, P. V. 1997. Granular flow behaviour in the transverse plane of a partially filled rotating cylinder. *J. Fluid Mech.* 330, 233±249.
6. Das Gupta S., Khakhar D. V. and Bhatia S. K. 1991. Axial transport of granular solids in horizontal rotating cylinders. Part 1: Theory. *Powder Technology*, 67.
7. Ding Y. L., Seville J.P.K., Forster R., Parker D.J., 2001. Solids motion in rolling mode rotating drums operated at low to medium rotational speeds. *Chemical Engineering Science* 56, 1769-1780.
8. Ding Y.L., Forster R., Seville J.P.K., Parker D.J.. 2002. Segregation of granular flow in the transverse plane of a rolling mode rotating drum. *Multiphase Flow* 28635–663.
9. Elperin T., Vikhansky A. 1998. Granular flow in a rotating cylindrical drum. *Europhysics Letters*, 42 (6), 619-623.
10. Felix G., V. Falk, D'Ortona U.. Segregation of dry granular material in rotating drum: experimental study of the flowing zone thickness. *Powder Technology* 128 , 314-319 (2002).
11. Hatzilyberis K. S. and Androustopoulos G.P.. 1999. An RTD study for the flow of lignite particles through a pilot rotary dryer Part 1: bare drum case. *Drying Technology* 17 (4&5), 745-757.

Reference

12. Hehl, M., Kroeger, H., Helmrich, H., Schuegerl, K., 1978. Longitudinal mixing in horizontal rotary drum reactors. *Powder Technology* 20 (1), 29-37.
13. Hogg R., Shoji K. and Austin L. G., 1973. Axial transport of dry powders in horizontal rotating cylinders. *Powder Technology* 9, 99-106.
14. Jain N., J. Ottino, R. Lueptow. 2002. An experimental study of the flowing granular layer in a rotating tumbler, *Physics of Fluids* 14 (2) 572– 582.
15. Kramers. H, Croockewit. P, 1952. The passage of granular solid through inclined rotary kilns. *Chemical Engineering Science* 1, 259-265.
16. Lehmborg J., Hehl M., and Schügerl K., Transverse mixing and heat transfer in a horizontal drum mixer. *Powder Technology*. 18, 149 (1977).
17. Li S.-Q., Yan J.-H., Li R.-D., Chi Y., Cen K.-F. 2002. Axial transport and residence time of MSW in rotary kilns Part 1. Experimental. *Powder technology* 126217-227.
18. Liu Xiao Yan, Specht E., Gonzalez O.Guerra, Walzel P. 2006. Analytical solution for the rolling-mode granular motion in rotary kilns. *Chemical Engineering and process* 45, 515-521.
19. Liu Xiao Yan, Specht E., Mellmann J.,2005. Experimental study of the lower and upper angles of repose of granular materials in rotating drums. *Powder Technology* 154 (2005) 125-131.
20. Liu Xiao Yan, Specht Eckehard. 2006. Mean residence time and holdup of solids in rotary kiln. *Chemical Engineering Science* 61, 5176-5181.
21. Liu. Xiao Yan, Specht E., Mellmann J.,2005. Experimental study of the lower and upper angles of repose of granular materials in rotating drums. *Powder Technology* 154 ,125-131.
22. Lori Sanfratello, Arvind Caprihan. 2007. Velocity depth profile of granular matter in a horizontal rotating drum. *Granular matter* 9, 1-6
23. Mellmann J., Specht E., Liu X.Y.. 2004. Prediction of rolling bed motion in rotating cylinders. *AIChE J.*, 50: 2783-2793
24. Mueller Ronny, Kleinebudde Peter, 2007. Prediction of tablet velocity in pan coaters

for scale-up. *Powder Technology* 173, 51-58.

25. Nicolas A. Pohlman, Julio M. Ottino, Richard M. Lueptow. 2006. End-wall effects in granular tumblers: From quasi-two-dimensional flow to three-dimensional flow. *Physical review E* 74, 031305.

26. Parker D. J., Dijkstra A.E., Martin T.W., J.P.K. Seville. 1997. Positron emission particles tracking studies of spherical particles motion in rotating drums. *Chemical Engineering Science*, Vol. 52, No.13, 2011-2022.

27. Perron, J. and BUI, R.T. , February 1990. Rotary cylinders: solid transport prediction by dimensional and rheological analysis. *The Canadian journal of chemical of chemical engineering*. Volume 68.

28. Preetanshu Pandey, Yongxin Song, Ferhan Kayihan, Richard Turton, 2006. Simulation of particle movement in a pan coating device using discrete element modeling and its comparison with video-imaging experiments. *Powder Technology* 161, 79–88.

29. Saeman, W.C. 1951 Passage of solids through rotary kilns: factors affecting time of passage, *Chemical Engineering Progress* 47, 508-514.

30. Sandadi S., Pandey P., Turton R., 2004. In-situ, near real-time acquisition of particle motion in a rotating pan coating equipment using imaging techniques, *Chemical Engineering Science* 59 (24) 5807– 5817.

31. Santomaso A.C., Ding Y.L., Lickiss J.R., York S.W., 2003. Investigation of the granular behaviour in a rotating drum operated over a wide range of rotational speed. *Trans IChmeE*, Vol 81, Part A. 936-945.

32. Spurling R.J., 2000. Granular flow in an inclined rotating cylinder: steady state and transients. PhD thesis. University of Cambridge, UK.

33. Sullivan, J.D., Maier, C.G., Ralson, O.C., 1927. Passage of solid particles through rotary cylindrical kilns. U.S. Bureau of Mines Technical Paper, No. 384.

34. Vahl L., and Kingma W.G., 1952. Transport of solids through horizontal rotating cylinders, *Chemical Engineering Science* 1, 253-258.

Figure abstract

- Fig.1** Rotary Kiln ($\Phi 6.2 \times 98\text{m}$) of a Clinker Production Line (Ch1)
- Fig.2** General production process in cement industry (Ch1)
- Fig.3** Clinker discharged at extremely high temperature and a falling height with 4-6m (Ch2)
- Fig.4** Particles discharging from rotary kiln with radial and axial velocity. Hot materials are cooled on the cooler (Ch2)
- Fig.5** Solid bed depth in transverse view and the depth change along the cylinder (Ch3.1)
- Fig.6** The boundary condition solving the solid bed depth in kilns (Ch3.1)
- Fig.7** Schematic structure of lab rotary kiln1 (Ch3.2.1, Ch4.2.1, Ch5.2.1)
- Fig.8** Schematic structure of lab rotary kiln2 (Ch3.2.1, Ch4.2.1, Ch5.2.1)
- Fig.9** Measurement of the dynamic angle of repose θ (Ch3.2.2)
- Fig.10** Real images of three experimental materials (Ch3.2.3, Ch 4.2.1, Ch5.2.1)
- Fig.11** Dynamic measuring the bed surface width at discharge end of kiln (Ch3.2.4)
- Fig.12** Variation of the scaled end depth of clinker with the bed depth number (Ch3.4)
- Fig.13** Variation of the scaled end depth of glass beads with the bed depth number
- Fig.14** Variation of the scaled end depth of sand with the bed depth number (Ch3.4)
- Fig.15** Correlation of the end filling degree with Bd for clinker (Ch3.5)
- Fig.16** Variation of the end filling degree sorted by the inclination angle for glass beads (Ch3.5)
- Fig.17** Influence of the particle property on the $Bd-F0$ correlation at 1° inclination (Ch3.6)
- Fig.18** Influence of the particle property on the $Bd-F0$ correlation at 3° inclination (Ch3.6)

Fig.19 Influence of the particle property on the $Bd-F0$ correlation at 4° inclination (Ch3.6)

Fig.20 Derivation of the fitting equation for the end filling degree $F0$ based on Bd (Ch3.7)

Fig.21 Particles flowing out of the discharge end with the downstream velocity v_{sd} and distributed in the grid box. (Ch4)

Fig.22 The influence of the kiln radius on the mean downstream velocity inside the kiln, based on analytical solution of Liu et al. [60]. (Ch4.1)

Fig.23 The influence of the rotational speed on the mean downstream velocity inside the kiln, based on analytical solution of Liu et al. [60]. (Ch4.1)

Fig.24 The grid box used to collect the out-flowing particle from the kiln discharge end in order to calculate the radial and axial velocity

Fig.25 Experimental setup to measure the radial downstream velocity of the out-flowing particles (Ch4.2.2)

Fig.26 Measured particles amount of radial out-flowing and the fitting curve with normal function for sand, 3rpm, 3° inclination (Ch4.5.1)

Fig.27 Measured particles amount of radial out-flowing and the fitting curve with normal function for sand, 5rpm, 3° inclination (Ch4.5.1)

Fig.28 Measured particles amount of radial out-flowing and the fitting curve with normal function for clinker, 2rpm, 3° inclination (Ch4.5.1)

Fig.29 Measured particles amount of radial out-flowing and the fitting curve with normal function for glass beads, 2rpm, 3° inclination (Ch4.5.1)

Fig.30 Influence of the mass flow on the downstream velocity at discharge end for clinker and glass beads (Ch4.5.1)

Fig.31 Influence of the mass flow on the downstream velocity at discharge end for sand (Ch4.5.1)

Fig.32 Measured particles amount of radial out-flowing and the fitting curve with normal function for clinker, 250kg/h, 3° inclination (Ch4.5.2)

Fig.33 Measured particles amount of radial out-flowing and the fitting curve with normal function for sand, 250kg/h, 3° inclination (Ch4.5.2)

Fig.34 Influence of the rotational speed on the radial downstream velocity at discharge end (Ch4.5.2)

Fig.35 Correlation of the scaled downstream velocity with the bed depth number for clinker , sand and glass beads at 3° inclination (Ch4.6.1)

Fig.36 Correlation of the scaled downstream velocity with the bed depth number for glass beads (Ch4.6.1)

Fig.37 Correlation of the scaled downstream velocity with the bed depth number for clinker (Ch4.6.1)

Fig.38 Comparison of the distributed range of out-flowing particles for three materials (Ch4.6.2)

Fig.39 The calculation of the downstream velocity fluctuation at kiln discharge end (Ch4.6.2)

Fig.40 Comparison of the maximal, minimal and mean downstream velocity at the discharge end for glass beads (Ch4.6.2)

Fig.41 Comparison of the maximal, minimal and mean downstream velocity at the discharge end for sand (Ch4.6.2)

Fig.42 Comparison of the maximal, minimal and mean downstream velocity at the discharge end for clinker (Ch4.6.2)

Fig.43 Particles flowing out of the kiln end with the axial velocity; The axial velocity is measured with grid box (Ch5)

Fig.44 Experimental setup to measure the axial velocity of the out-flowing particles (Ch5.2.2)

Fig.45 Measured particle amount and the fitting curve with normal distribution for glass beads, 2rpm, 3° inclination (Ch5.5.1)

Fig.46 Measured particle amount and the fitting curve with normal distribution for clinker, 1.5rpm, 5° inclination (Ch5.5.1)

Fig.47 Influence of the mass flow on the axial velocity at discharge end (Ch5.5.1)

Fig.48 Measured particle amount and the fitting curve with normal distribution for clinker, 250kg/h, 3° inclination (Ch5.5.1)

Fig.49 Influence of the rotational speed on the axial velocity at discharge end (Ch5.5.2)

Fig.50 Comparison of the axial velocity at discharge end between experimental values and theoretical values (Ch5.6.1)

Fig.51 Correlation of the scaled axial velocity with the bed depth number (Ch5.6.2)

Fig.52 Comparison of the distributed range of out-flowing particles for three materials (Ch5.6.2)

Fig.53 The velocity fluctuation for glass beads (Ch5.6.3)

Fig.54 The velocity fluctuation for glass beads. (Ch5.6.3)

Fig.55 The velocity fluctuation for clinker. (Ch5.6.3)



Fig.1 Rotary Kiln ($\Phi 6.2 \times 98\text{m}$) of a Clinker Production Line (Ch1)

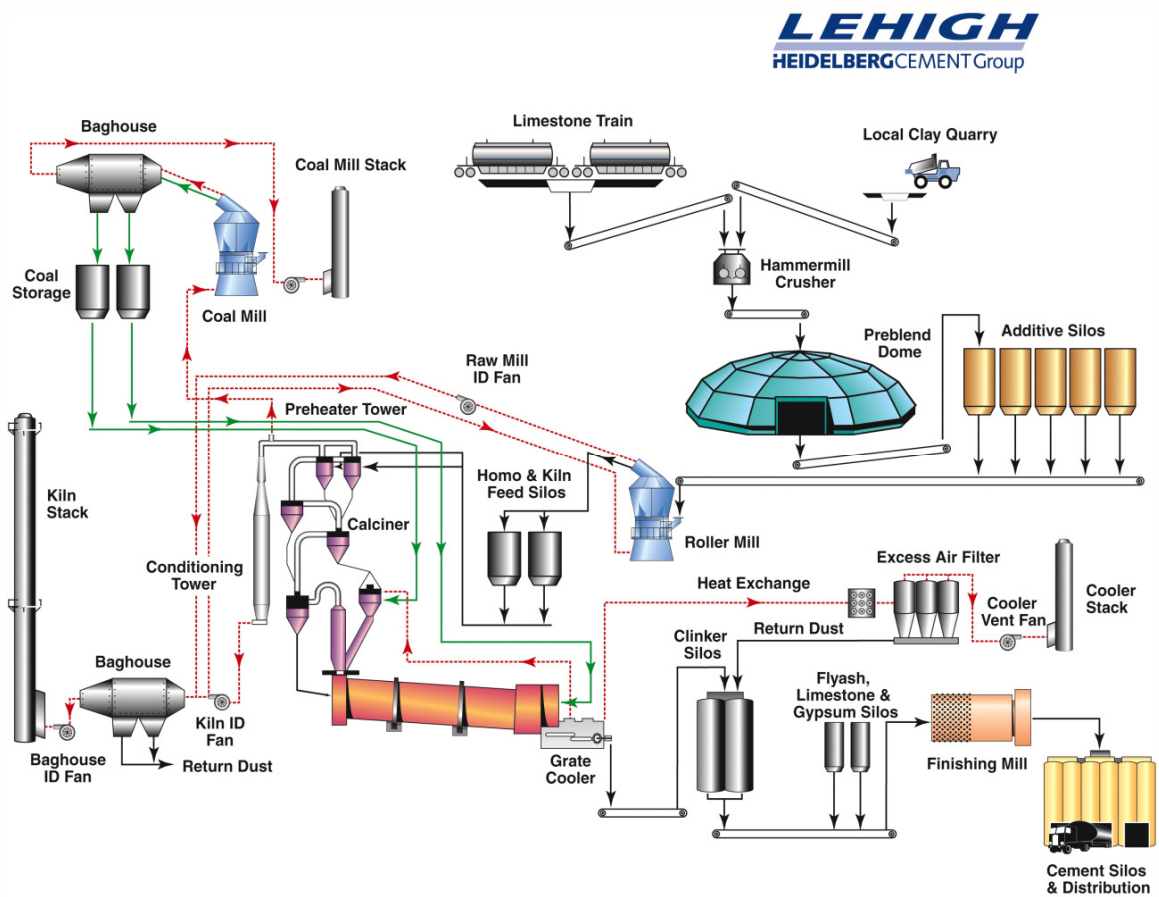


Fig.2 General production process in cement industry (Ch1)



Fig.3 Clinker discharged at extremely high temperature and a falling height with 4-6m (Ch2)

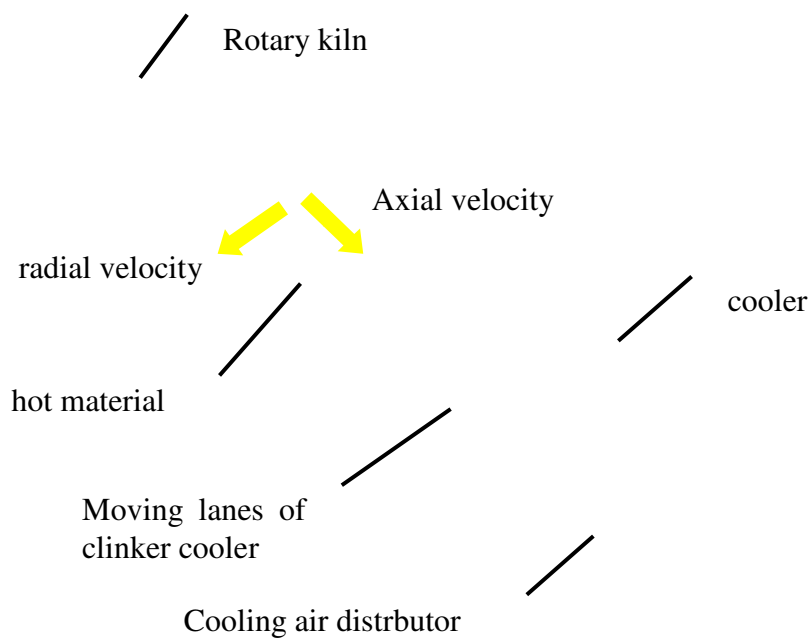


Fig.4 Particles discharging from rotary kiln with radial and axial velocity. Hot materials are cooled on the cooler (Ch2)

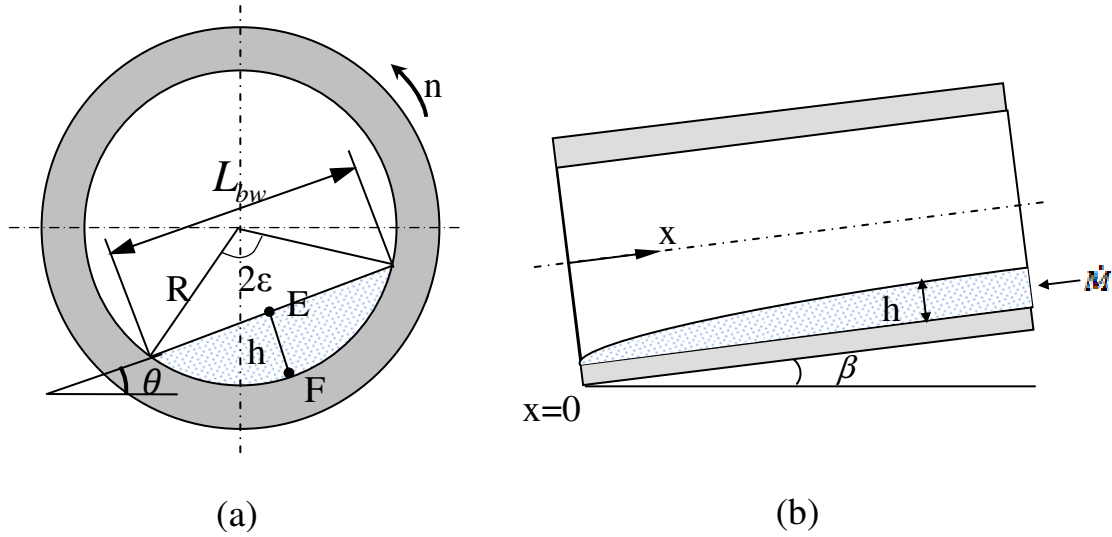


Fig.5 Solid bed depth in transverse view and the depth change along the cylinder (Ch3.1)

Note: (a).Solid bed depth h at the mid-chord length, shown as the line \overline{EF} ; Corresponding bed surface width L_{bw} ; The parameters: rotational speed n ; kiln radius R , filling angle ϵ , dynamic angle of repose θ . (b). Solid bed depth change along the cylinder; the parameters: mass flow rate \dot{M} ; inclination angle β .

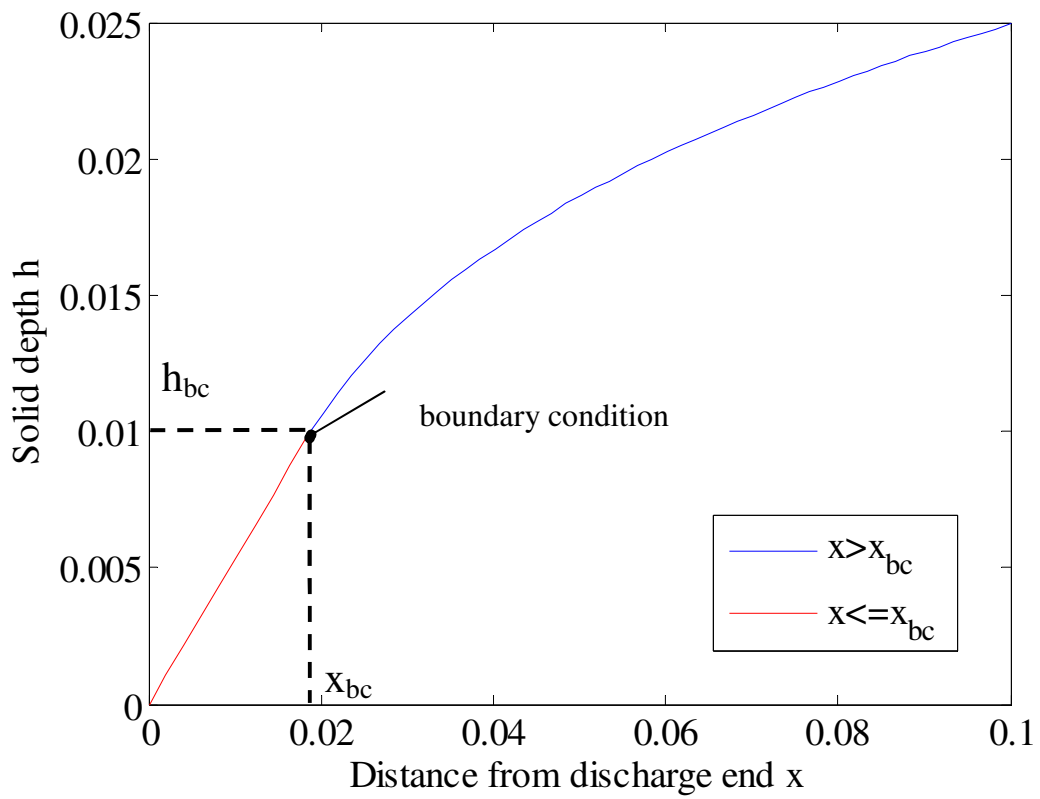


Fig.6 The boundary condition solving the solid bed depth in kilns (Ch3.1)

Note: The boundary condition (x_{bc} , h_{bc}) is derived with Eq.(12) and Eq.(13) to solve the equation for the solid bed depth profile in the kiln.

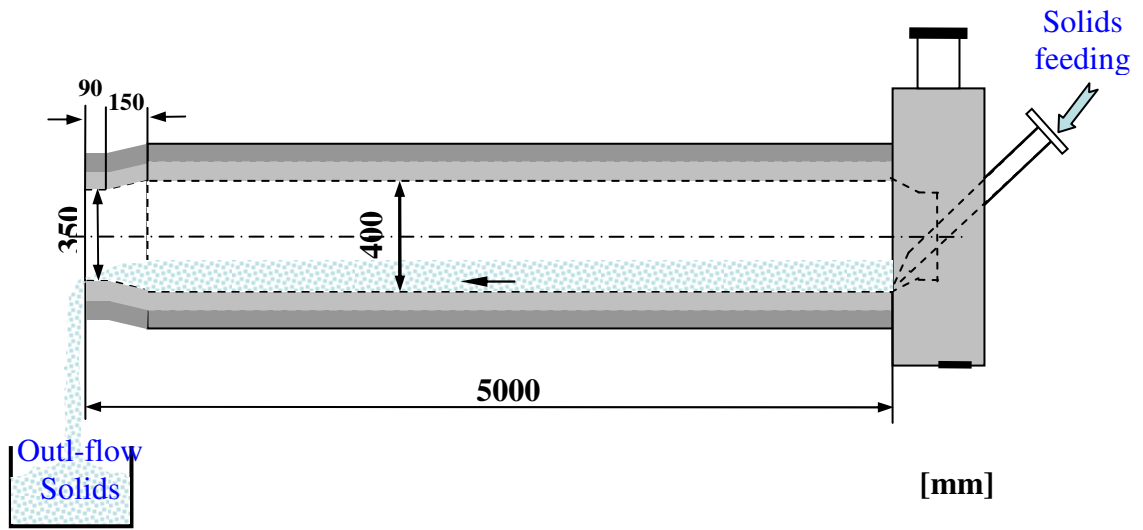


Fig.7 Schematic structure of lab rotary kiln1 (Ch3.2.1, Ch4.2.1, Ch5.2.1)

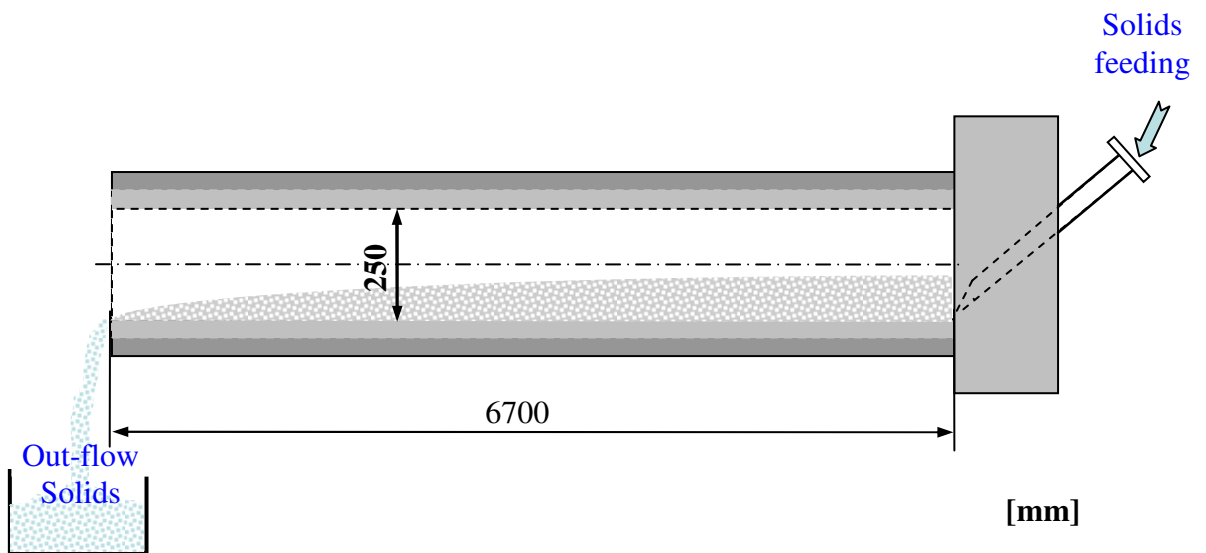


Fig.8 Schematic structure of lab rotary kiln2 (Ch3.2.1, Ch4.2.1, Ch5.2.1)

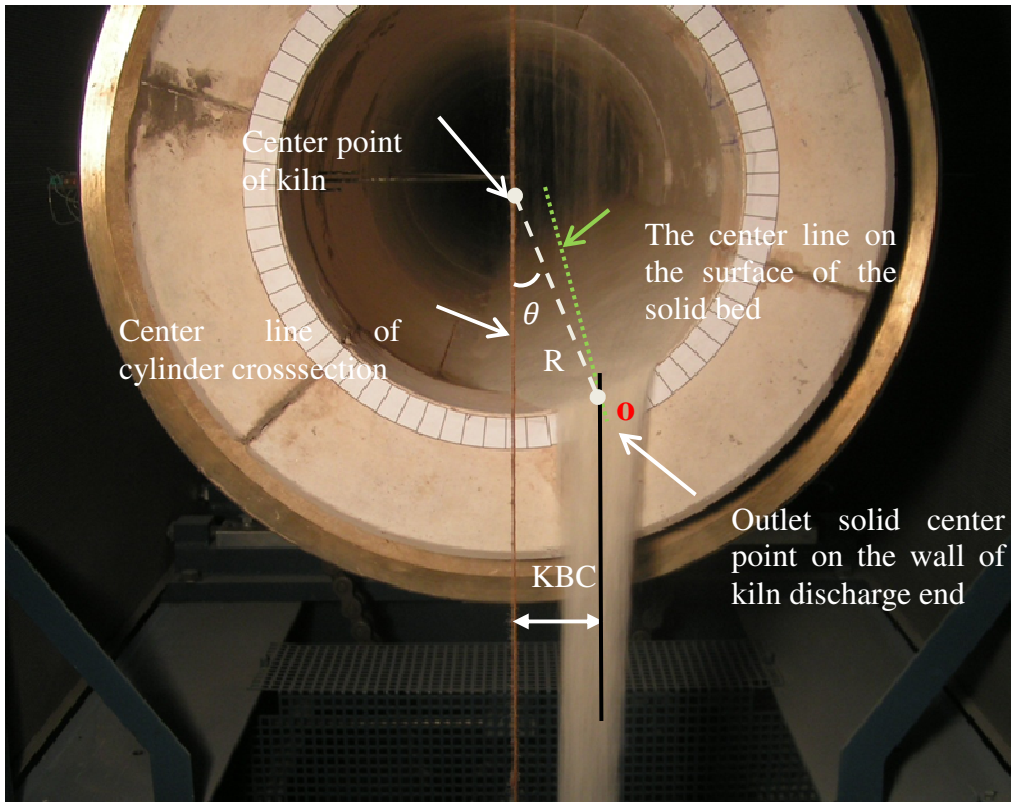


Fig.9 Measurement of the dynamic angle of repose θ (Ch3.2.2)

Note: The center line of the solid bed in the axial direction is found (the green line) and extended to the discharge end. A center point O of the discharge bed is marked on the kiln wall. The horizontal distance from the kiln center line (the brown line) to the point O is measured as KBC. The dynamic angle of repose can be calculated with Eq. (14).

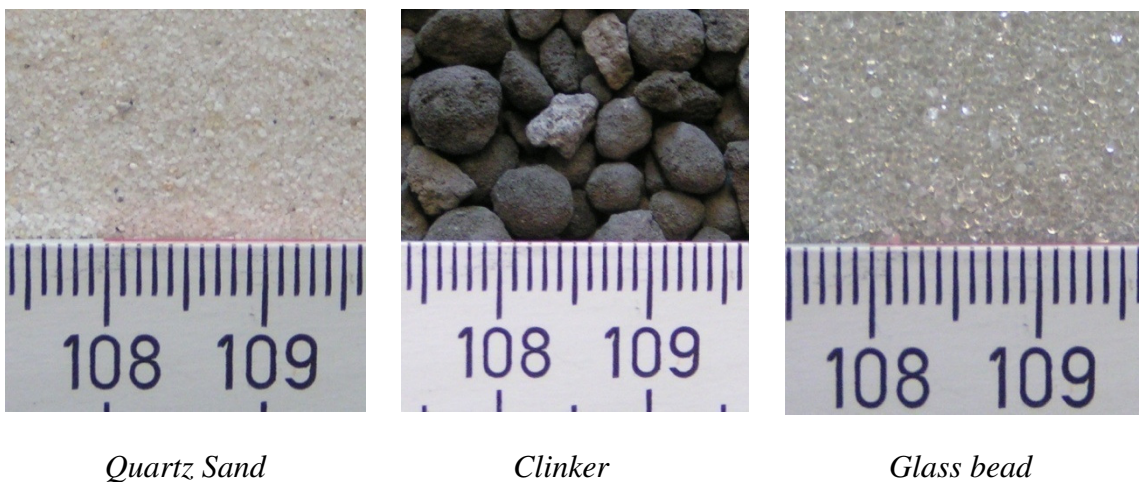


Fig.10 Real images of three experimental materials (Ch3.2.3, Ch 4.2.1, Ch5.2.1)

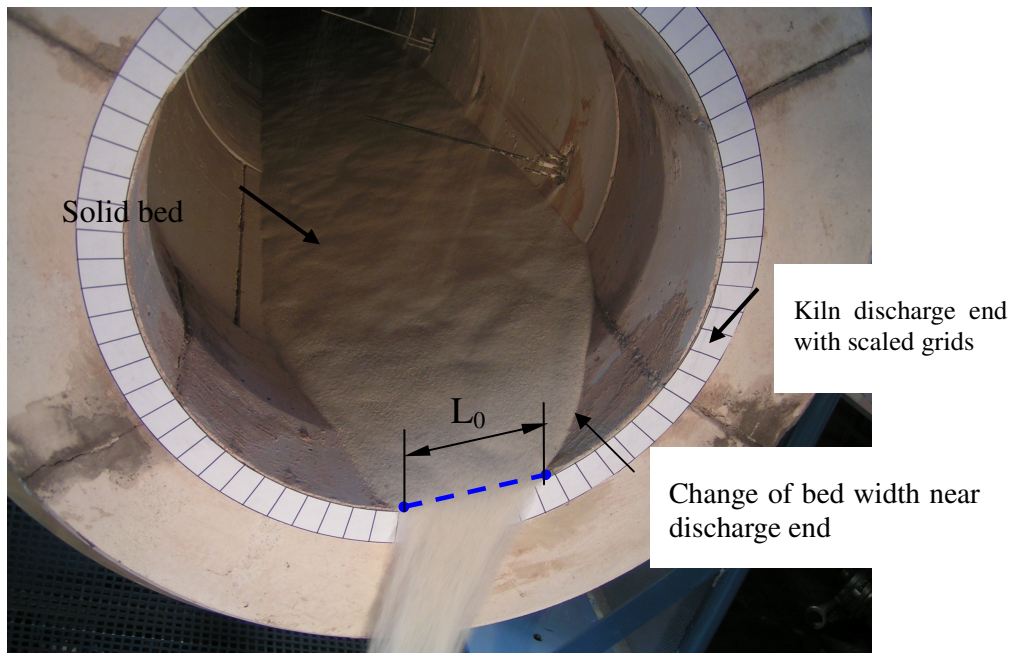


Fig.11 Dynamic measuring the bed surface width at discharge end of kiln (Ch3.2.4)

Note: The end condition of the bed is observed. The end depth is extremely low. The surface width L_0 of the solid bed is alternatively measured with rotation of cylinder.

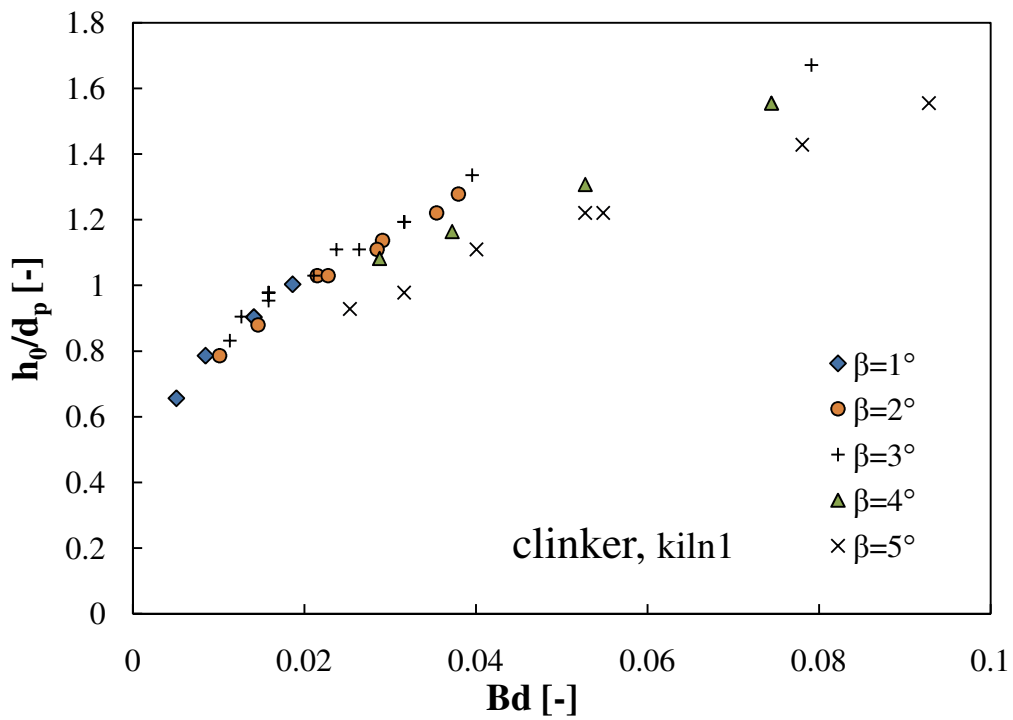


Fig.12 Variation of the scaled end depth of clinker with the bed depth number (Ch3.4)

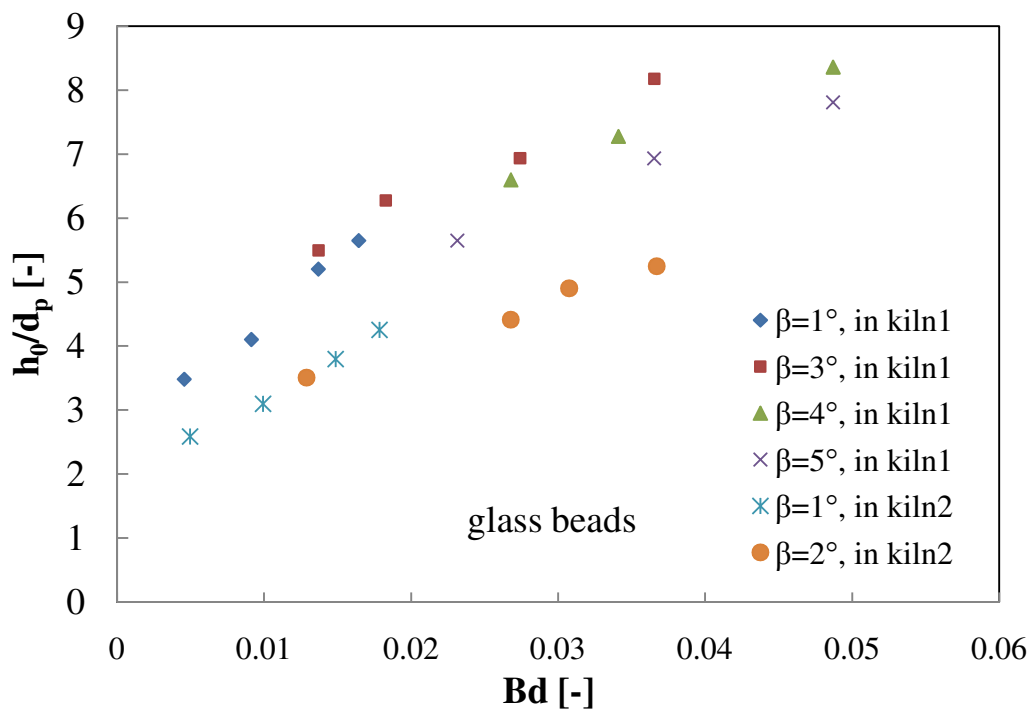


Fig.13 Variation of the scaled end depth of glass beads with the bed depth number (Ch3.4)

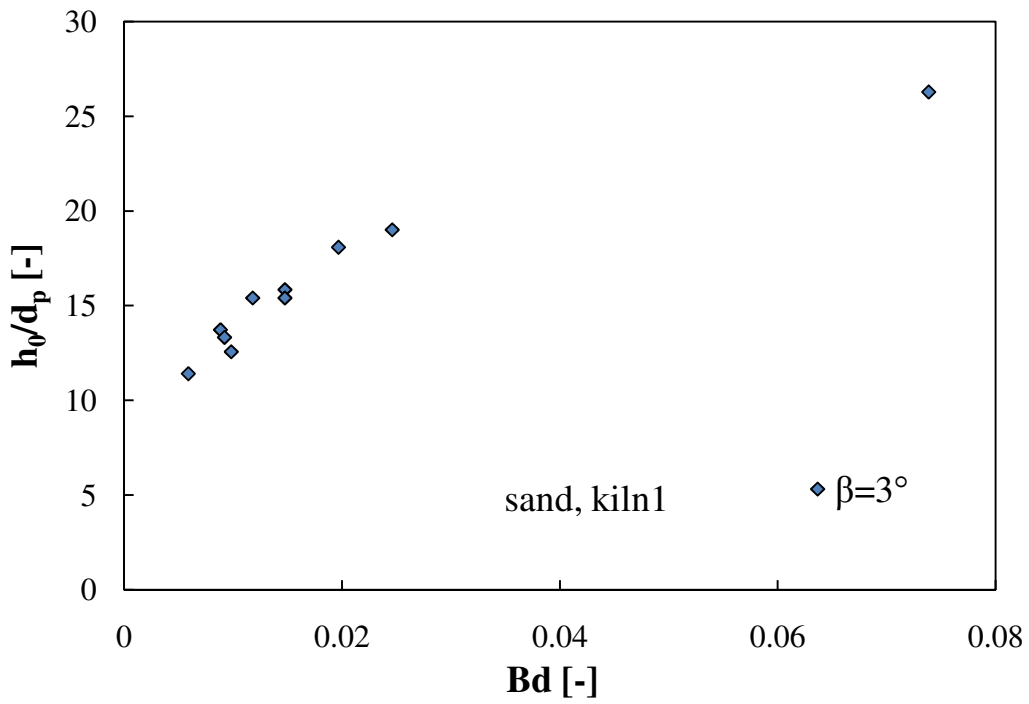


Fig.14 Variation of the scaled end depth of sand with the bed depth number (Ch3.4)

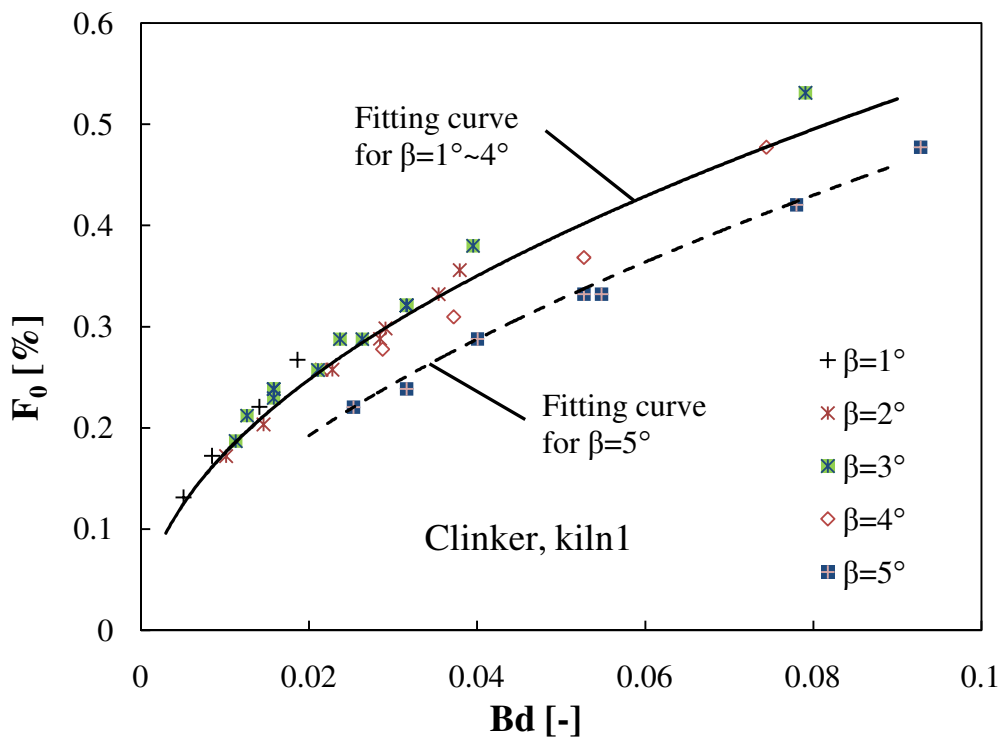


Fig.15 Correlation of the end filling degree with Bd for clinker (Ch3.5)

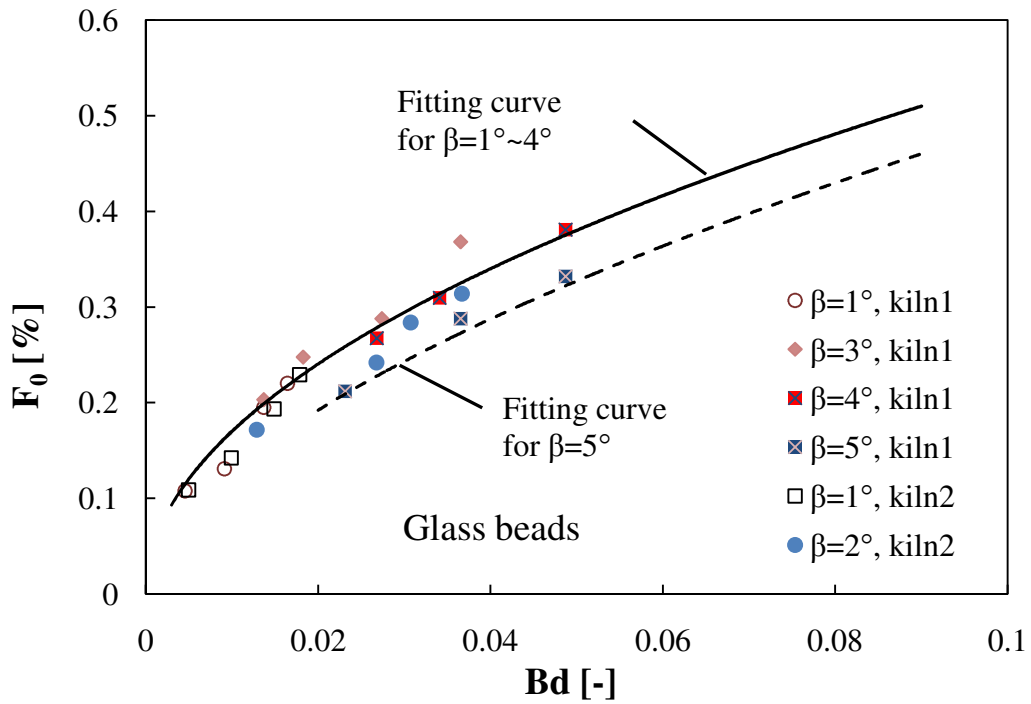


Fig.16 Variation of the end filling degree sorted by the inclination angle for glass beads (Ch3.5)

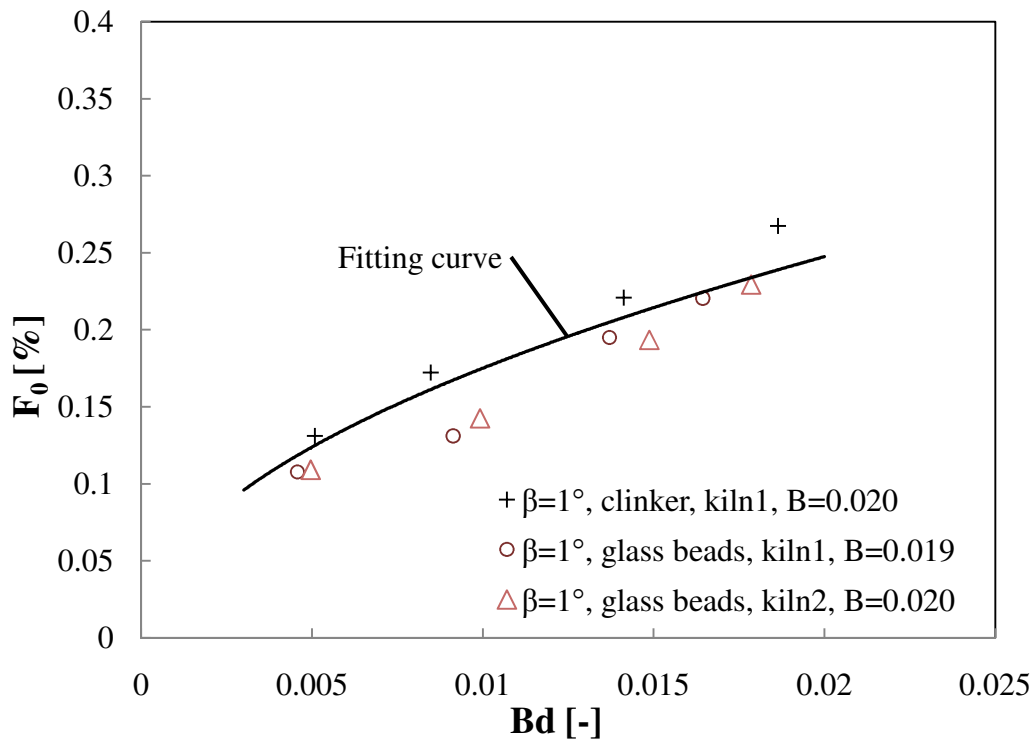


Fig.17 Influence of the particle property on the $Bd-F_0$ correlation at 1° inclination (Ch3.6)

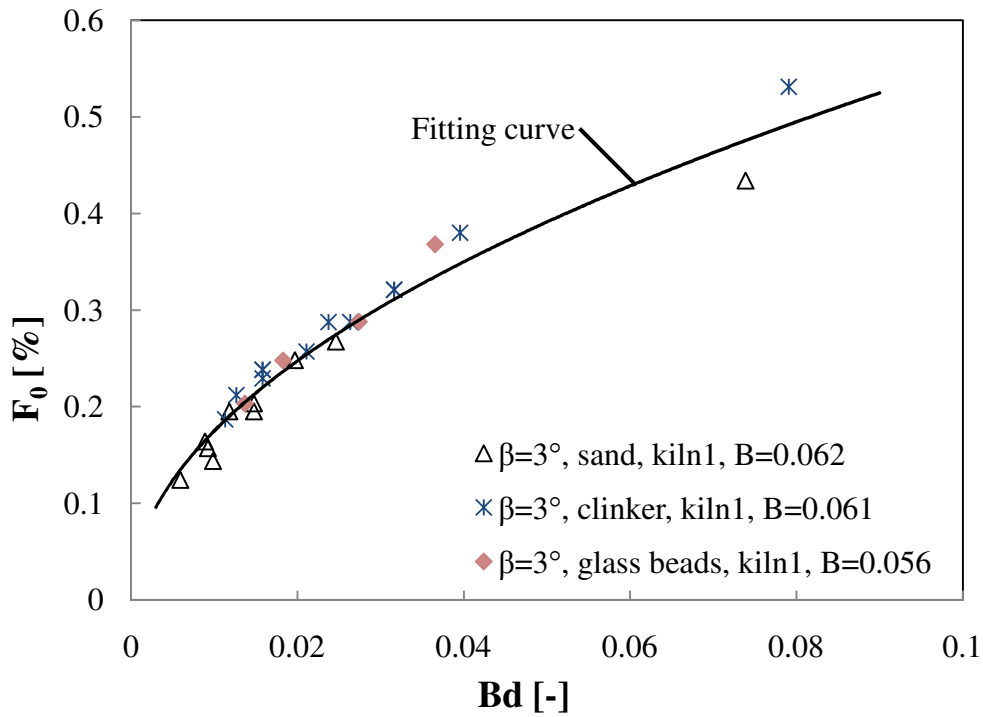


Fig.18 Influence of the particle property on the $Bd-F_0$ correlation at 3° inclination (Ch3.6)

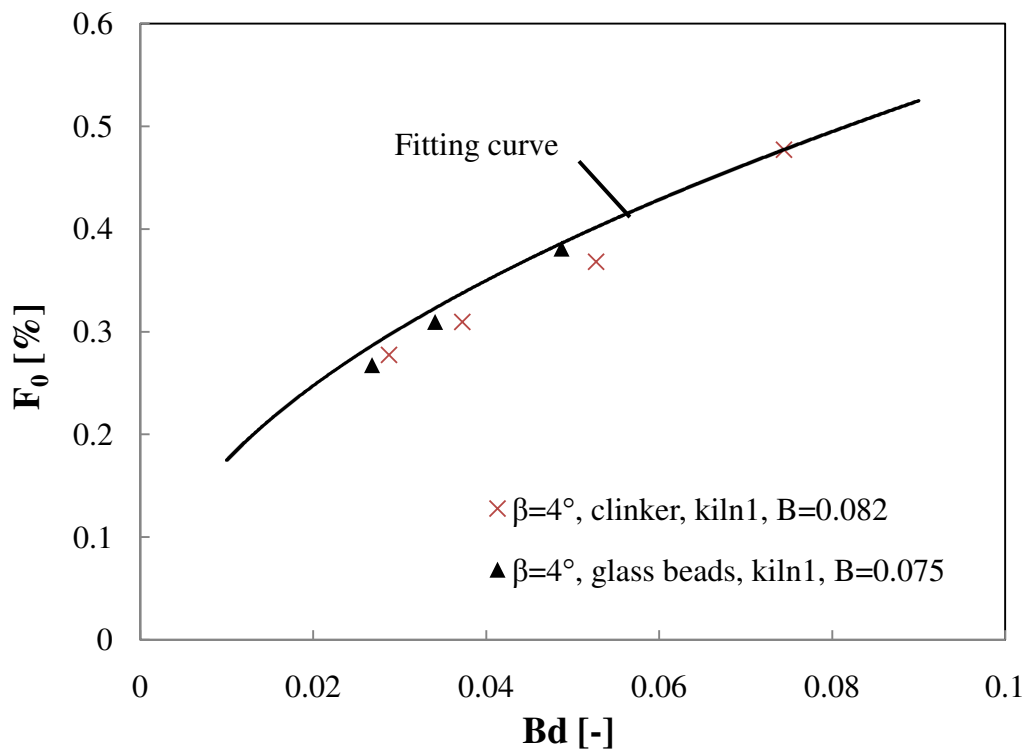


Fig.19 Influence of the particle property on the $Bd-F_0$ correlation at 4° inclination (Ch3.6)

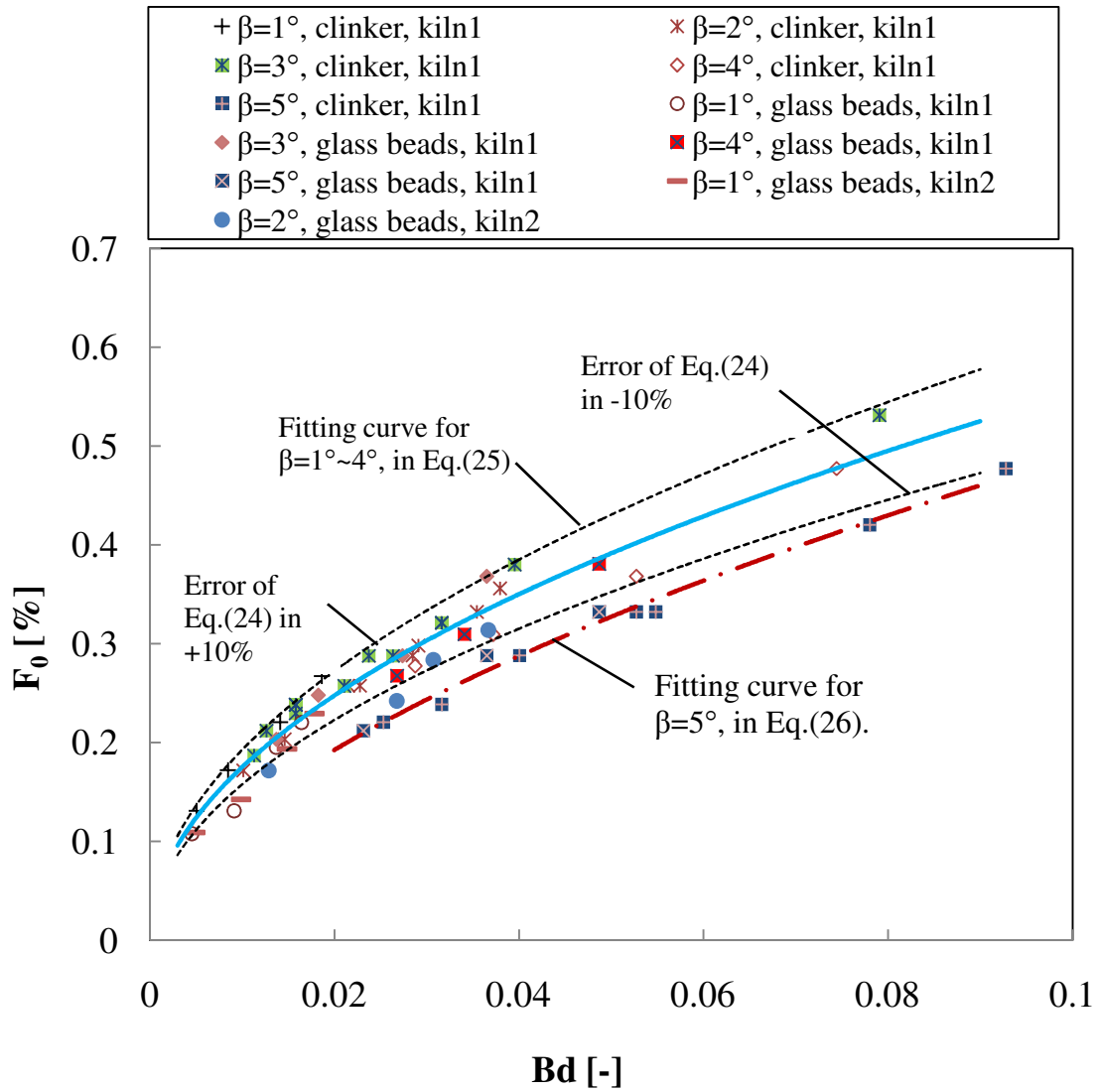


Fig.20 Derivation of the fitting equation for the end filling degree F_0 based on Bd (Ch3.7)

Note: All experimental data are fitted to find out the correlation for F_0 and Bd . The blue curve shows the fitting for data at $1^\circ\sim 4^\circ$, in Eq.. At 5° inclination the data deviates from other, shown by the red curve.

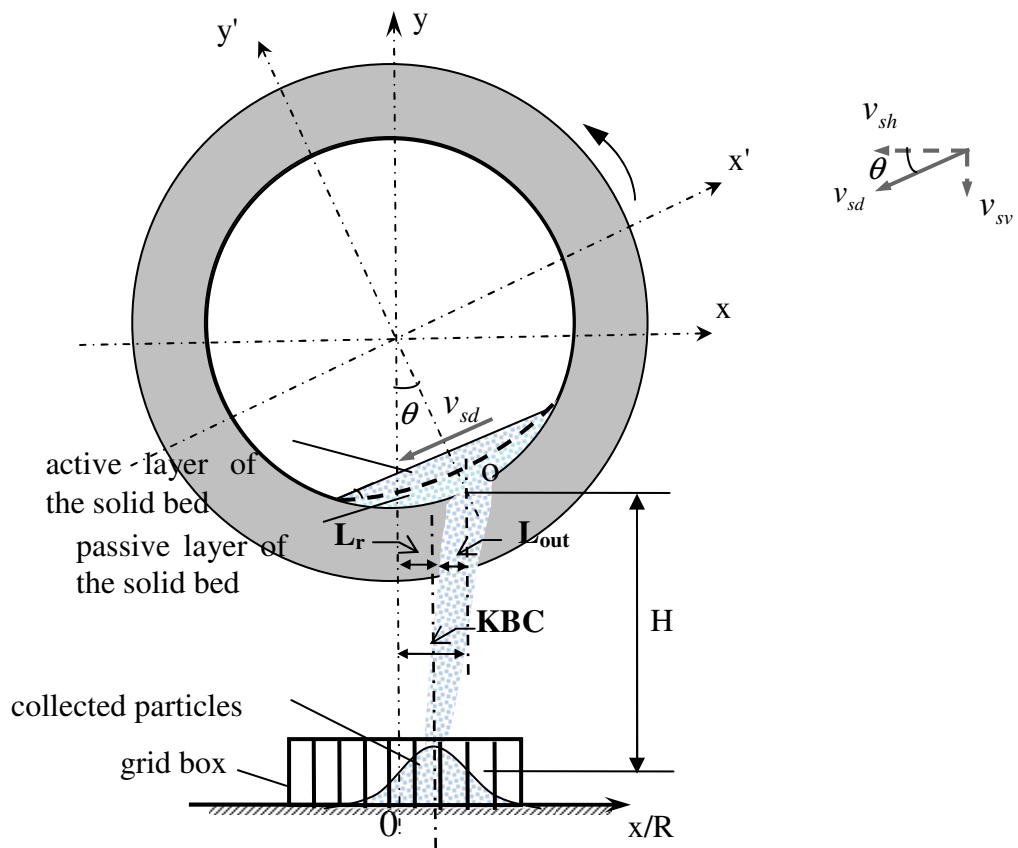


Fig.21 Particles flowing out of the discharge end with the downstream velocity v_{sd} and distributed in the grid box. (Ch4)

Note: The particle on the bed surface flow out of the rotary kiln with the velocity v_{sd} . Discharged particle distribution is measured with a grid box. The mean velocity is calculated with the displacement of the distribution. L_r is the horizontal distance from the kiln center line to the distribution center line. L_{out} is the horizontal distance from the distribution center line to the discharge center point O .

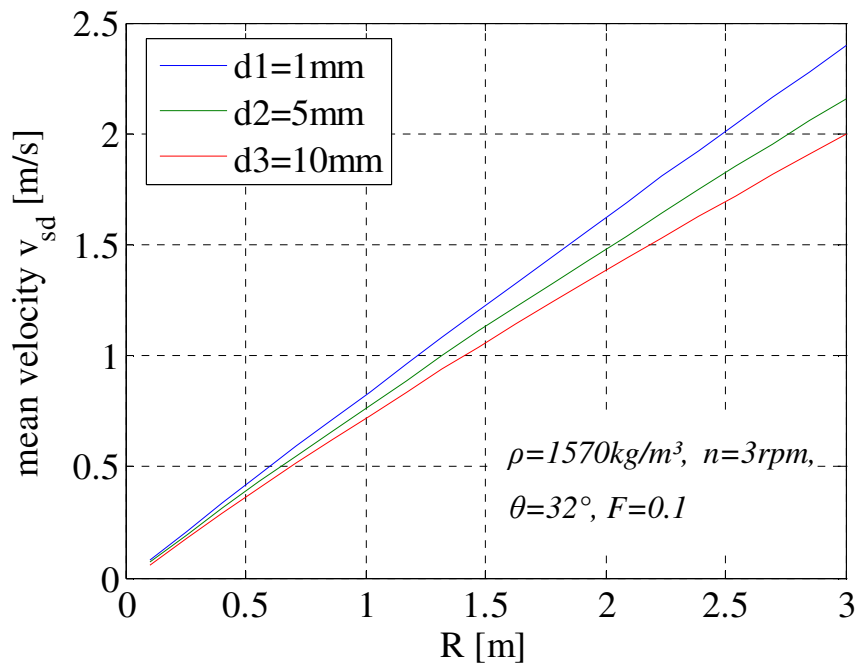


Fig.22 The influence of the kiln radius on the mean downstream velocity inside the kiln, based on analytical solution of Liu et al. [60]. (Ch4.1)

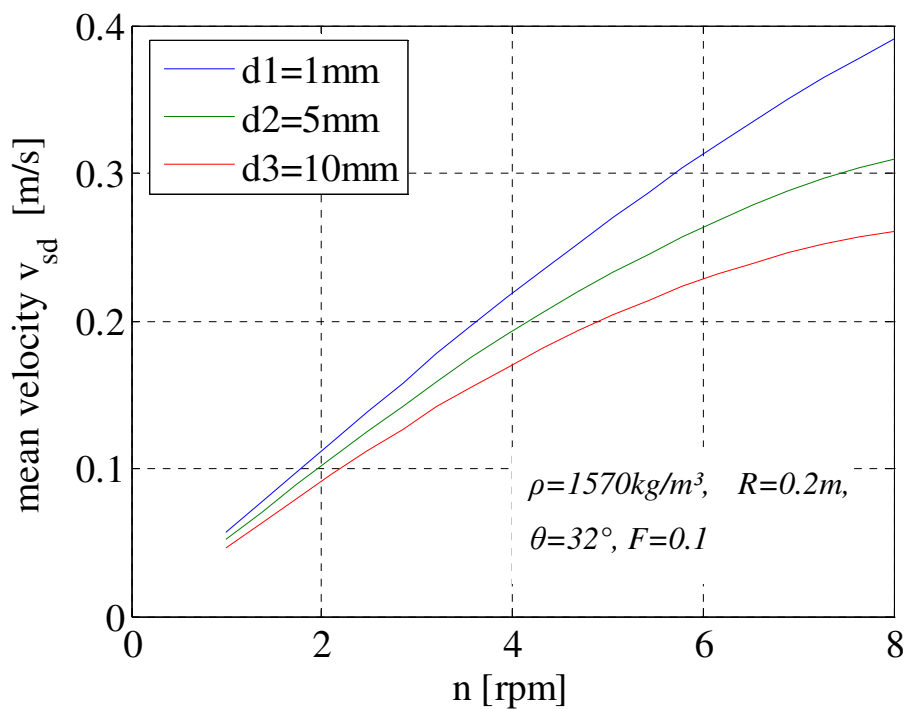


Fig.23 The influence of the rotational speed on the mean downstream velocity inside the kiln, based on analytical solution of Liu et al. [60]. (Ch4.1)

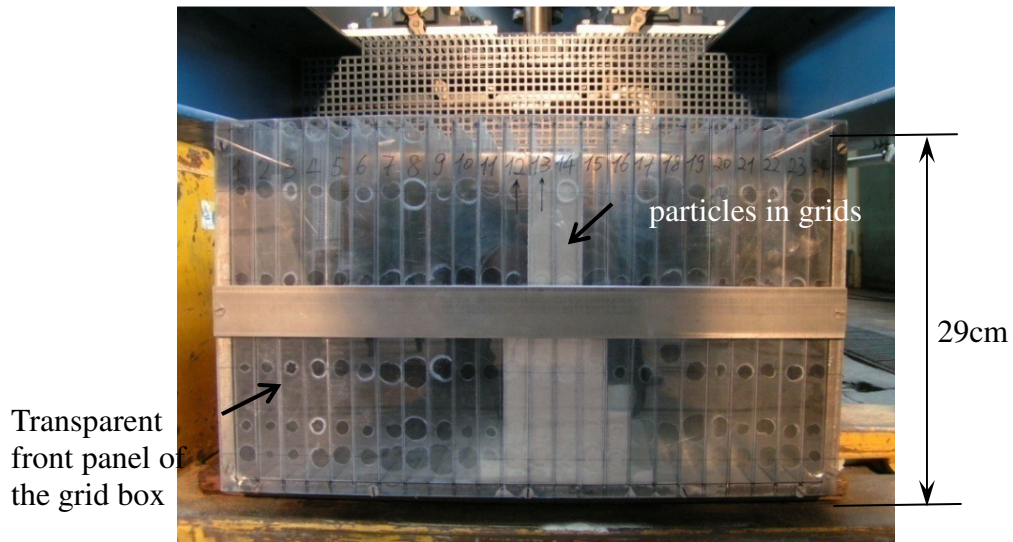


Fig.24 The grid box used to collect the out-flowing particle from the kiln discharge end in order to calculate the radial and axial velocity (Ch4.2.2. Ch5.2.2)

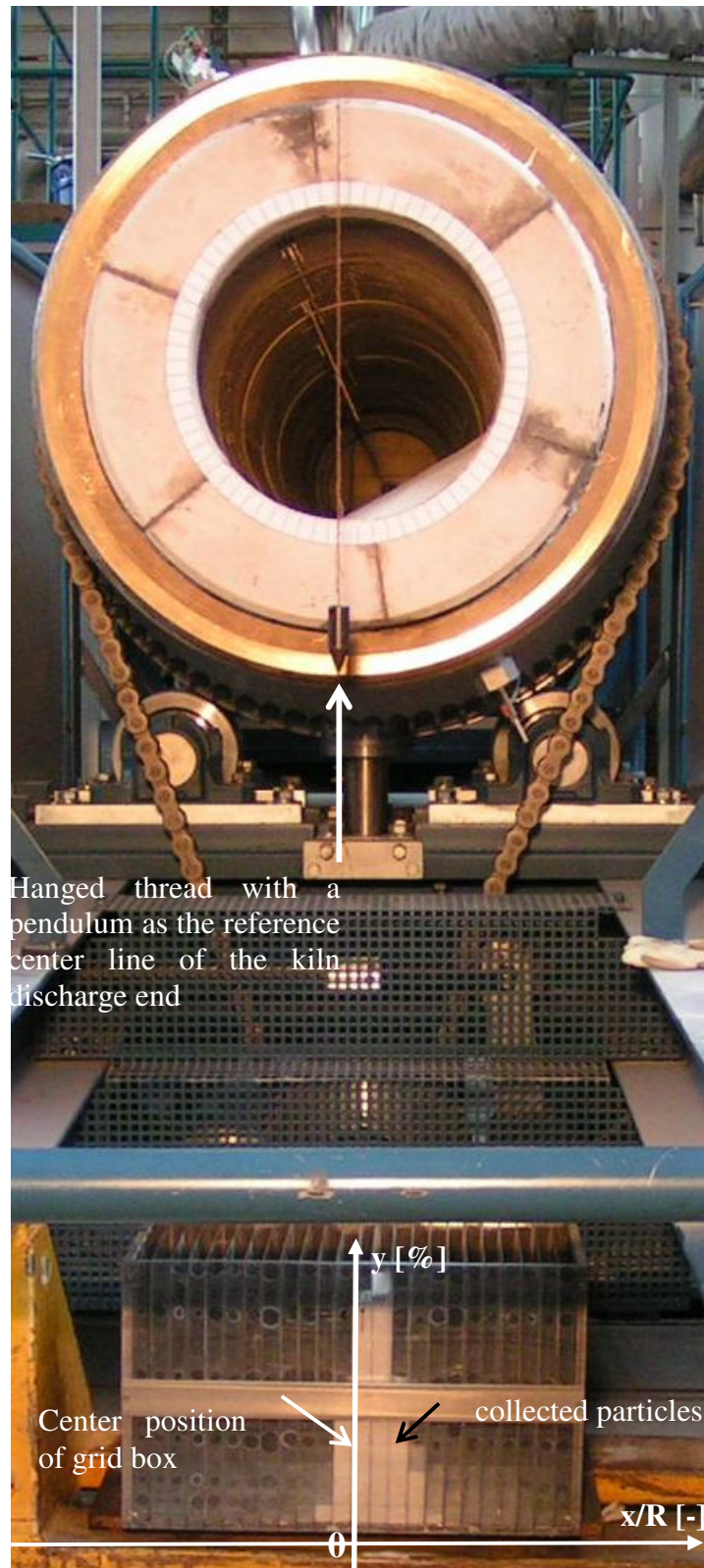


Fig.25 Experimental setup to measure the radial downstream velocity of the out-flowing particles (Ch4.2.2)

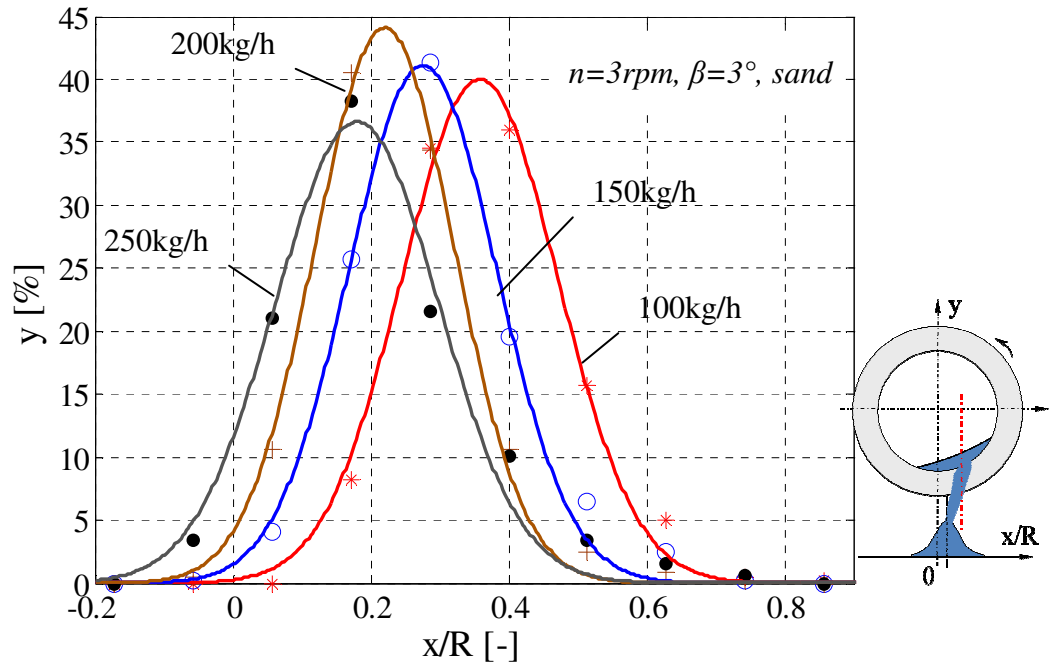


Fig.26 Measured particles amount of radial out-flowing and the fitting curve with normal function for sand, 3rpm, 3° inclination (Ch4.5.1)

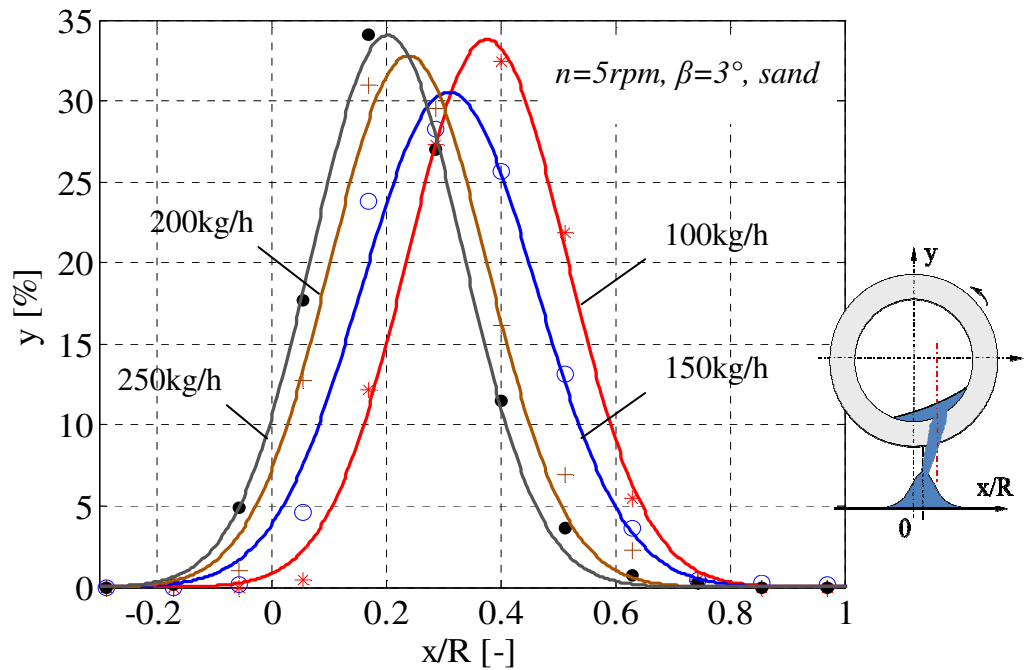


Fig.27 Measured particles amount of radial out-flowing and the fitting curve with normal function for sand, 5rpm, 3° inclination (Ch4.5.1)

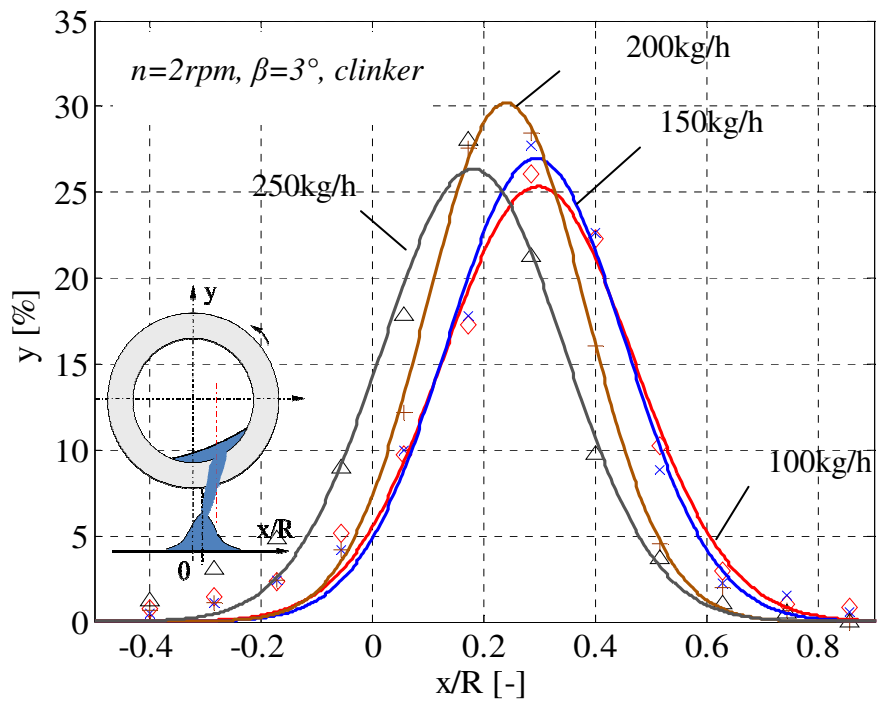


Fig.28 Measured particles amount of radial out-flowing and the fitting curve with normal function for clinker, 2rpm, 3° inclination (Ch4.5.1)

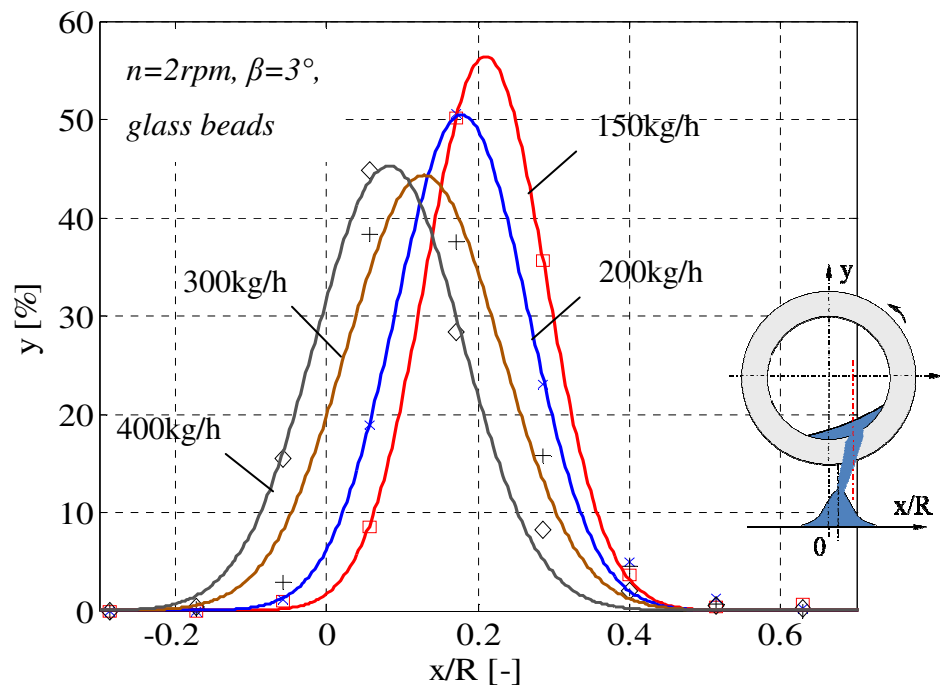


Fig.29 Measured particles amount of radial out-flowing and the fitting curve with normal function for glass beads, 2rpm, 3° inclination (Ch4.5.1)

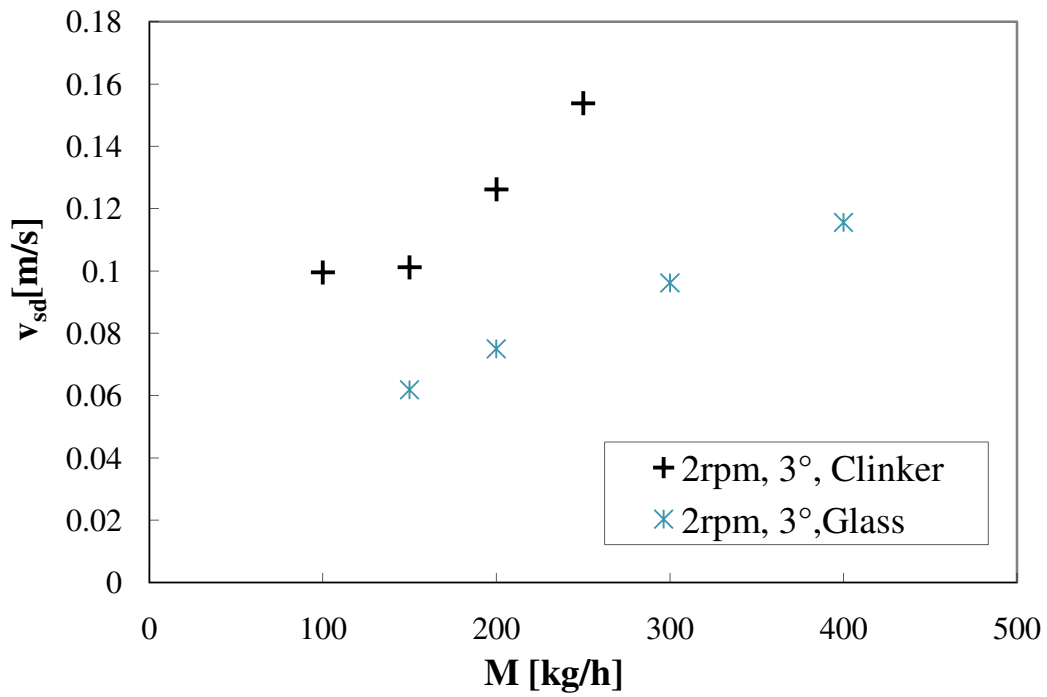


Fig.30 Influence of the mass flow on the downstream velocity at discharge end for clinker and glass beads (Ch4.5.1)

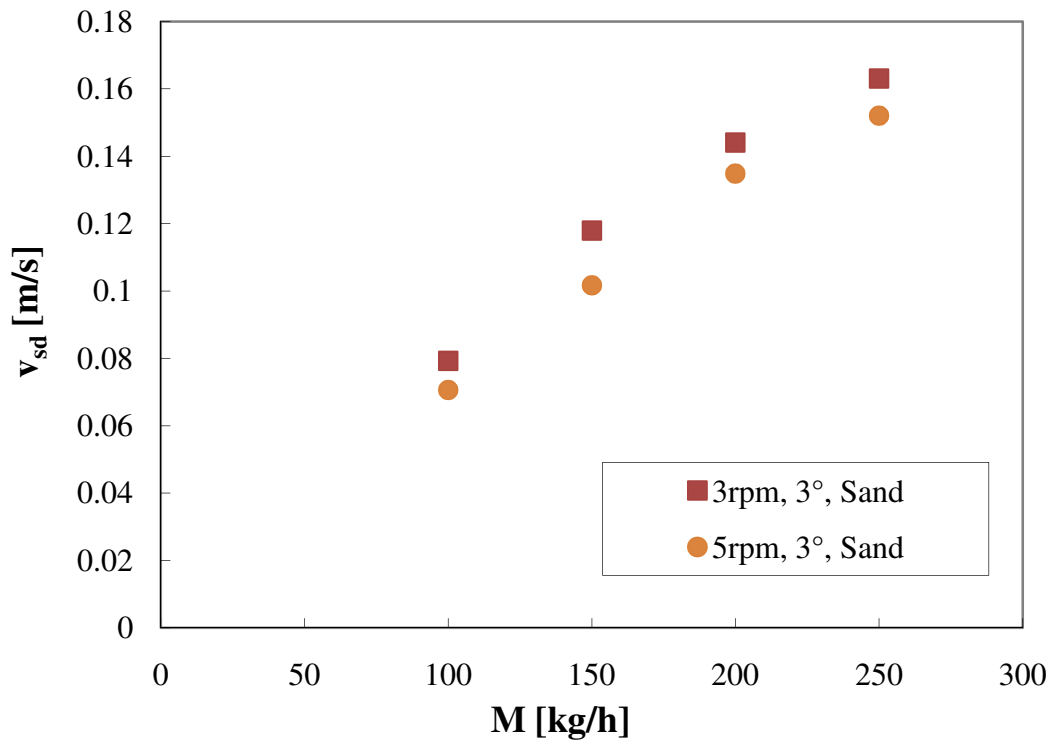


Fig.31 Influence of the mass flow on the downstream velocity at discharge end for sand (Ch4.5.1)

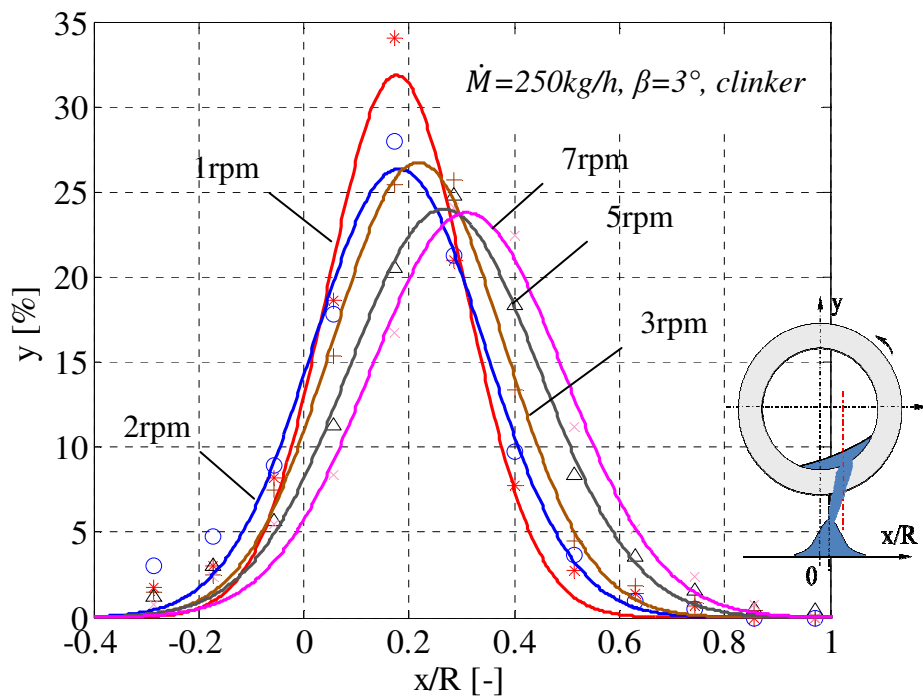


Fig.32 Measured particles amount of radial out-flowing and the fitting curve with normal function for clinker, 250kg/h, 3° inclination (Ch4.5.2)

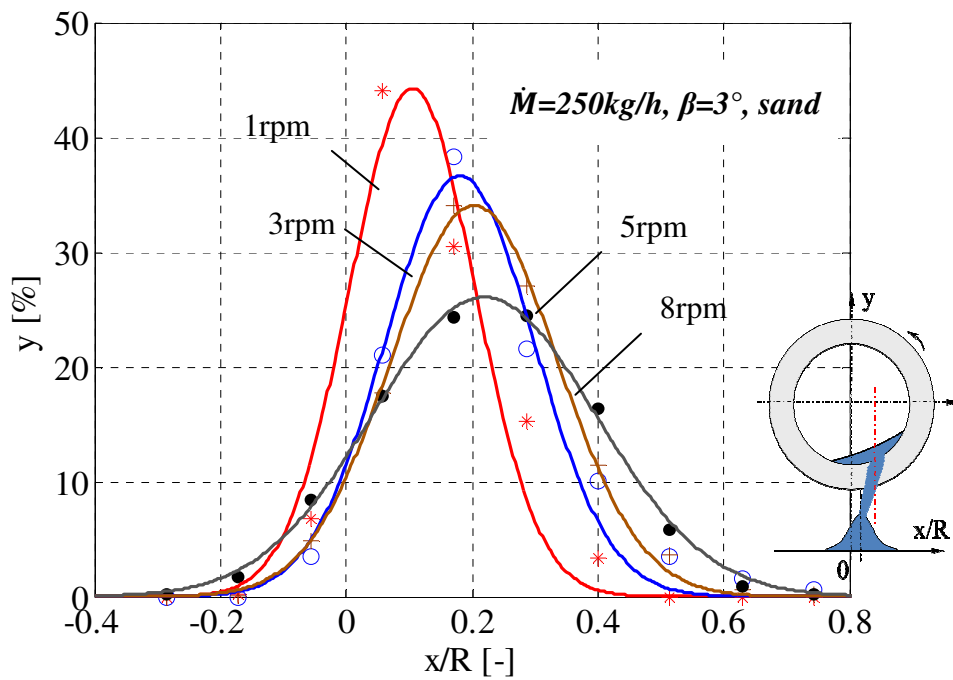


Fig.33 Measured particles amount of radial out-flowing and the fitting curve with normal function for sand, 250kg/h, 3° inclination (Ch4.5.2)

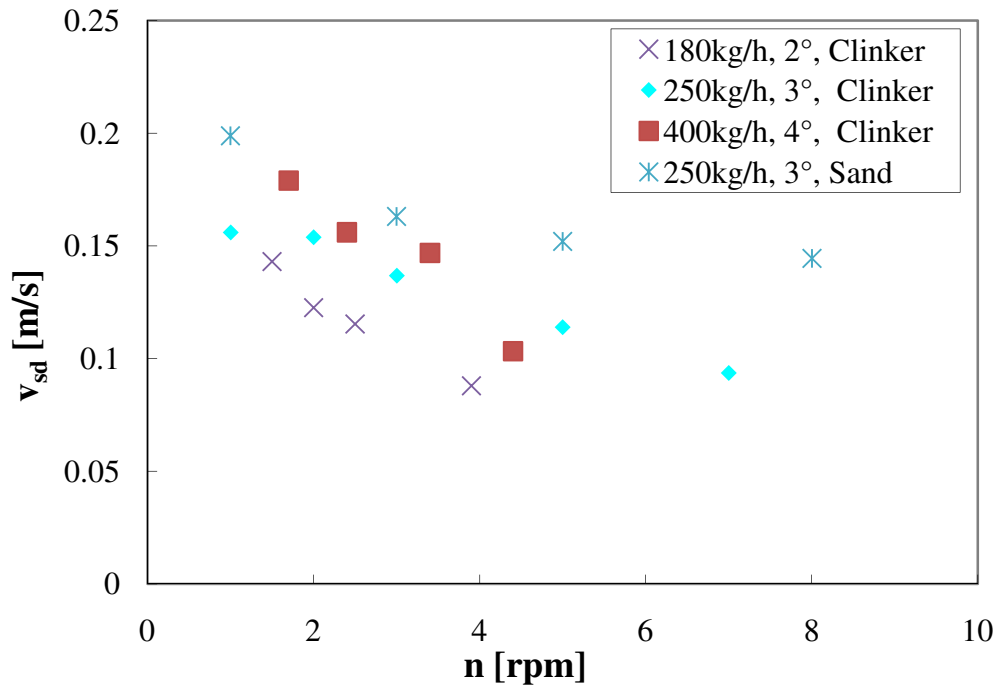


Fig.34 Influence of the rotational speed on the radial downstream velocity at discharge end (Ch4.5.2)

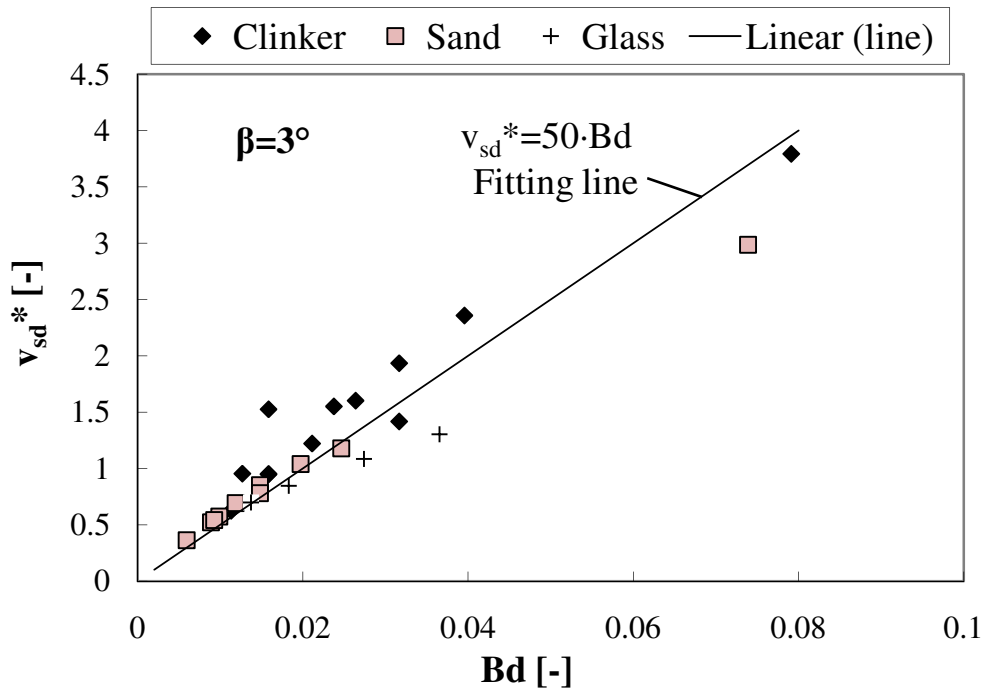


Fig.35 Correlation of the scaled downstream velocity with the bed depth number for clinker, sand and glass beads at 3° inclination (Ch4.6.1)

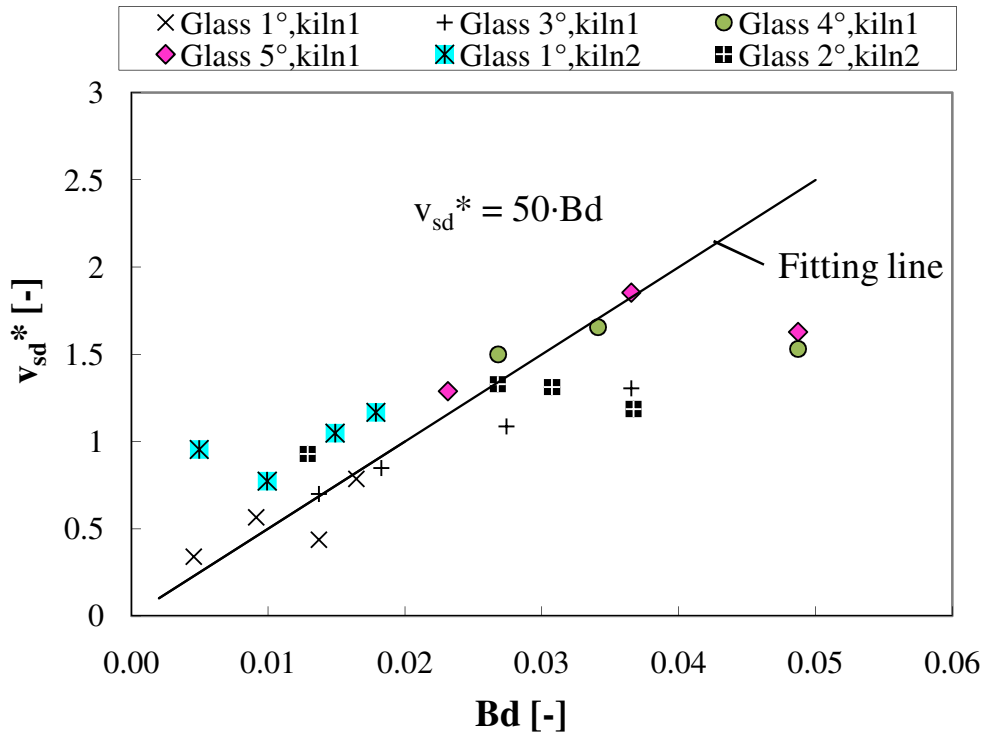


Fig.36 Correlation of the scaled downstream velocity with the bed depth number for glass beads (Ch4.6.1)

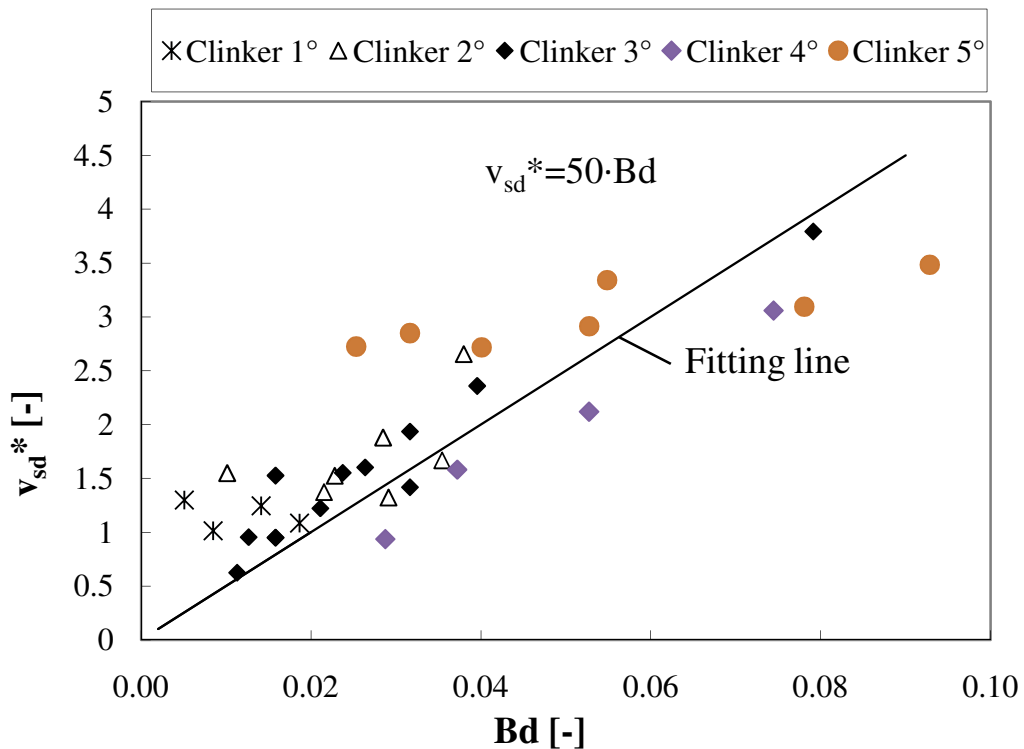


Fig.37 Correlation of the scaled downstream velocity with the bed depth number for clinker (Ch4.6.1)

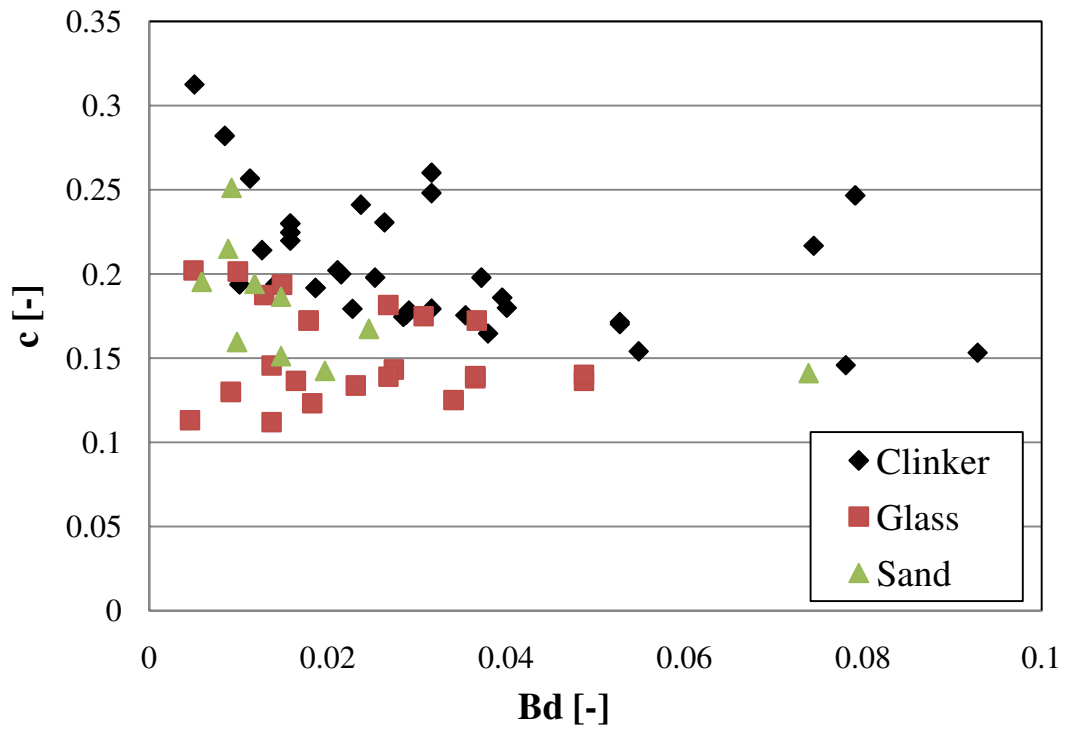


Fig.38 Comparison of the distributed range of out-flowing particles for three materials (Ch4.6.2)

Note: The values c in Eq.(37) is derived from the fitting result of the particle distribution.

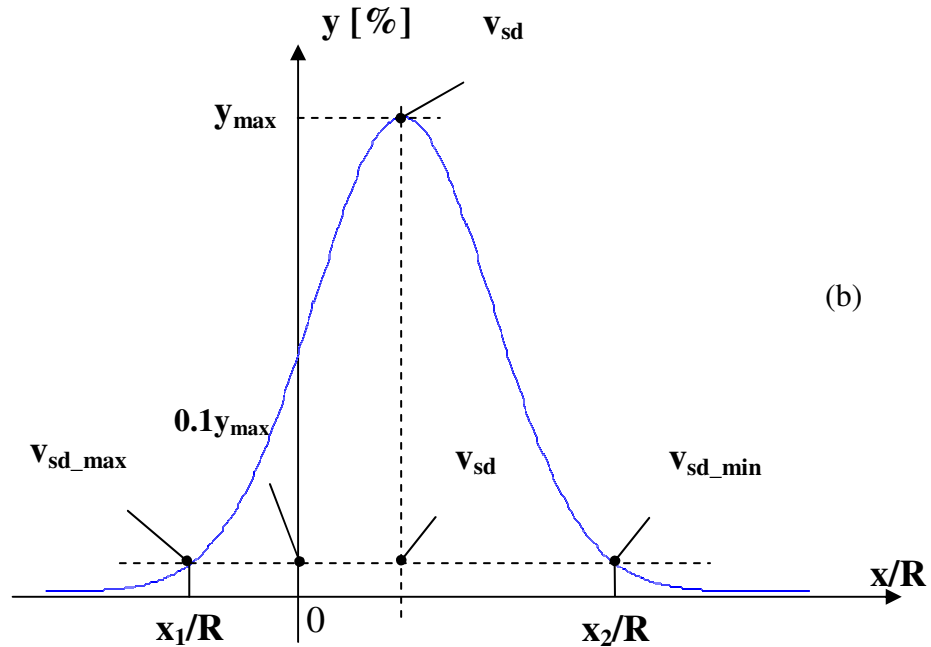
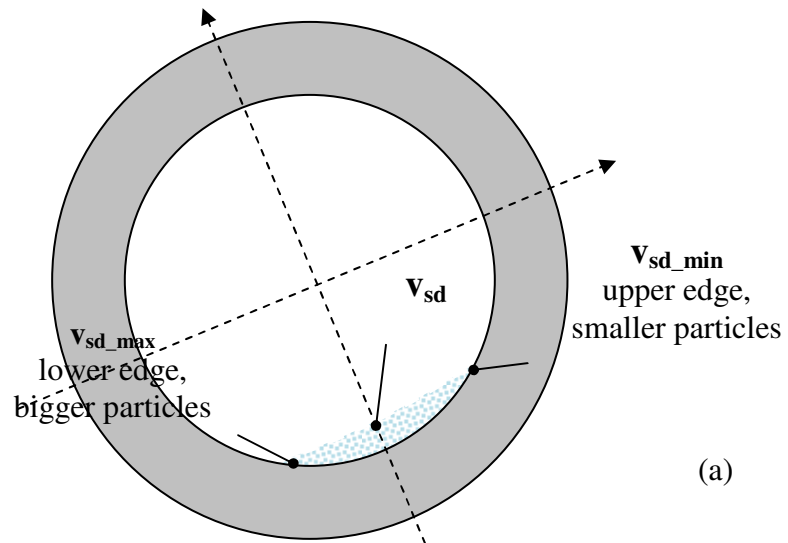


Fig.39 The calculation of the downstream velocity fluctuation at kiln discharge end
(Ch4.6.2)

Note: (a). the particles at the lower edge of the bed are found to have the maximal velocity v_{sd_max} ; the particles at the upper edge of the bed are found to have the minimal velocity v_{sd_min} . (b). Both extreme values of the velocity are calculated at the positions x_1/R and x_2/R , where the particle amount is 10% of the maximal amount y_{max} .

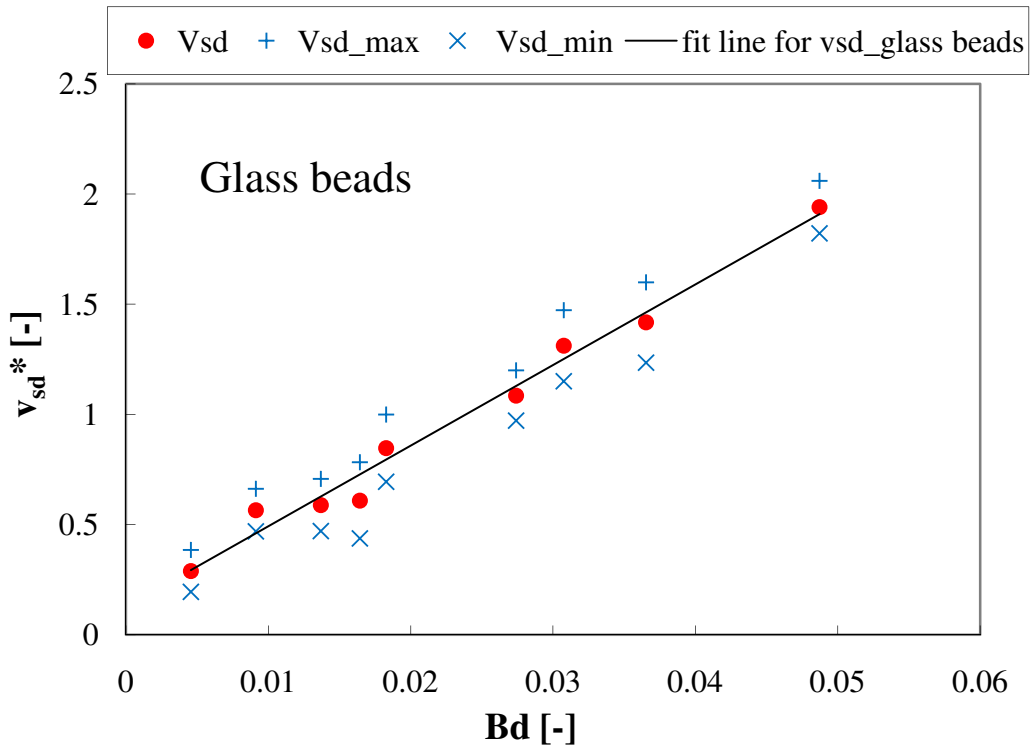


Fig.40 Comparison of the maximal, minimal and mean downstream velocity at the discharge end for glass beads (Ch4.6.2)

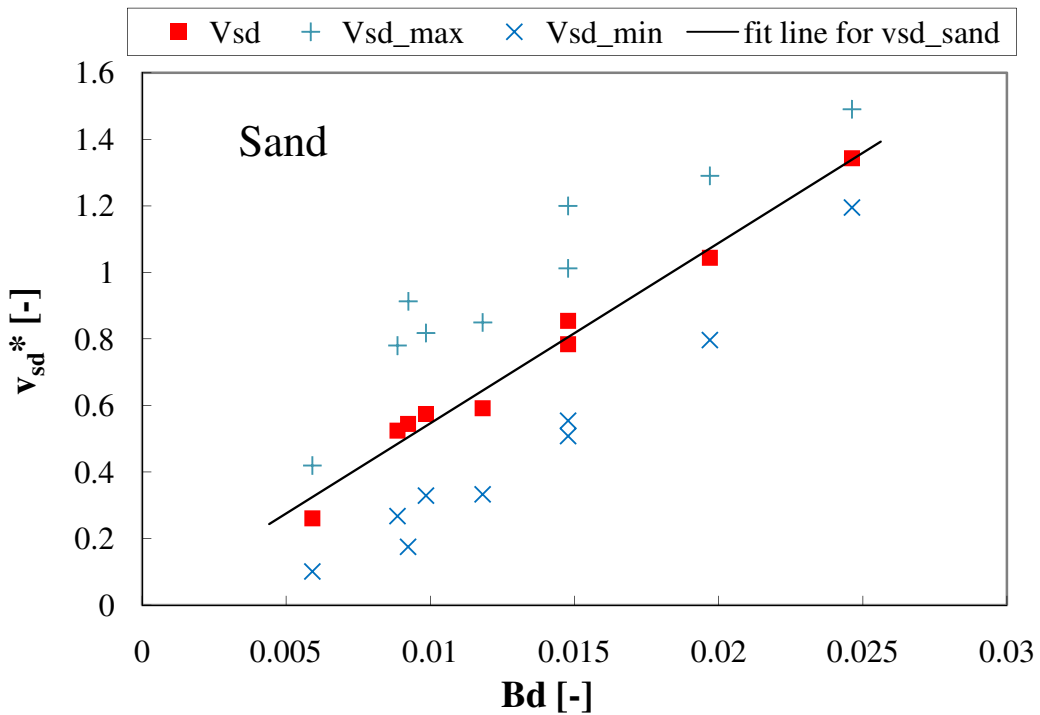


Fig.41 Comparison of the maximal, minimal and mean downstream velocity at the discharge end for sand (Ch4.6.2)

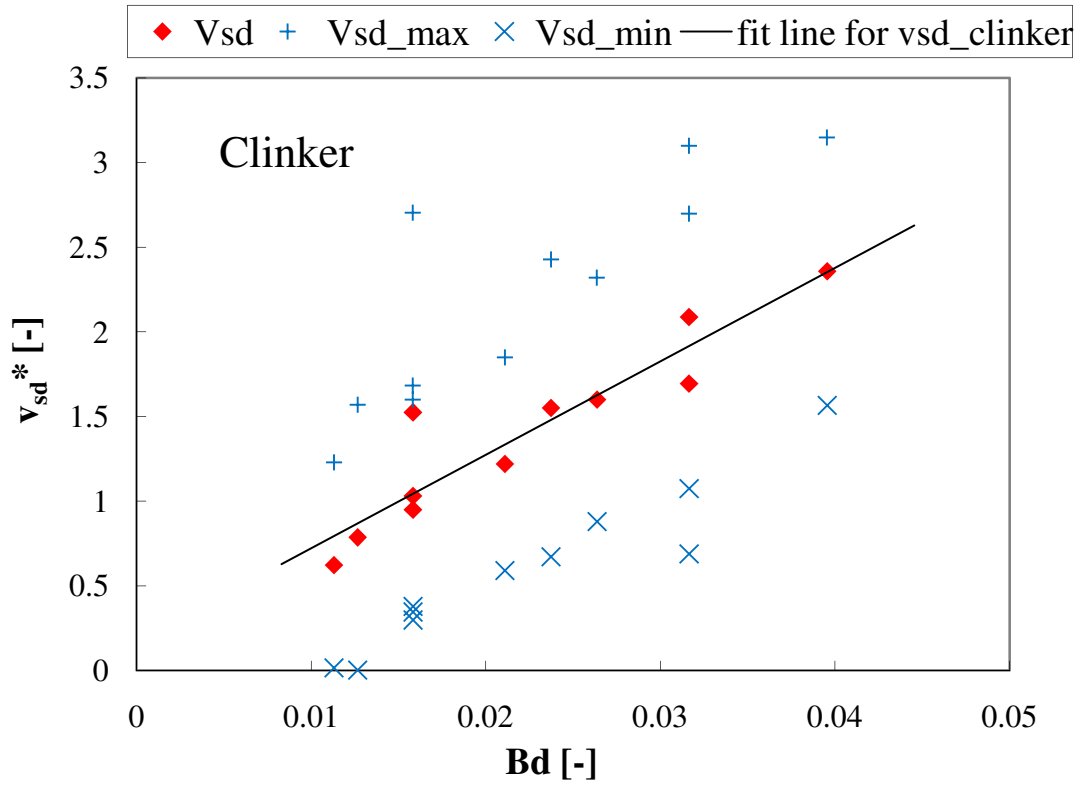


Fig.42 Comparison of the maximal, minimal and mean downstream velocity at the discharge end for clinker (Ch4.6.2)

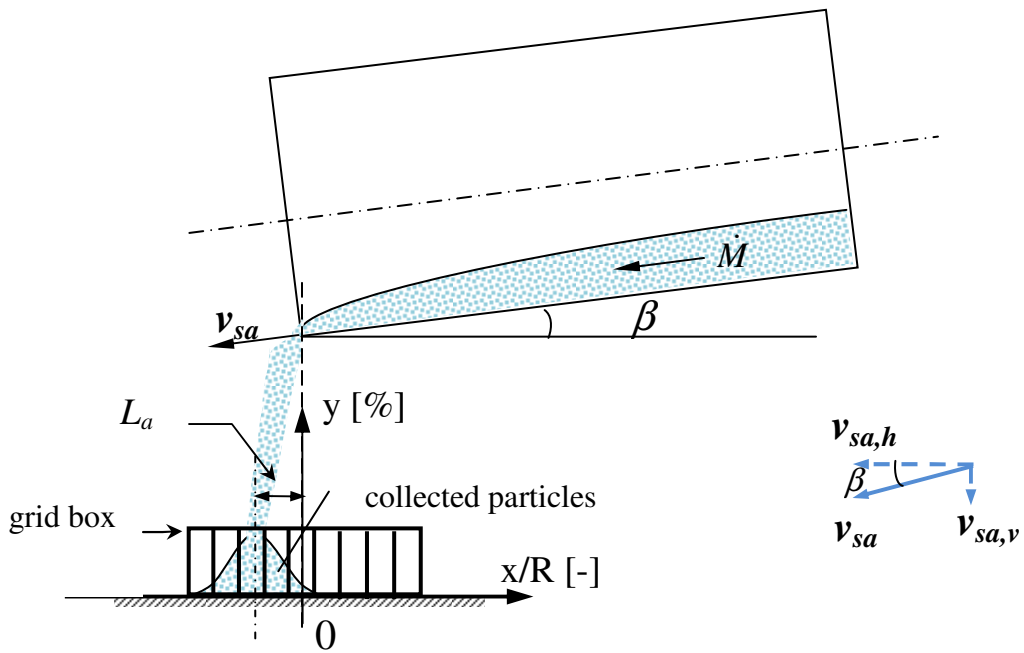


Fig.43 Particles flowing out of the kiln end with the axial velocity; The axial velocity is measured with grid box (Ch5)

Note: The particle distribution obtained in the axial direction is measured with the grid box. The axial displacement L_a is derived to calculate the experimental value of the axial velocity.

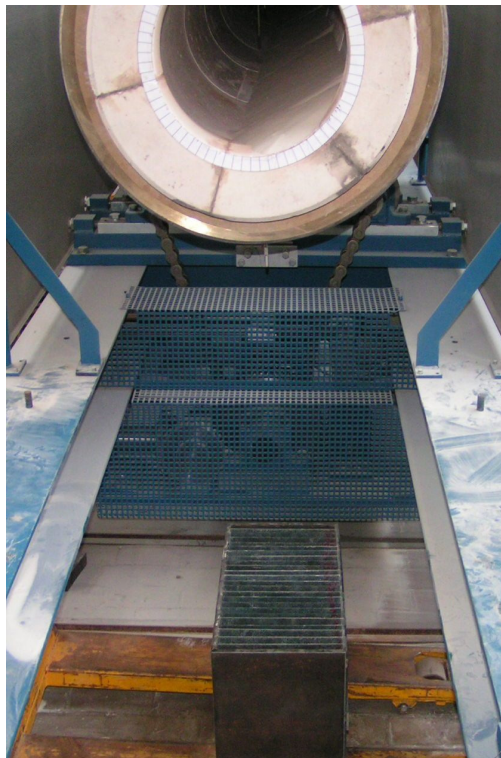


Fig.44 Experimental setup to measure the axial velocity of the out-flowing particles (Ch5.2.2)

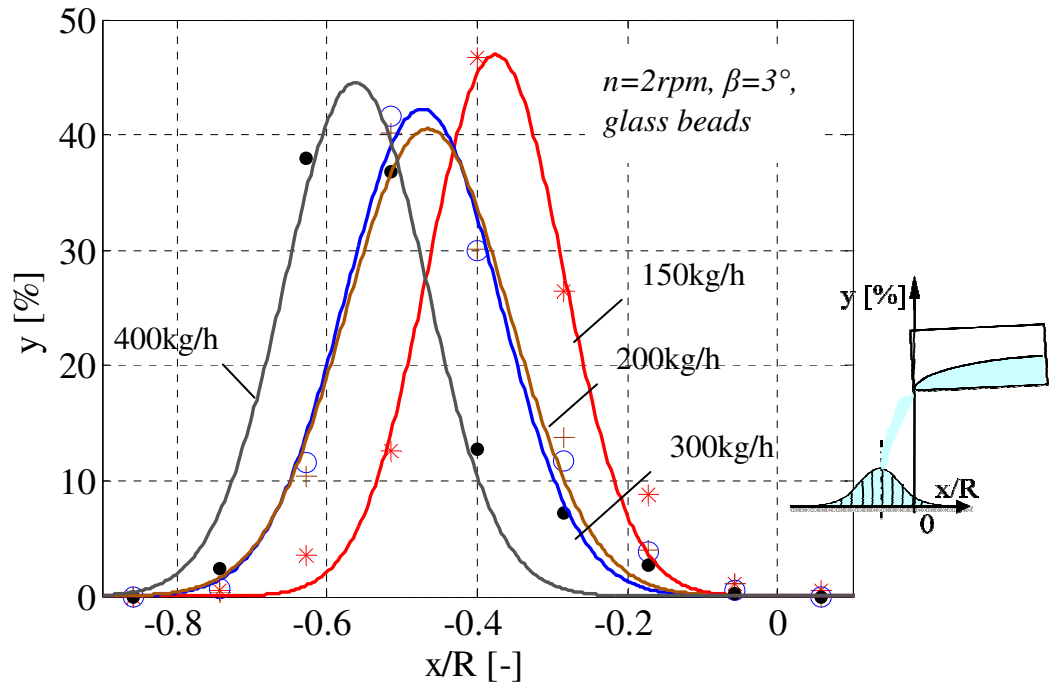


Fig.45 Measured particle amount and the fitting curve with normal distribution for glass beads, 2rpm, 3° inclination (Ch5.5.1)

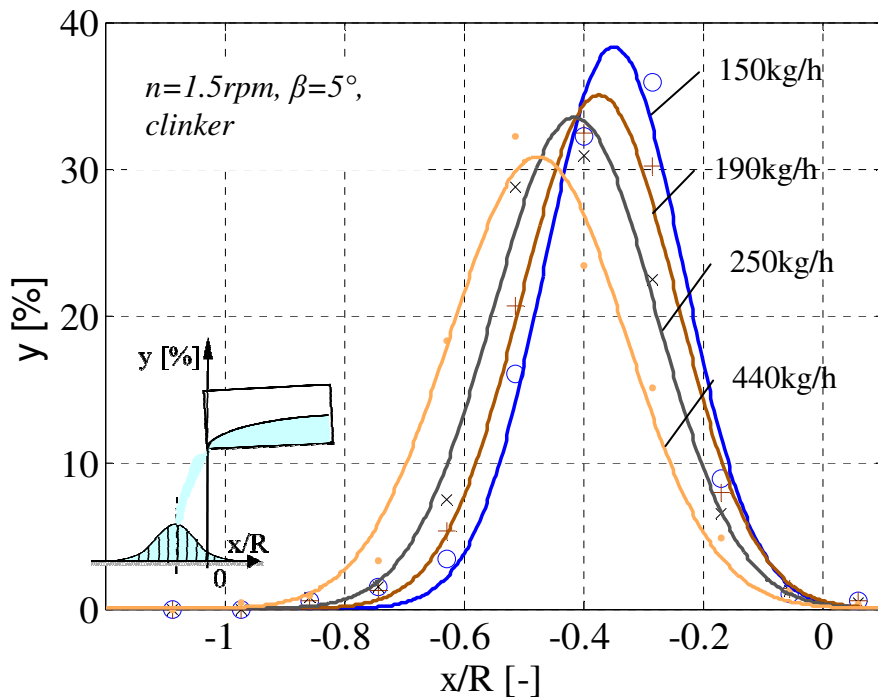


Fig.46 Measured particle amount and the fitting curve with normal distribution for clinker, 1.5rpm, 5° inclination (Ch5.5.1)

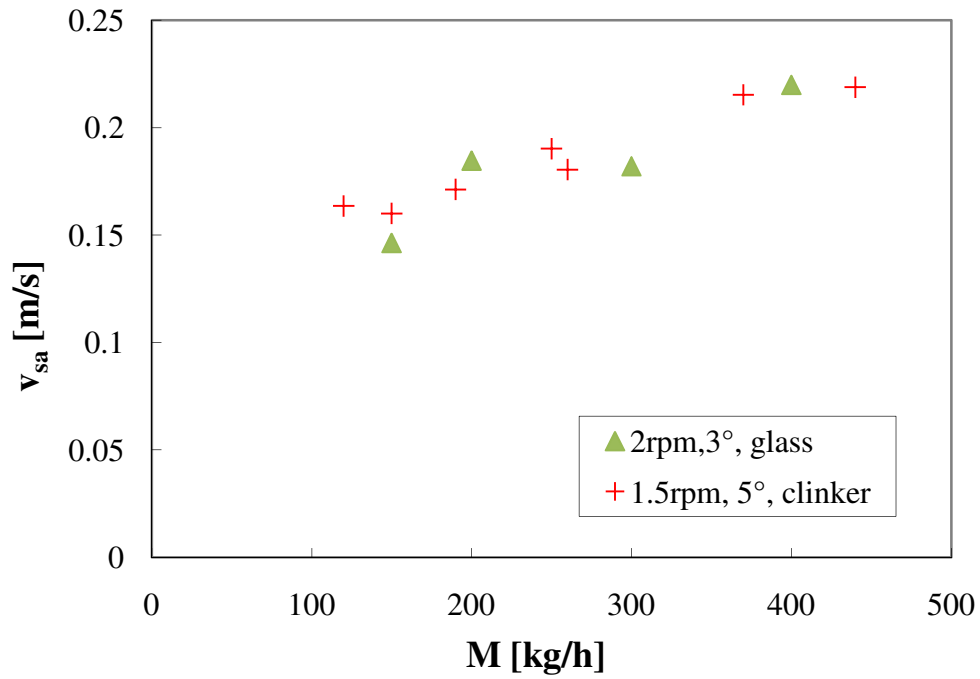


Fig.47 Influence of the mass flow on the axial velocity at discharge end (Ch5.5.1)

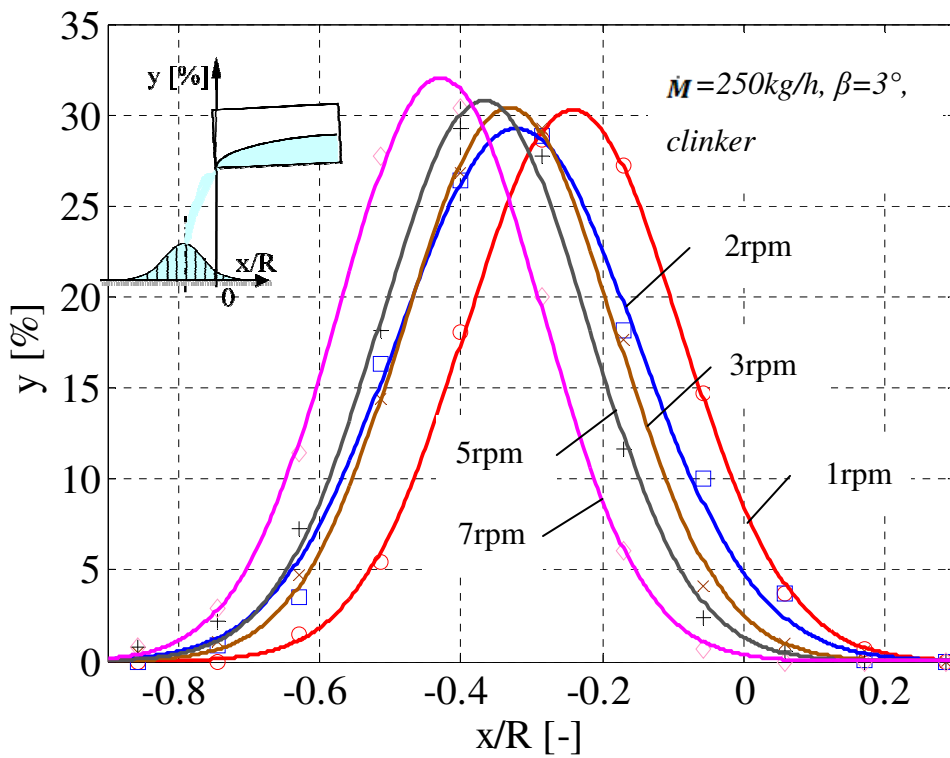


Fig.48 Measured particle amount and the fitting curve with normal distribution for clinker, 250kg/h, 3° inclination (Ch5.5.1)

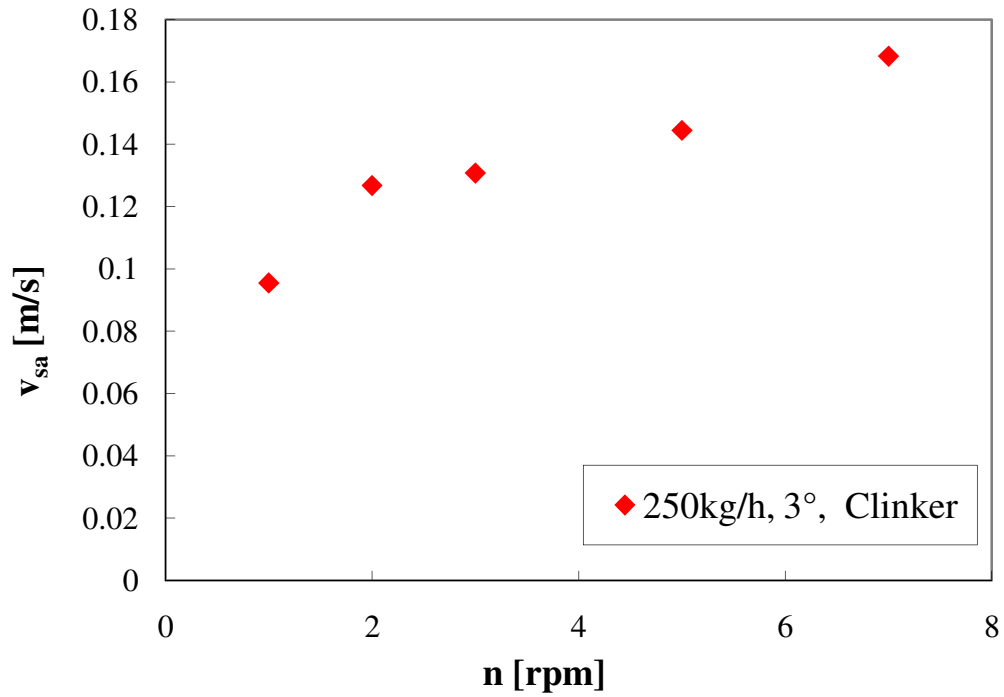


Fig.49 Influence of the rotational speed on the axial velocity at discharge end (Ch5.5.2)

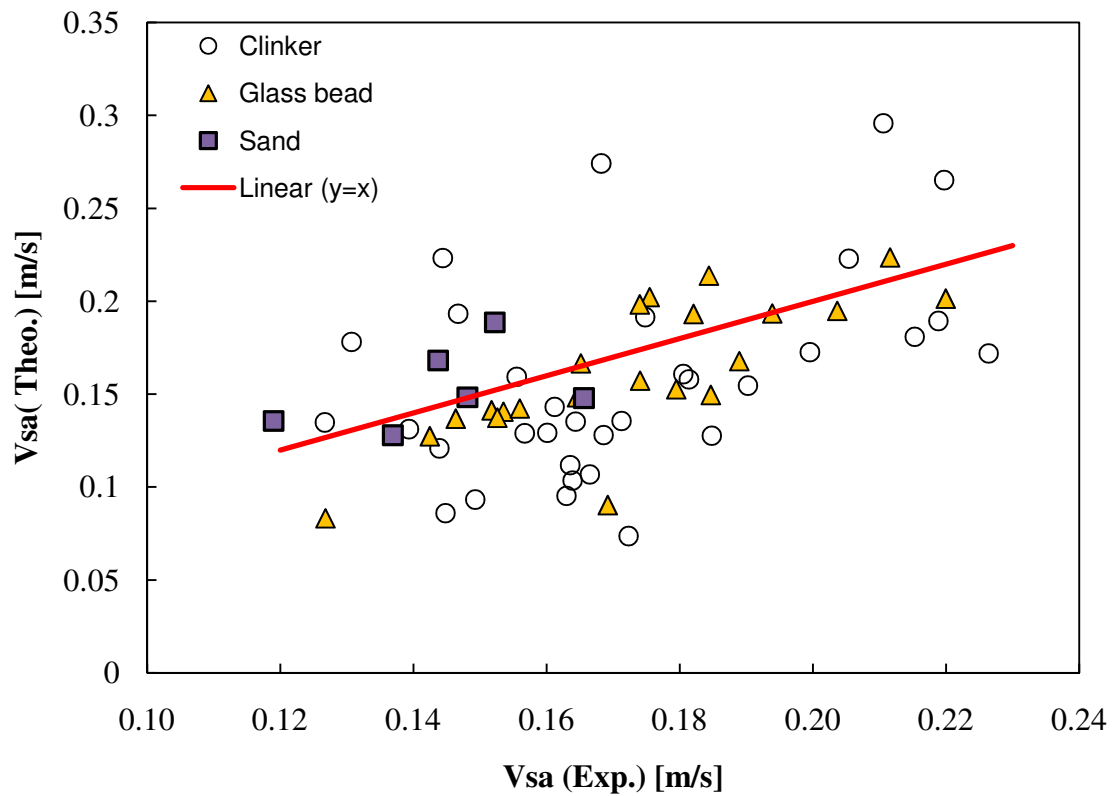


Fig.50 Comparison of the axial velocity at discharge end between experimental values and theoretical values (Ch5.6.1)

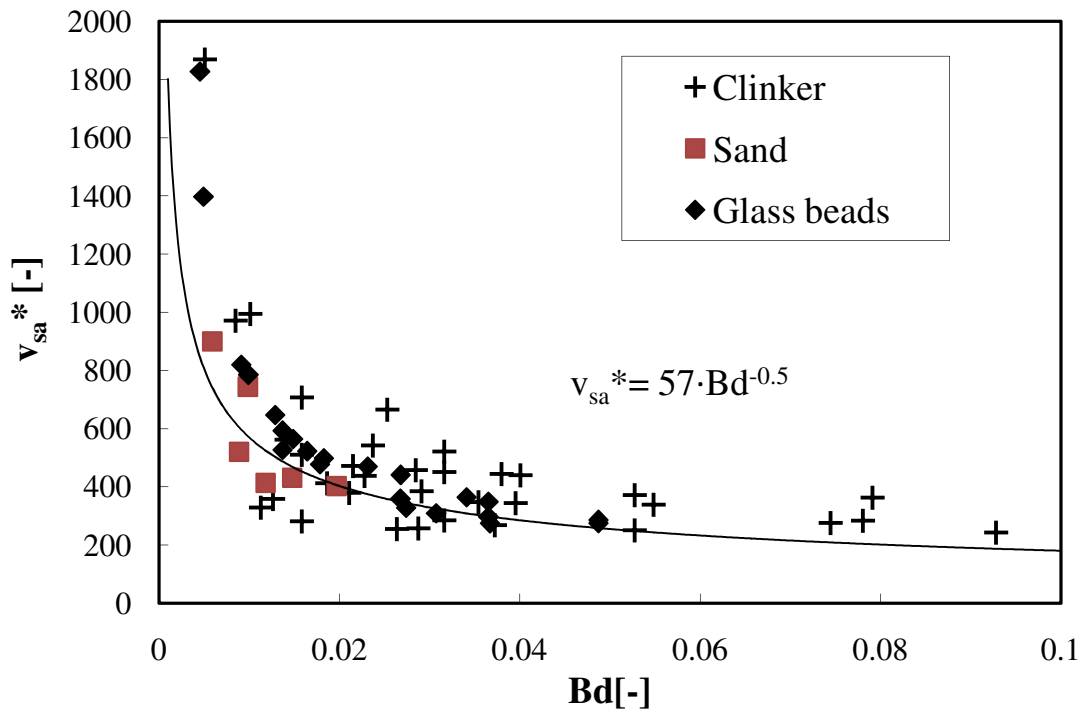


Fig.51 Correlation of the scaled axial velocity with the bed depth number (Ch5.6.2)

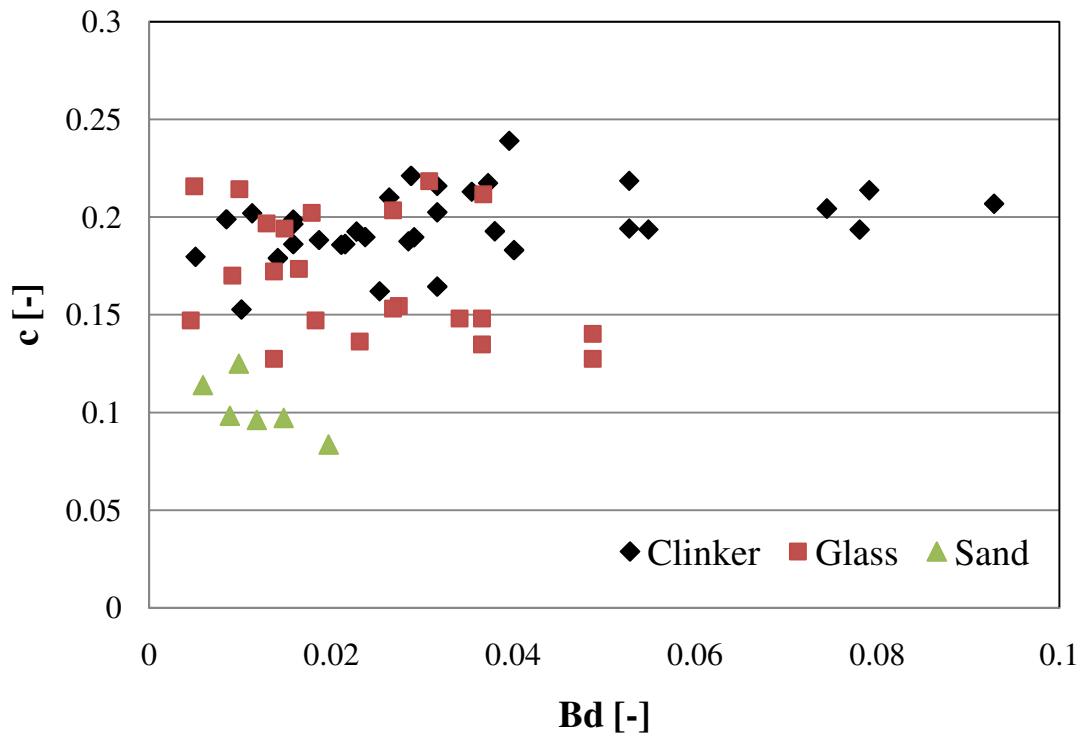


Fig.52 Comparison of the distributed range of out-flowing particles for three materials (Ch5.6.2)

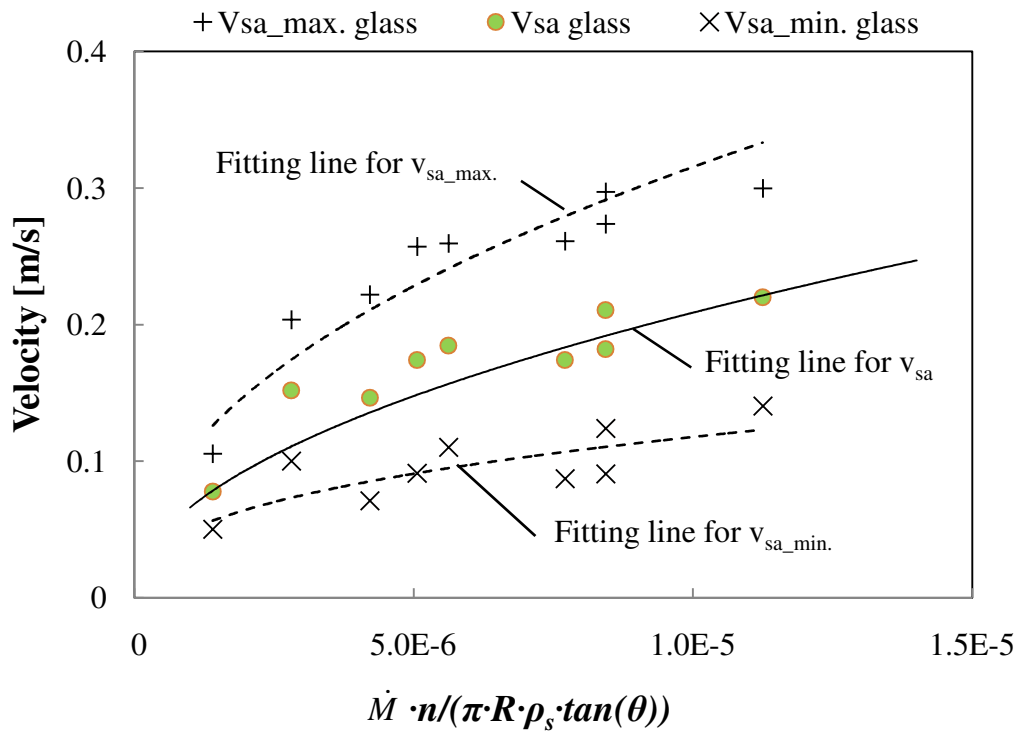


Fig.53 The velocity fluctuation for glass beads (Ch5.6.3)

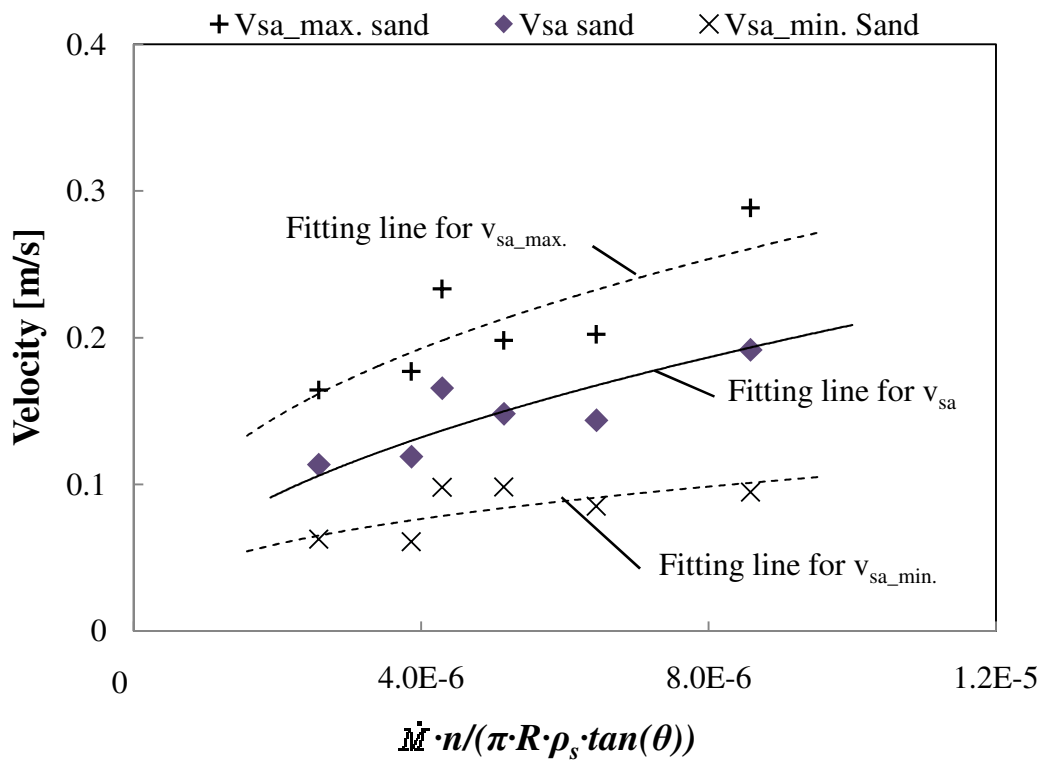


Fig.54 The velocity fluctuation for glass beads. (Ch5.6.3)

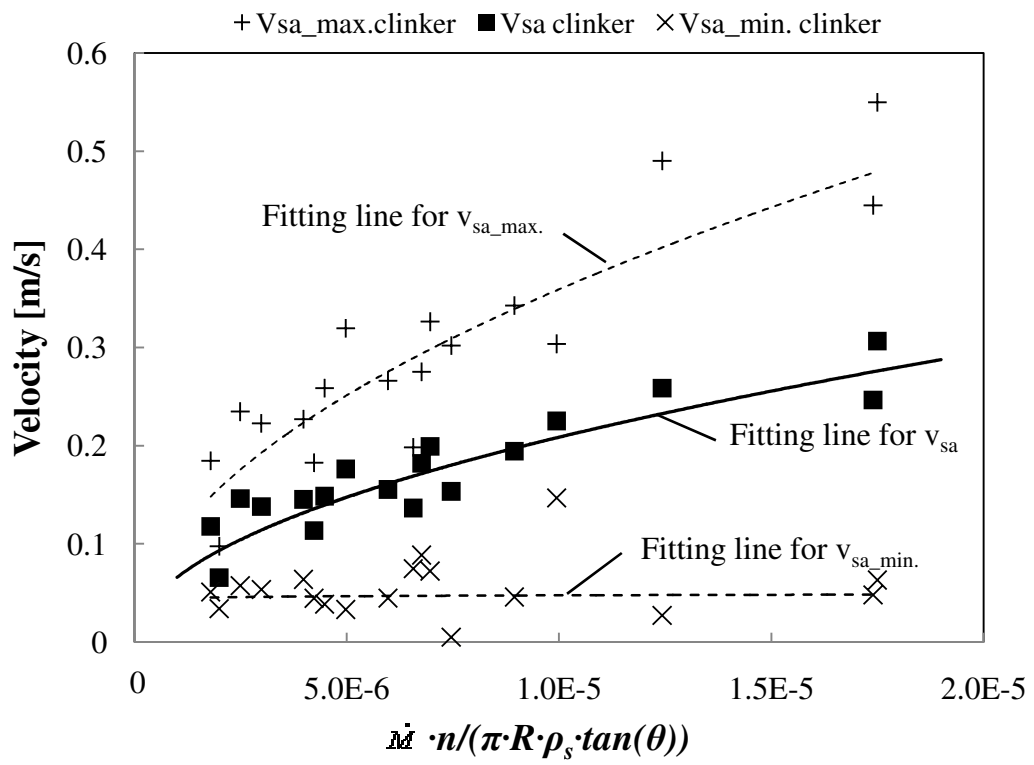
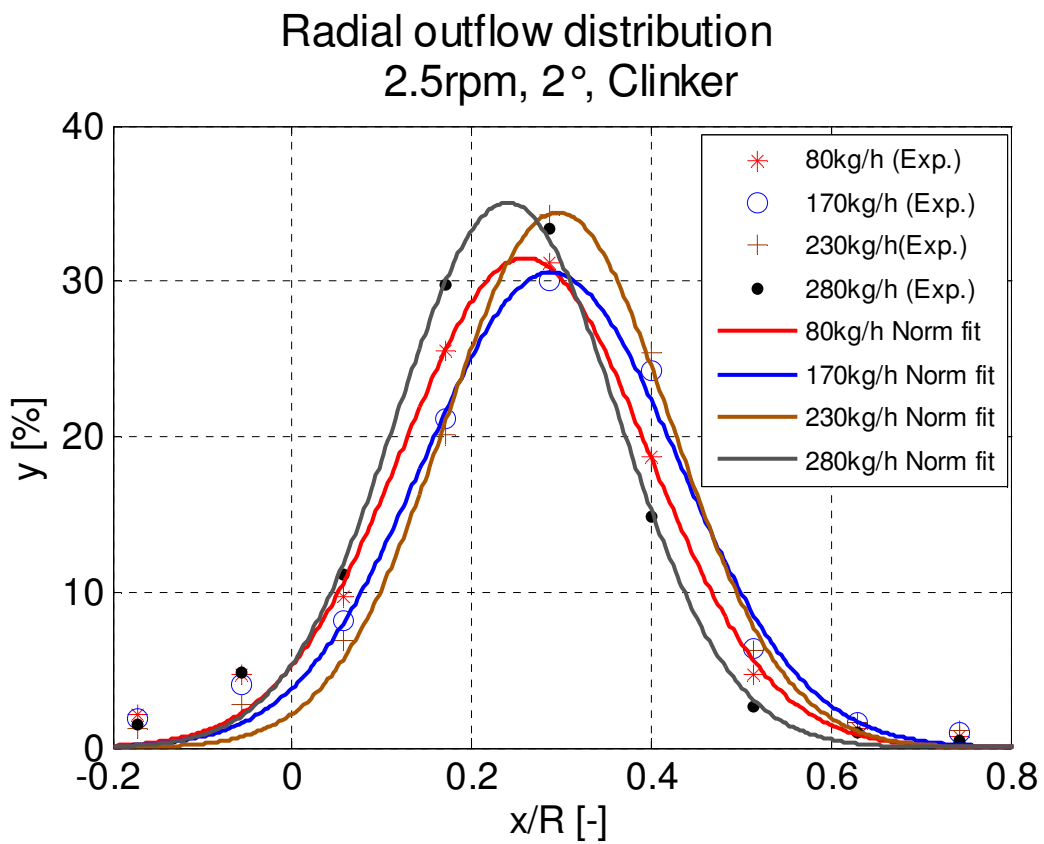
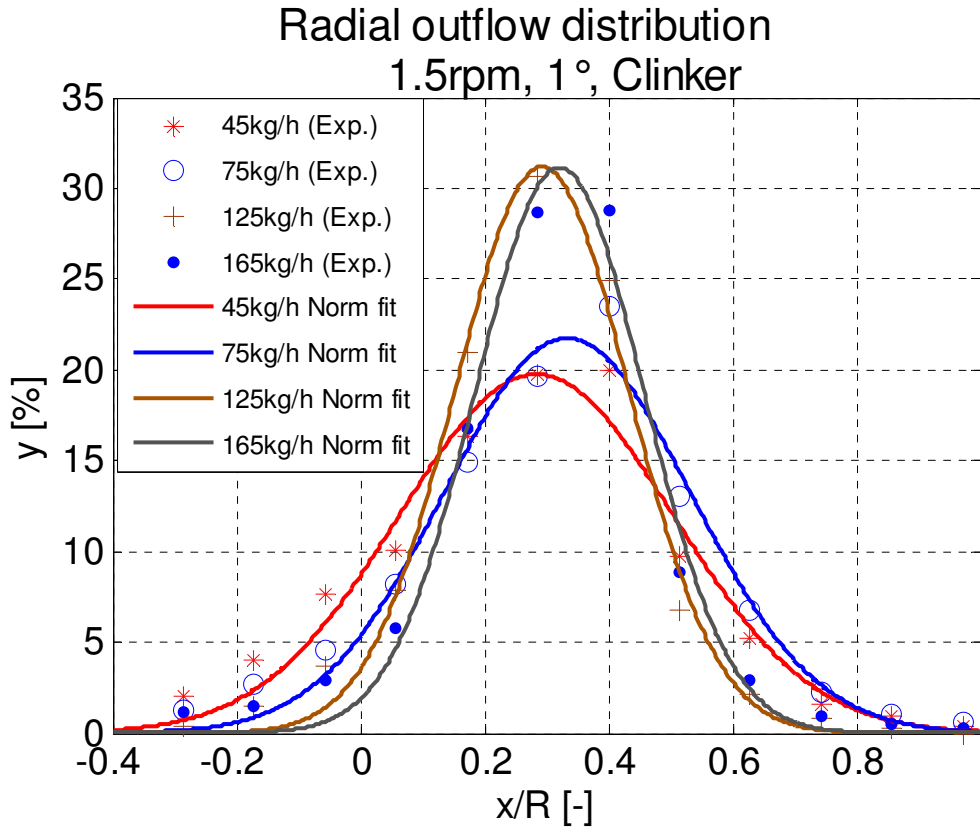
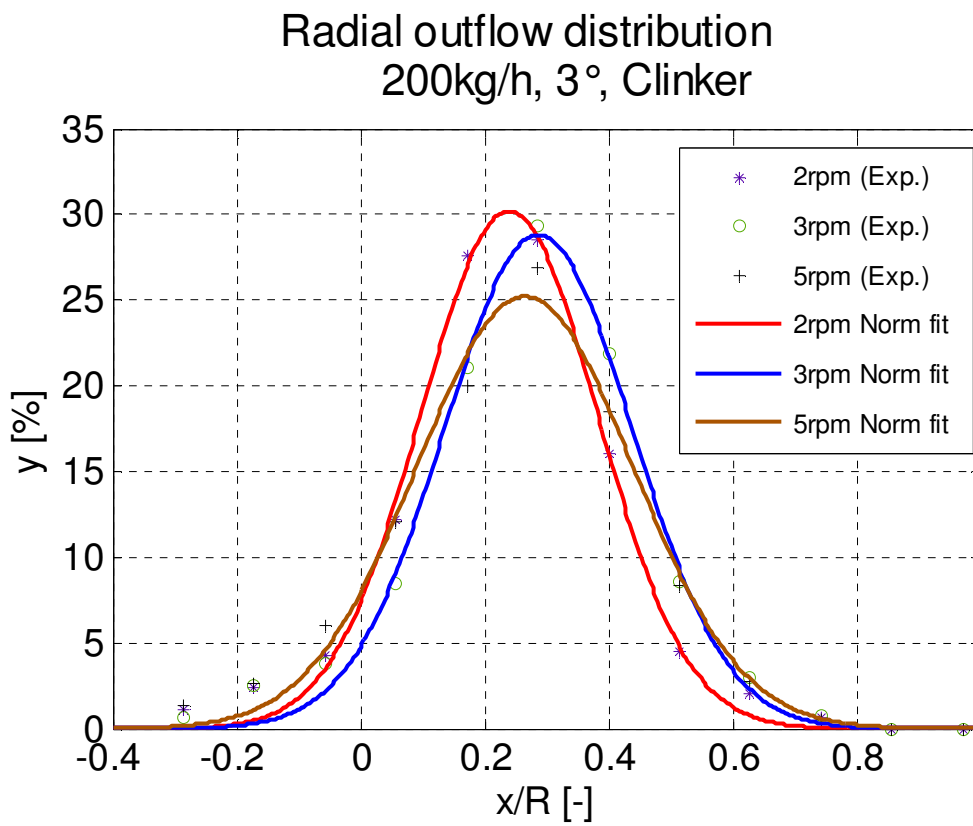
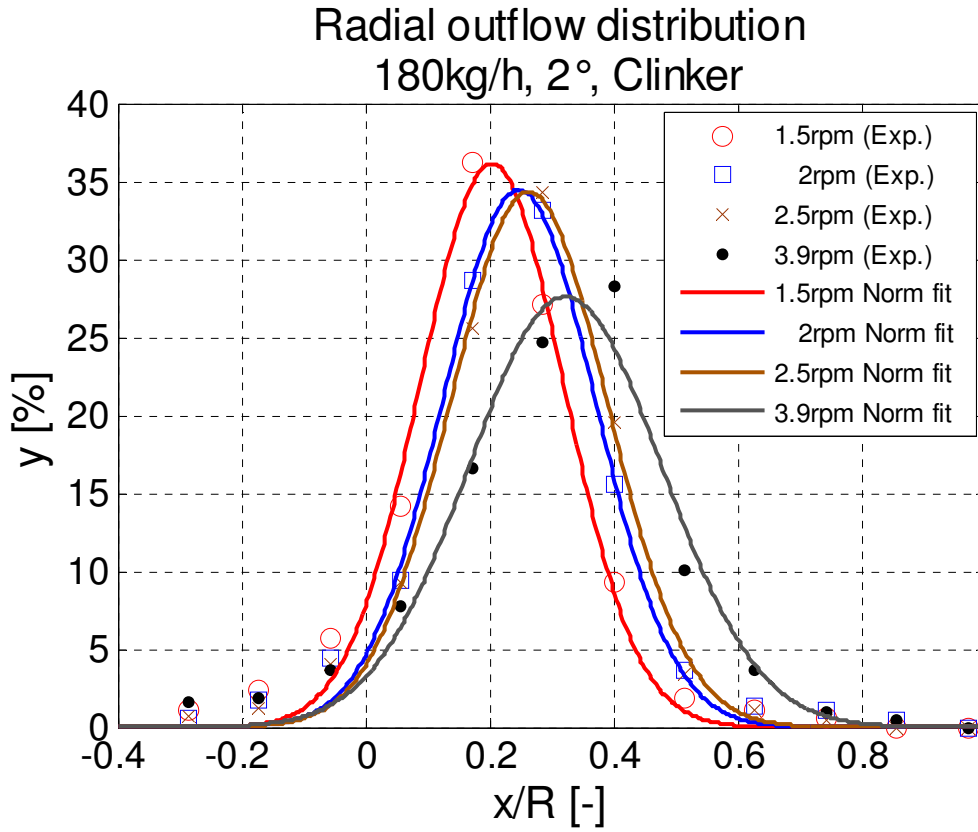


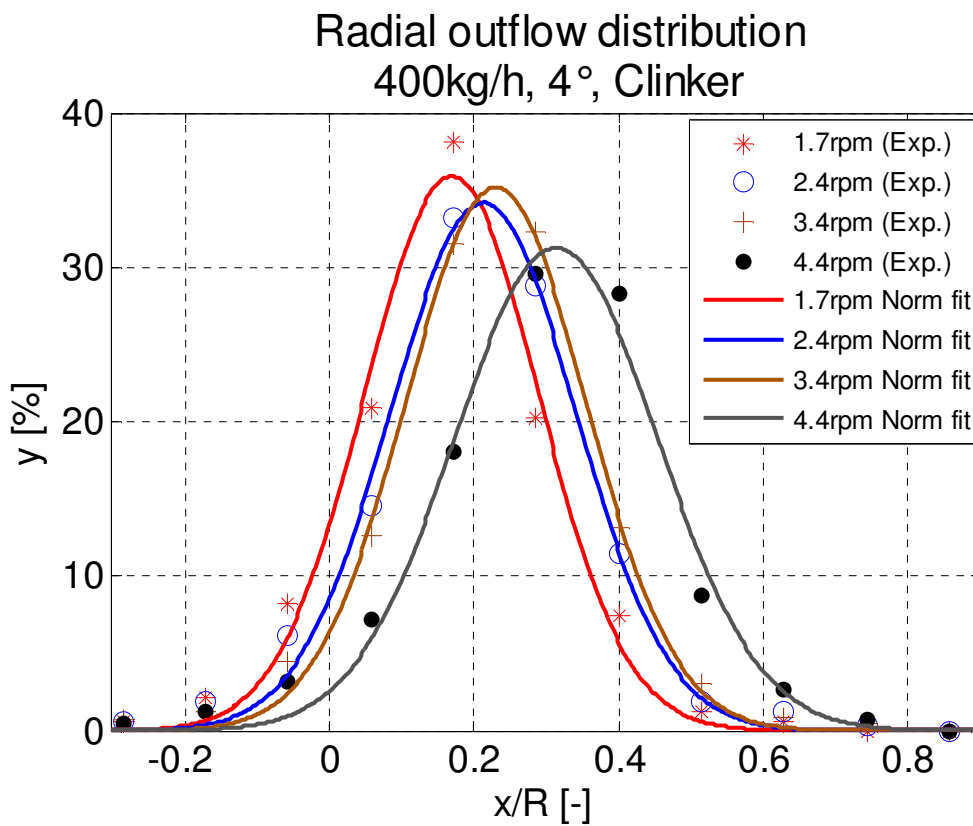
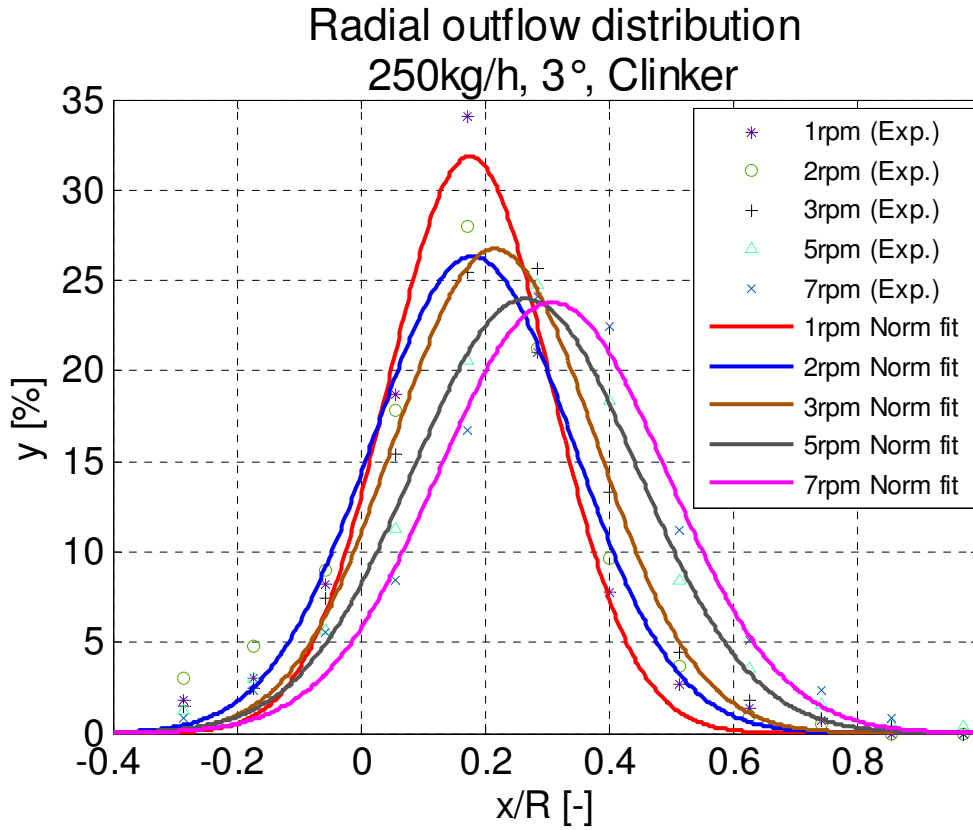
Fig.55 The velocity fluctuation for clinker. (Ch5.6.3)

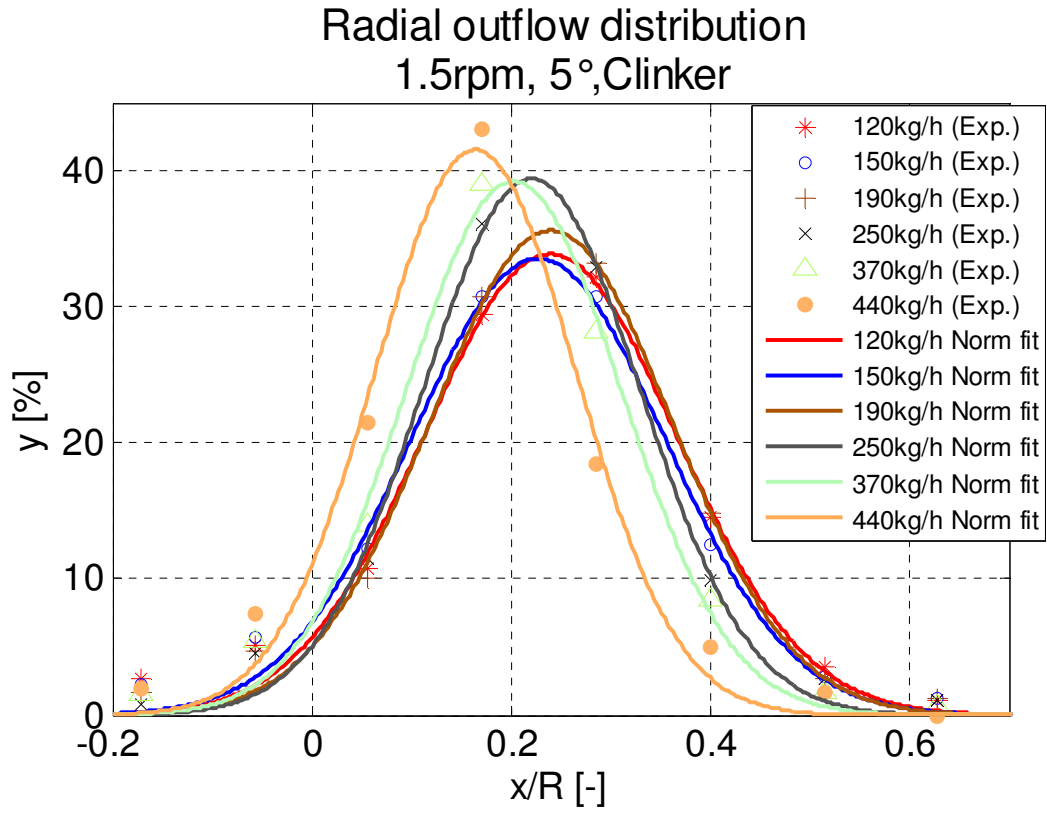
Appendix

A 1.1 Fitting results in the radial direction (clinker)	100
A 1.2 Fitting results in the radial direction (sand)	104
A 1.3 Fitting results in the radial direction (glass beads)	106
A 2.1 Fitting results in the axial direction (clinker)	109
A 2.2 Fitting results in the axial direction (sand)	113
A 2.3 Fitting results in the axial direction (glass beads)	114
A 3.1 Experimental parameters and data (clinker)	117
A 3.2 Experimental parameters and data (sand)	123
A 3.3 Experimental parameters and data (glass beads)	125

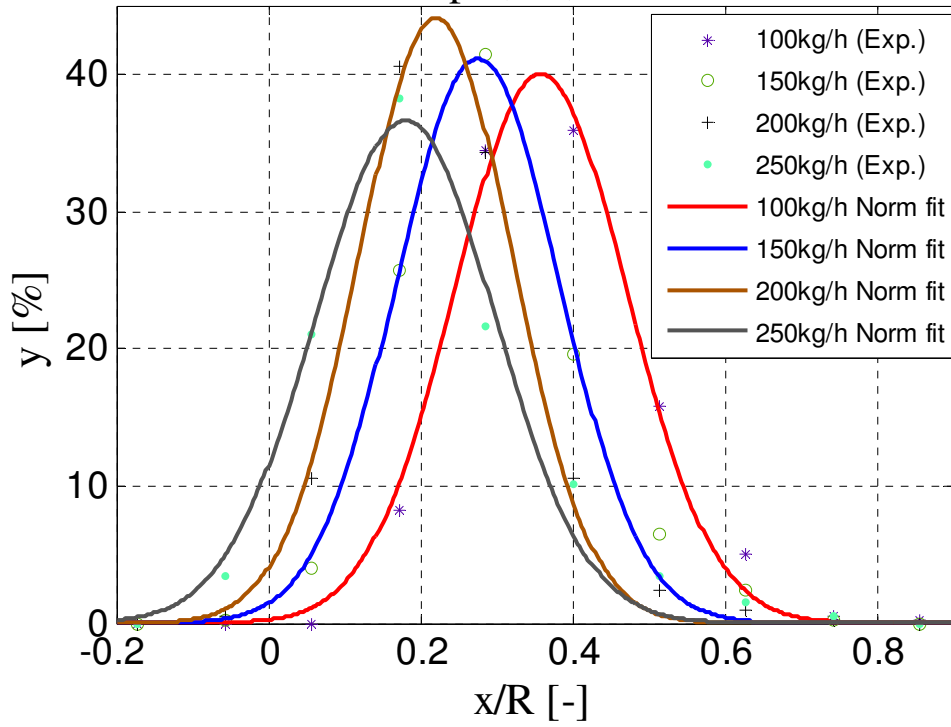




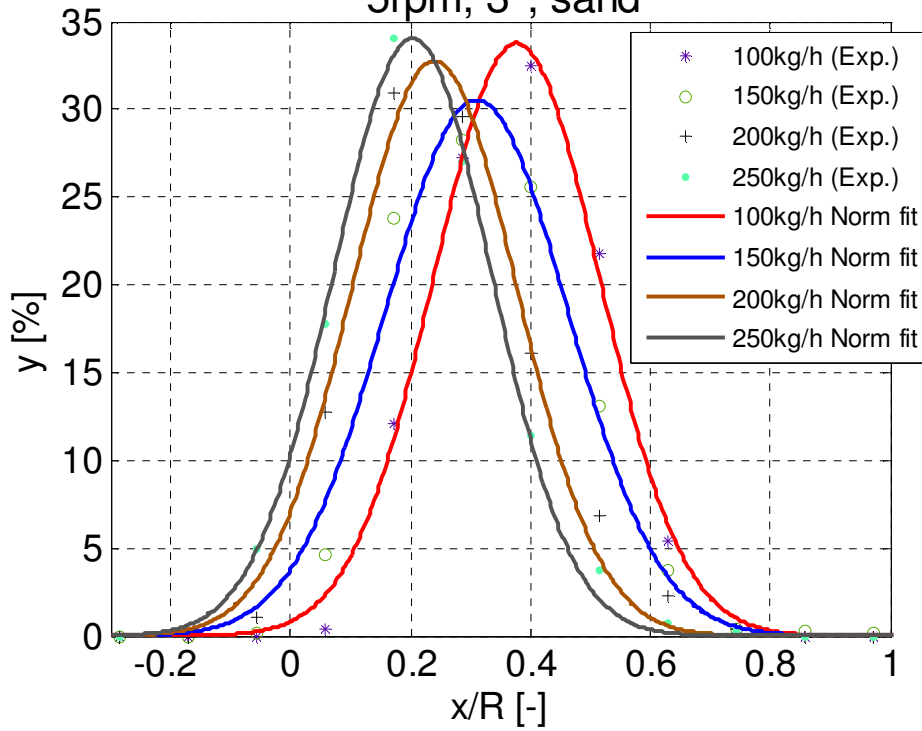


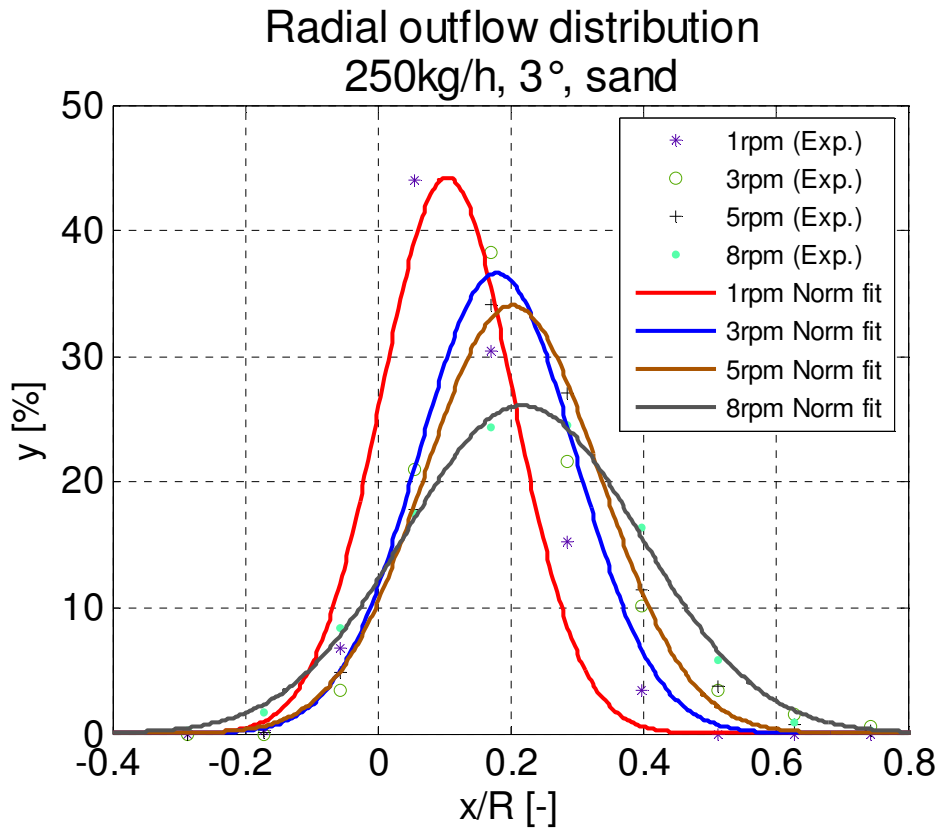


Radial outflow distribution
3rpm, 3°, Sand

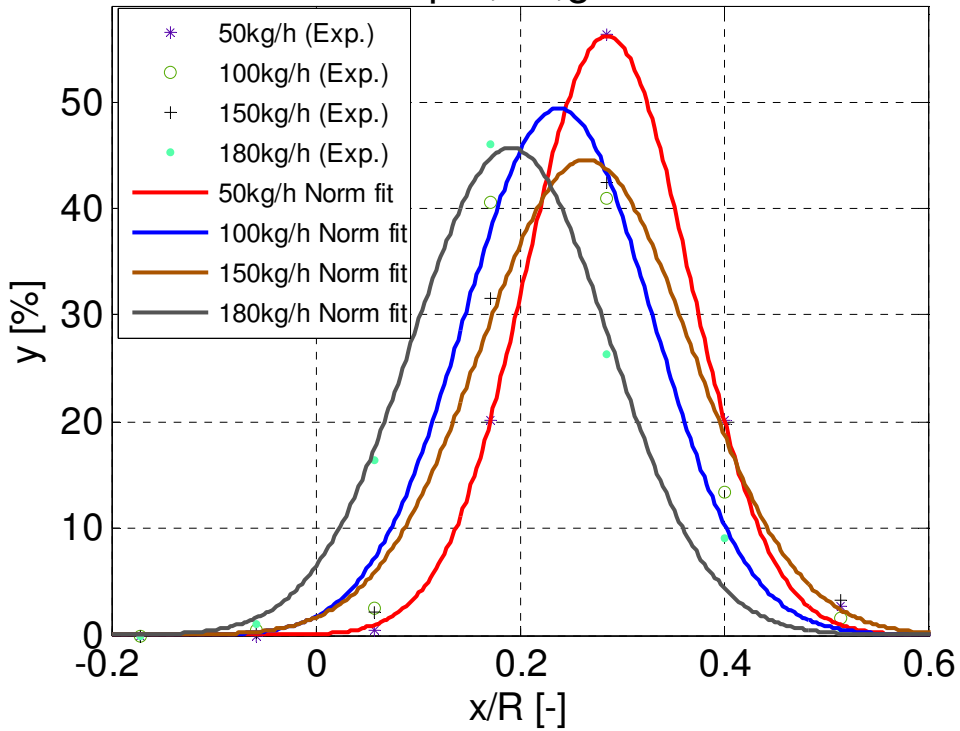


Radial outflow distribution
5rpm, 3°, sand

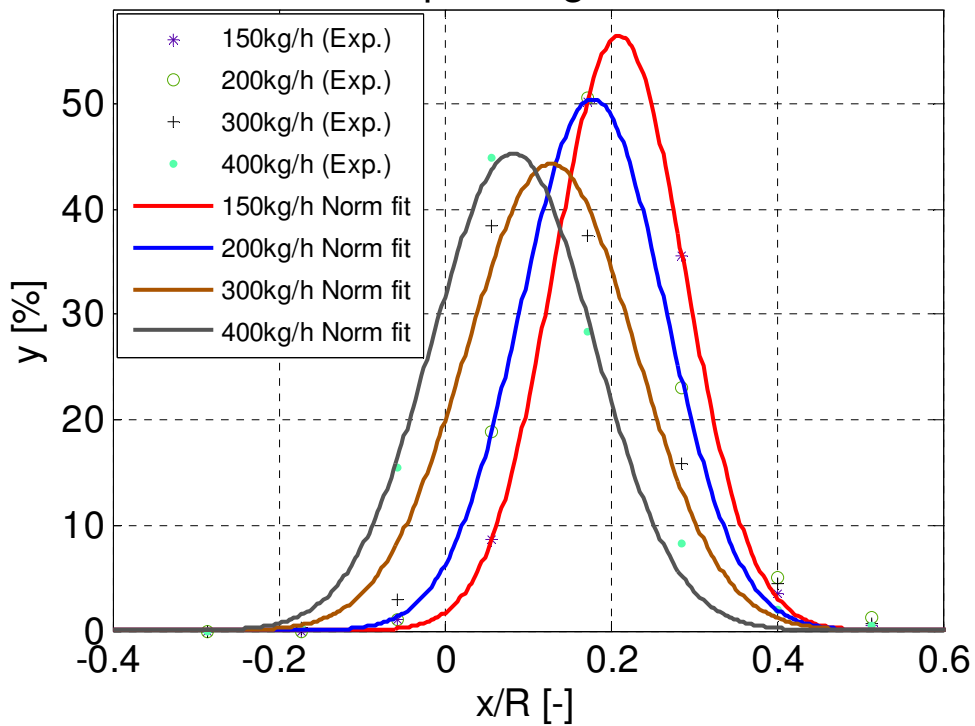




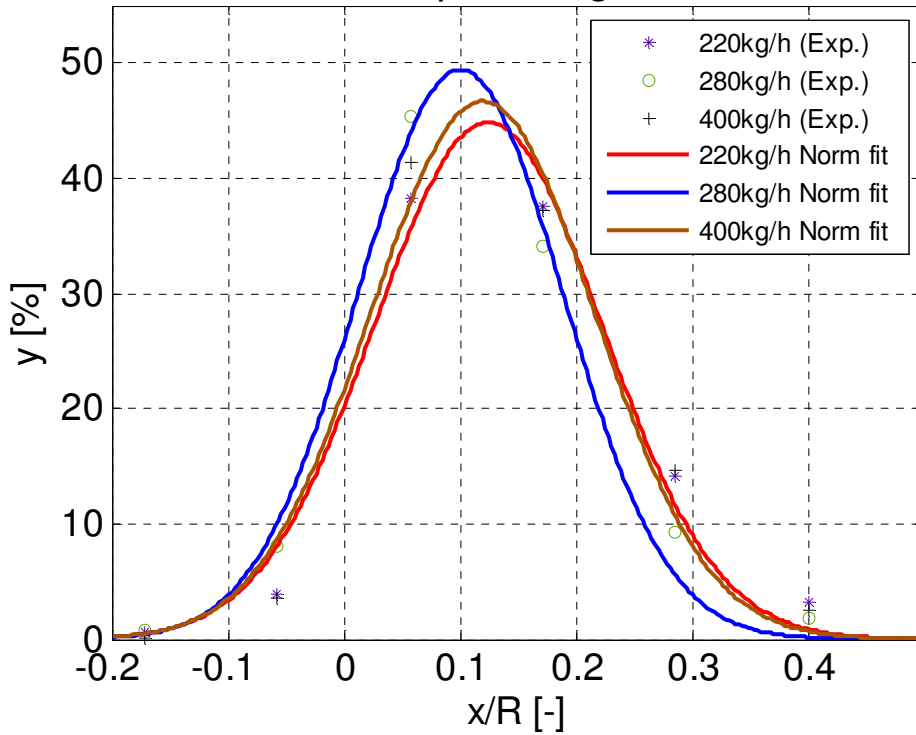
Radial outflow distribution 2rpm, 1°, glass



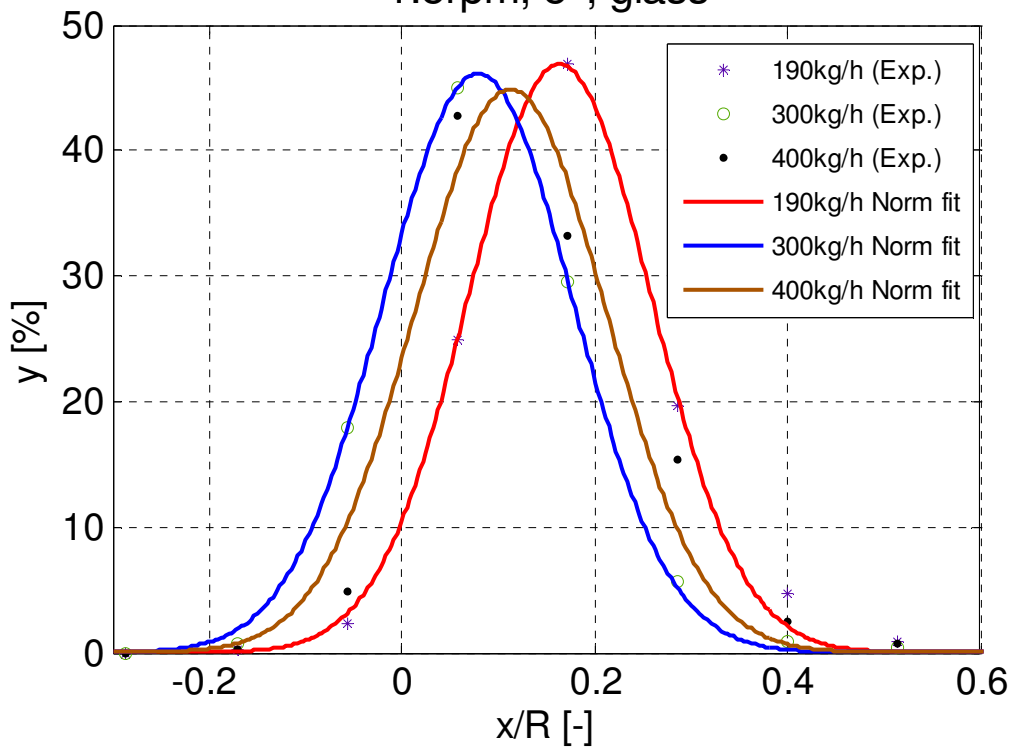
Radial outflow distribution 2rpm, 3°, glass



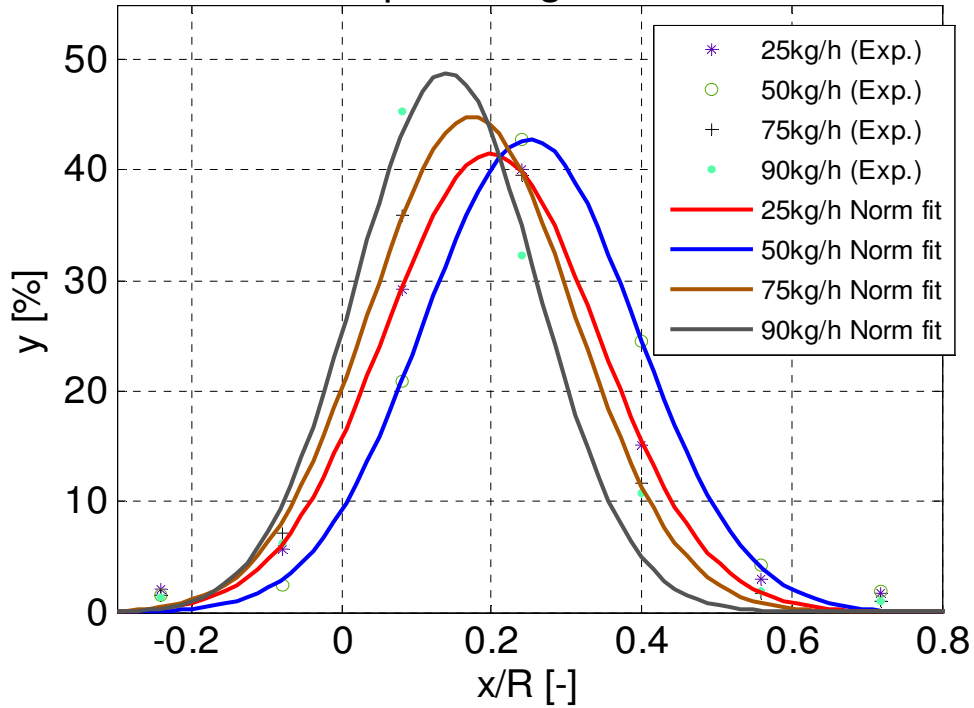
Radial outflow distribution
1.5rpm, 4°, glass



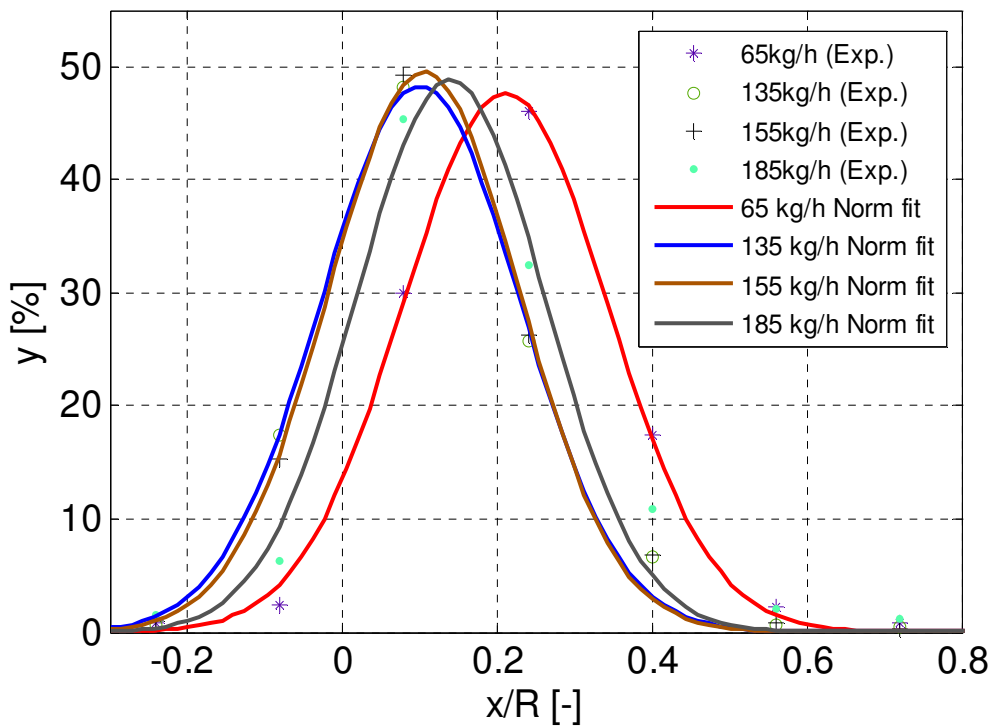
Radial outflow distribution
1.5rpm, 5°, glass

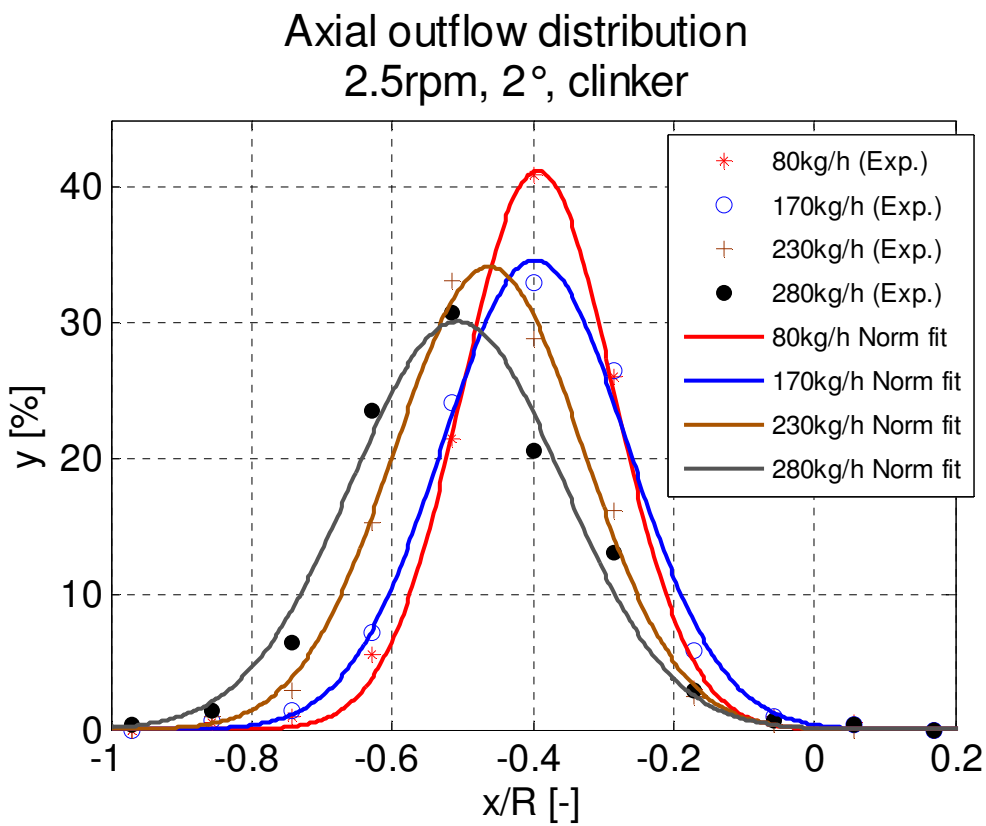
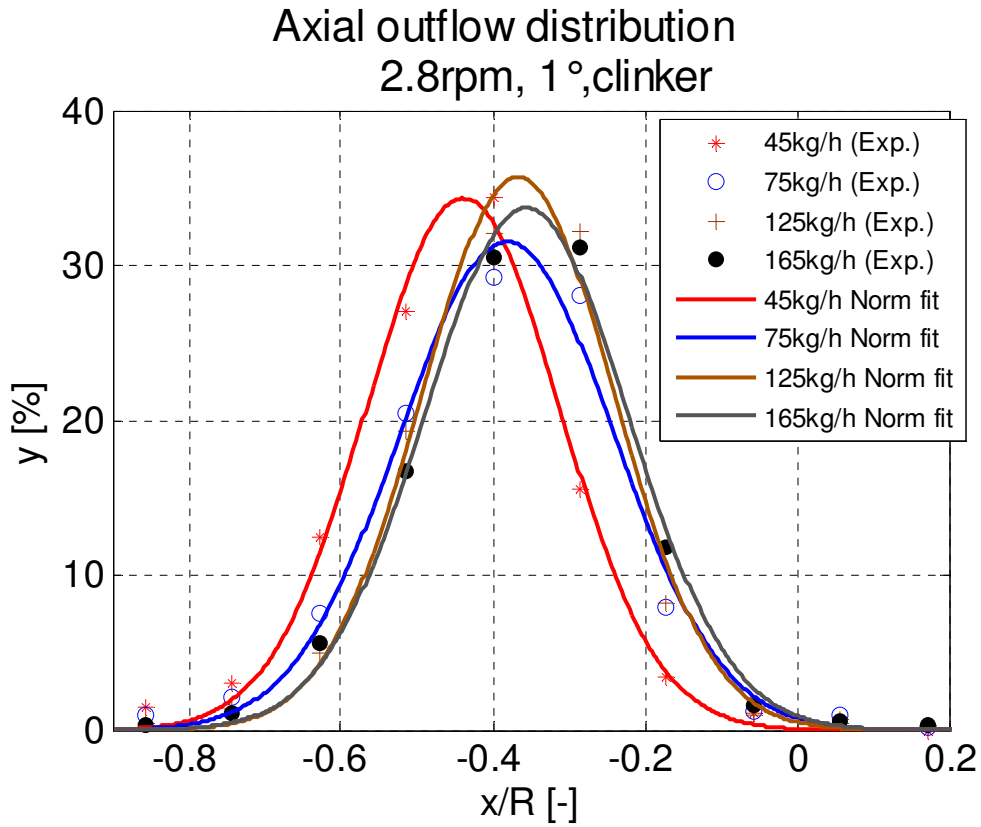


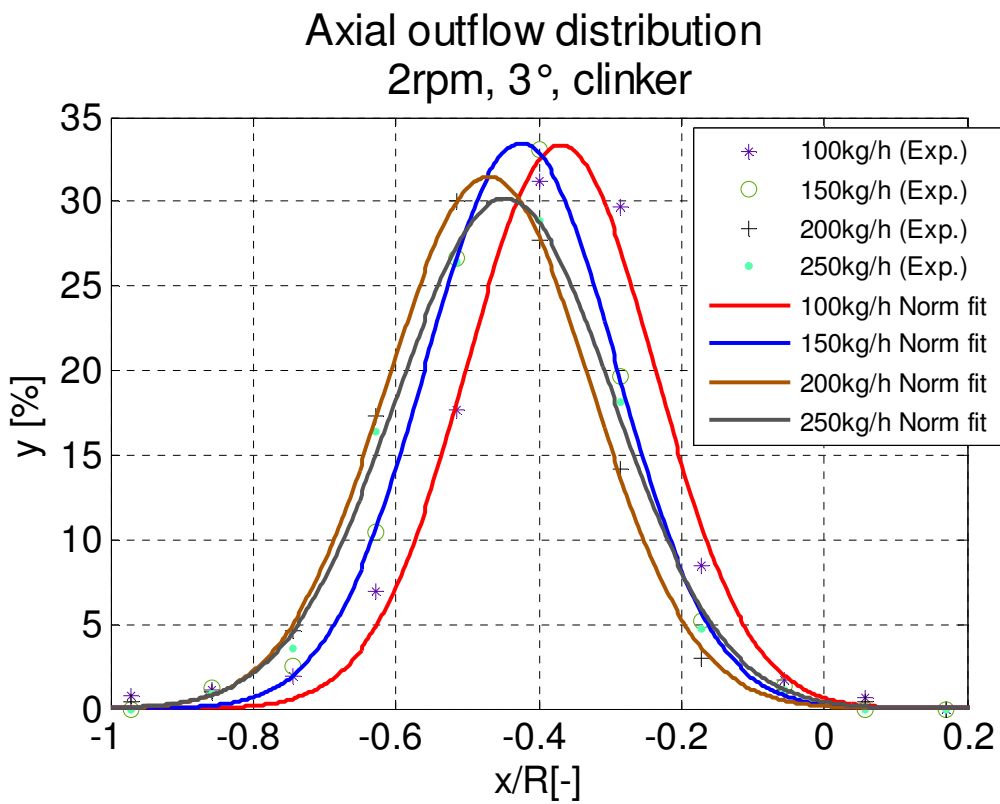
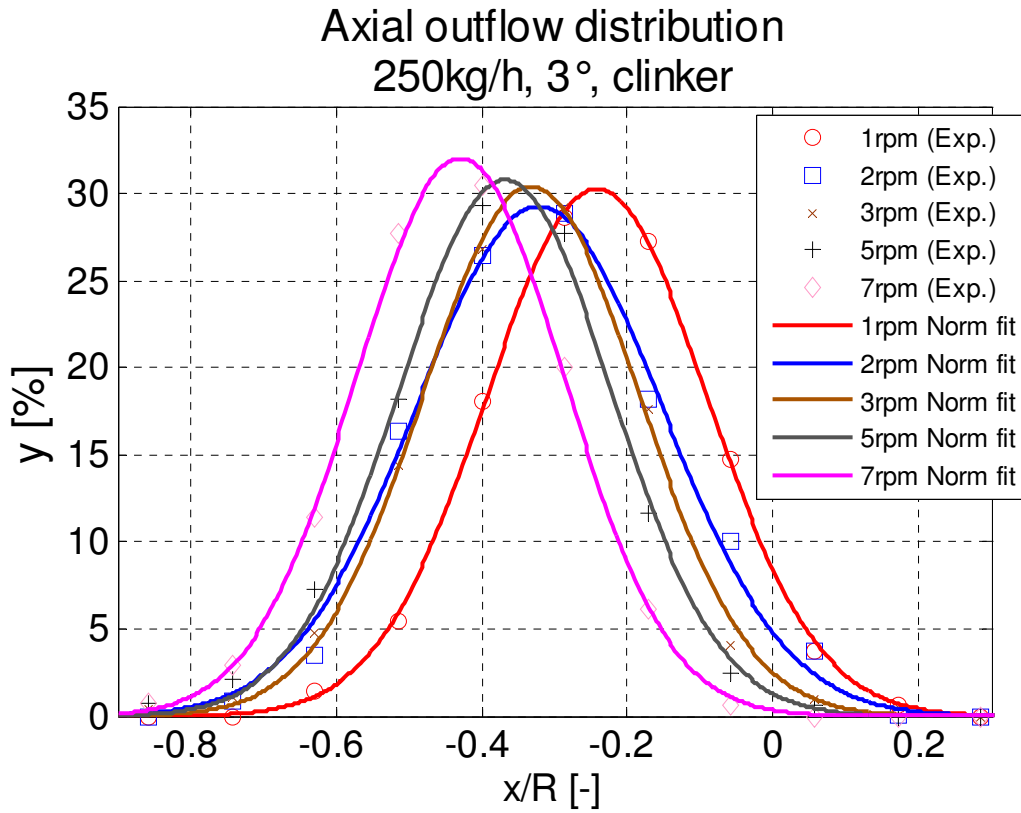
Radial outflow distribution
3.5rpm, 1°, glass, kiln2

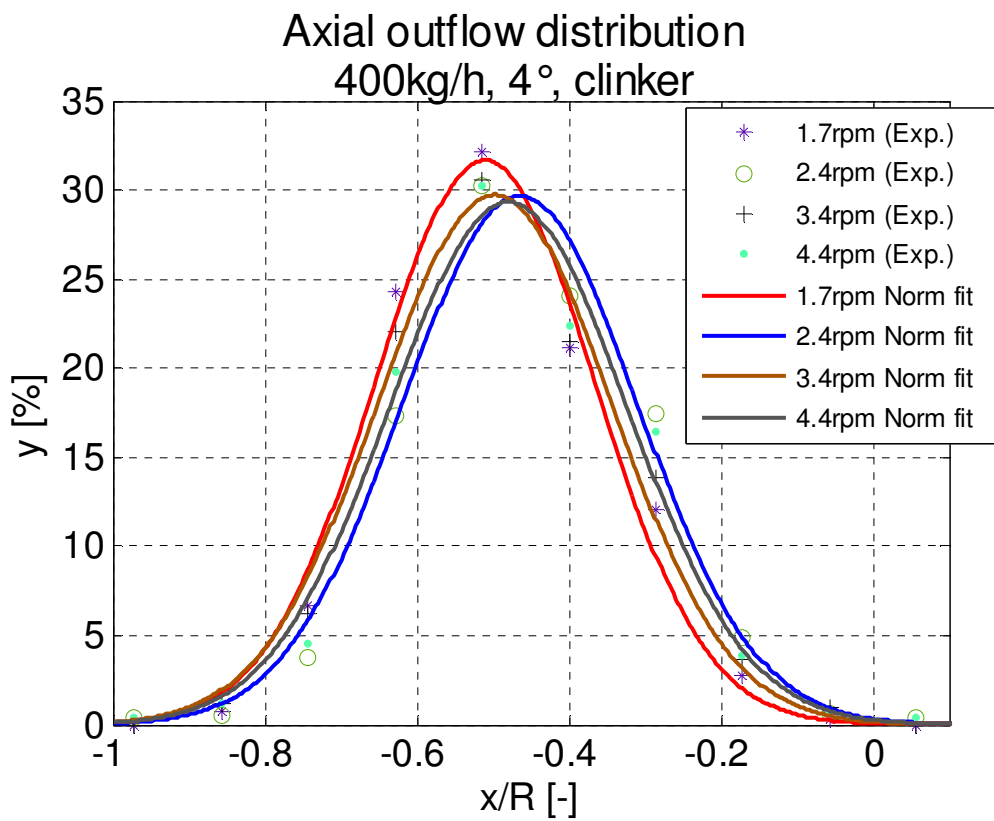
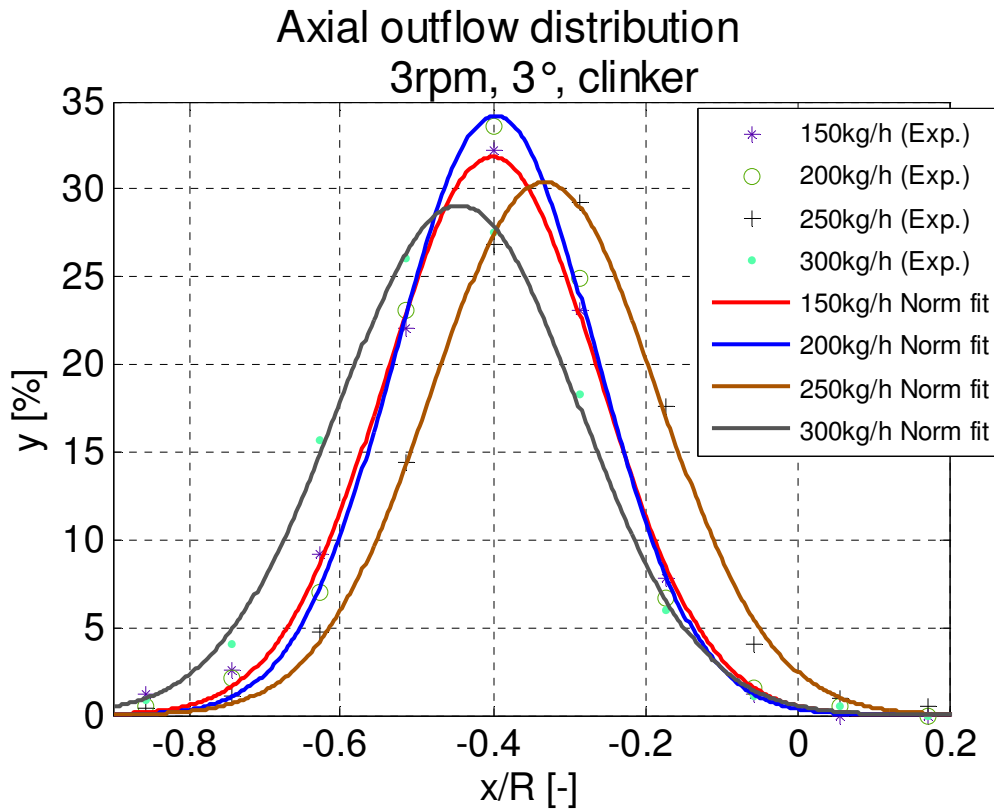


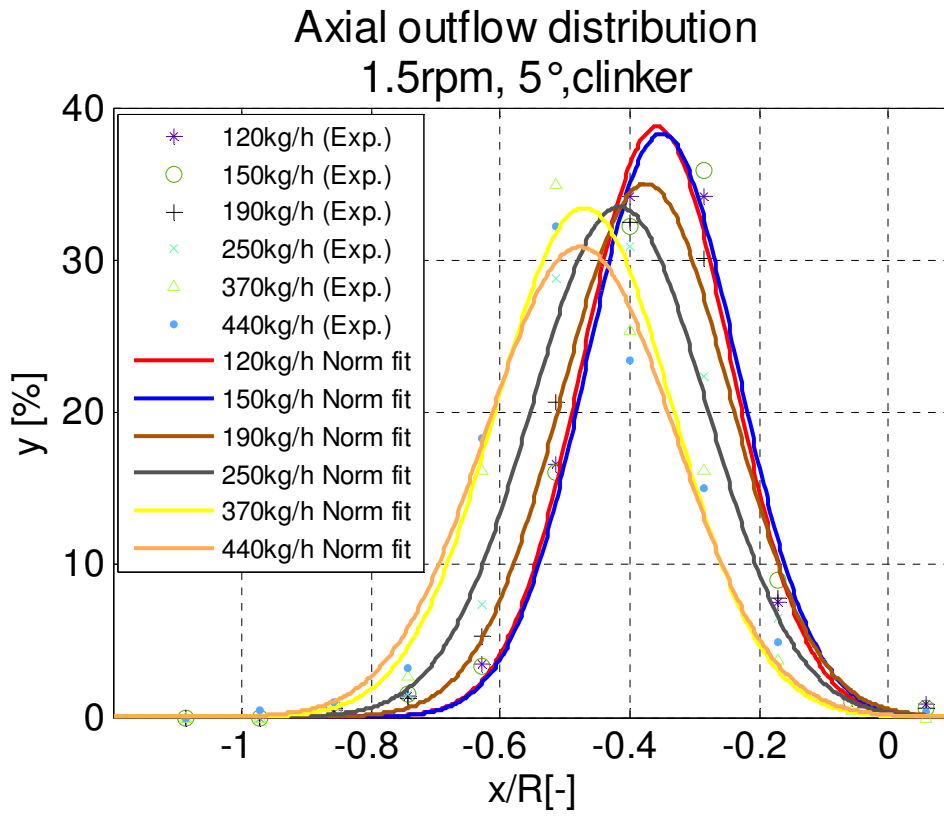
Radial outflow distribution
3.5rpm, 2°, glass, kiln2



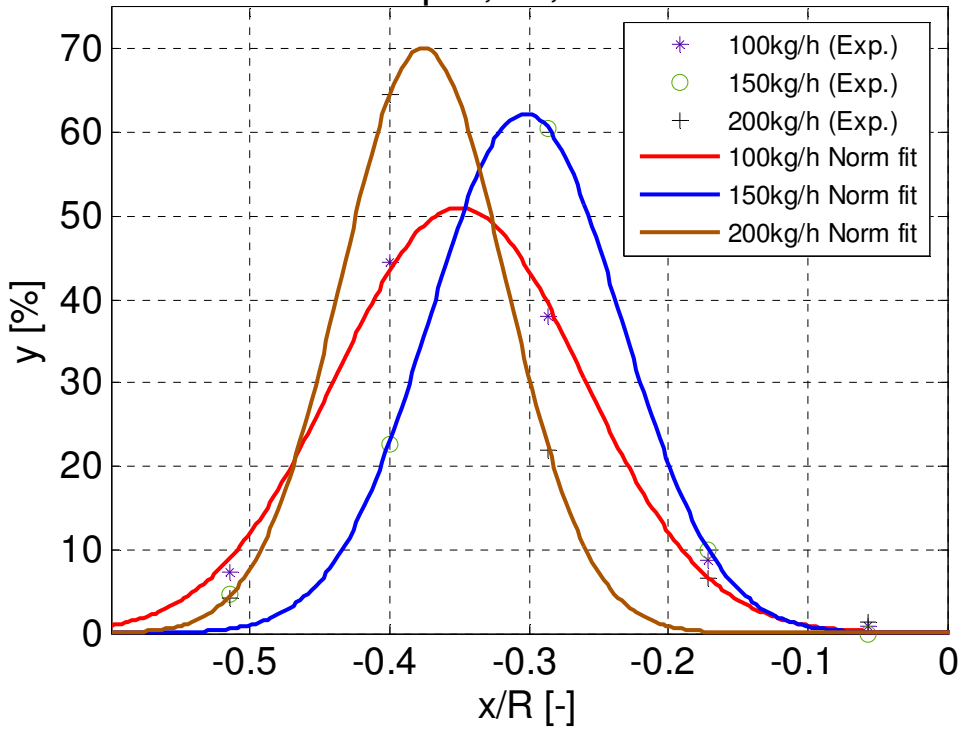




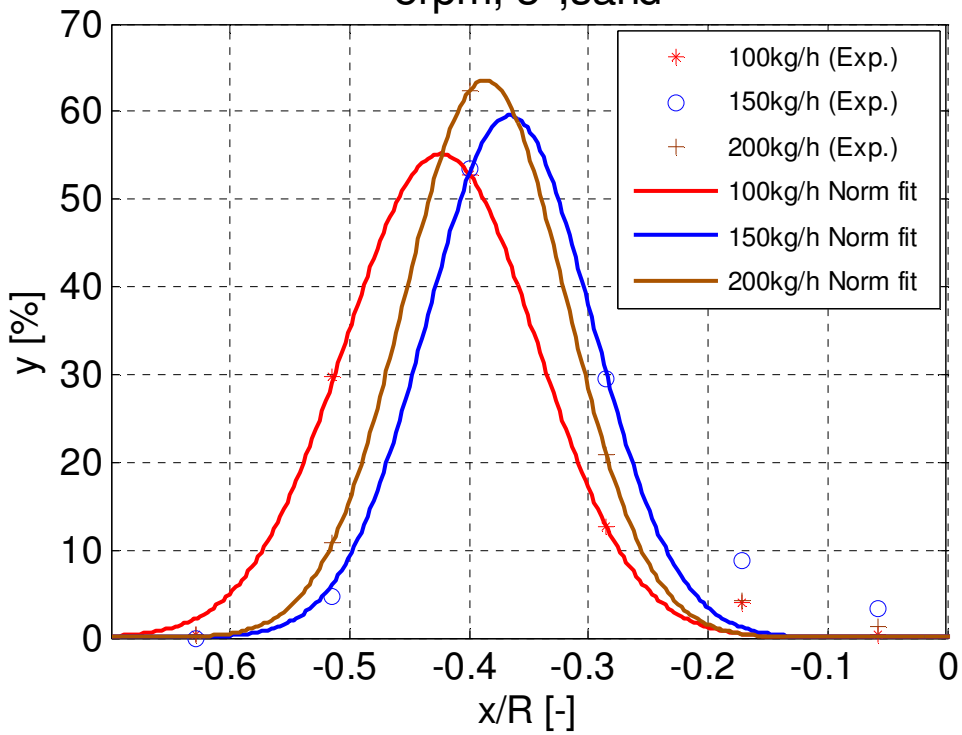


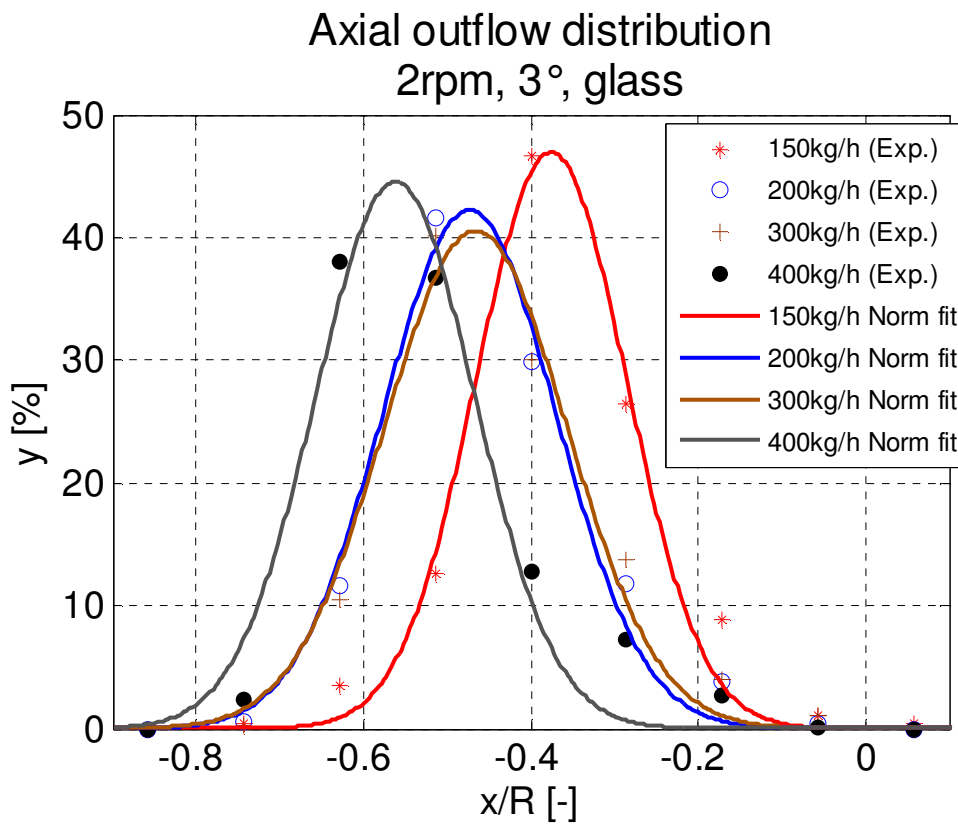
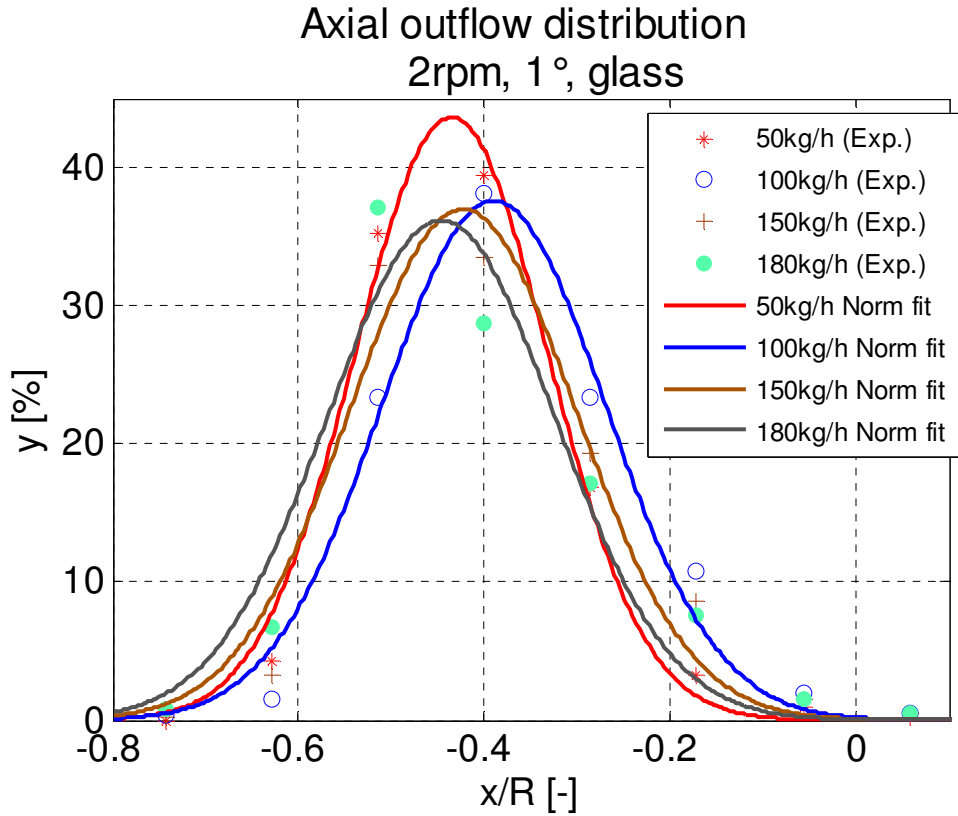


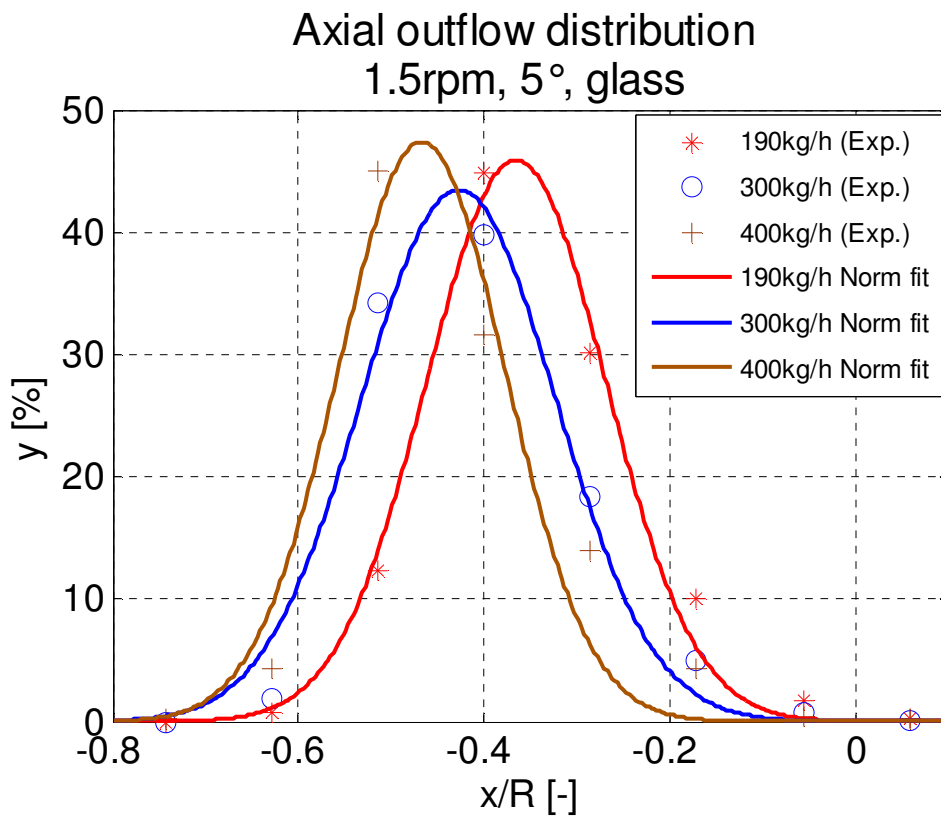
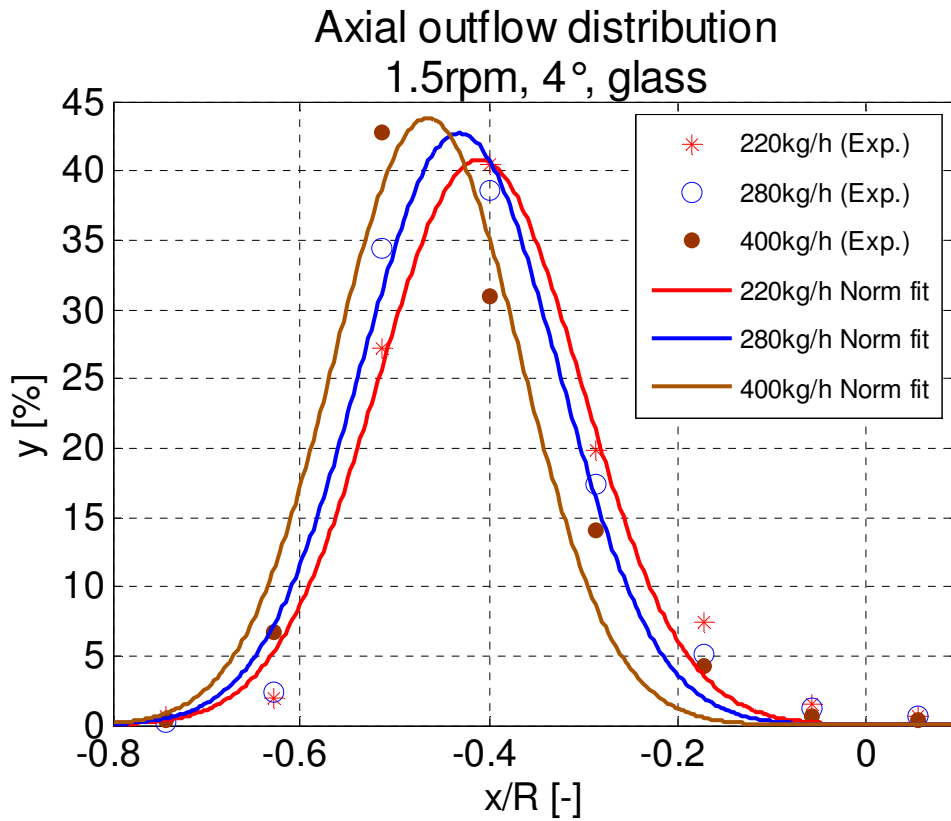
Axial outflow distribution
3rpm, 3°, sand



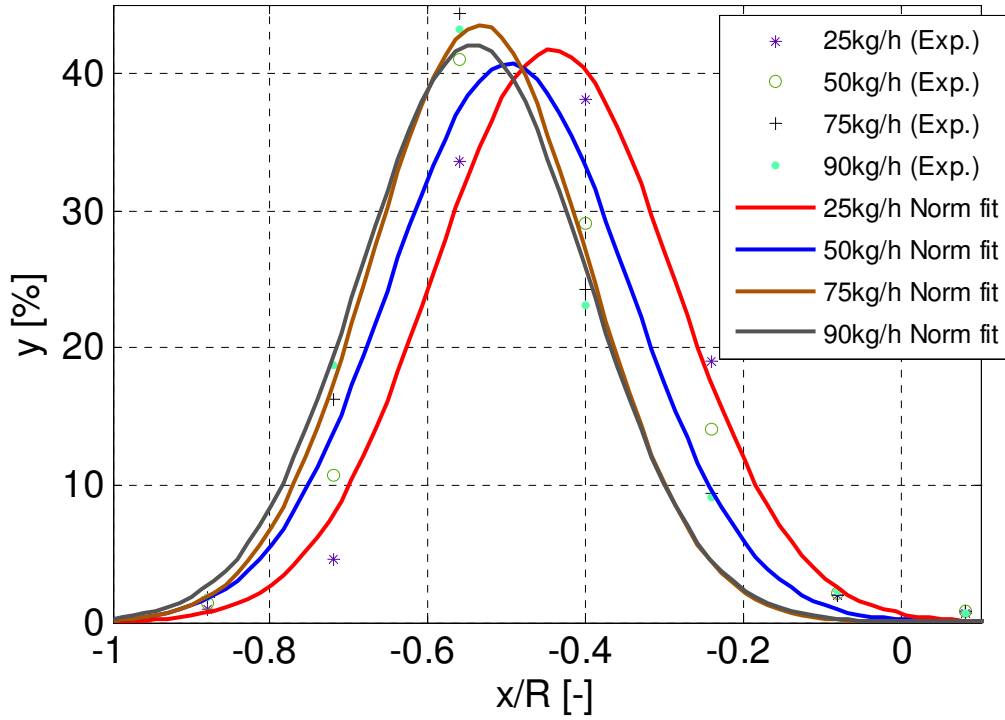
Axial outflow distribution
5rpm, 3°, sand



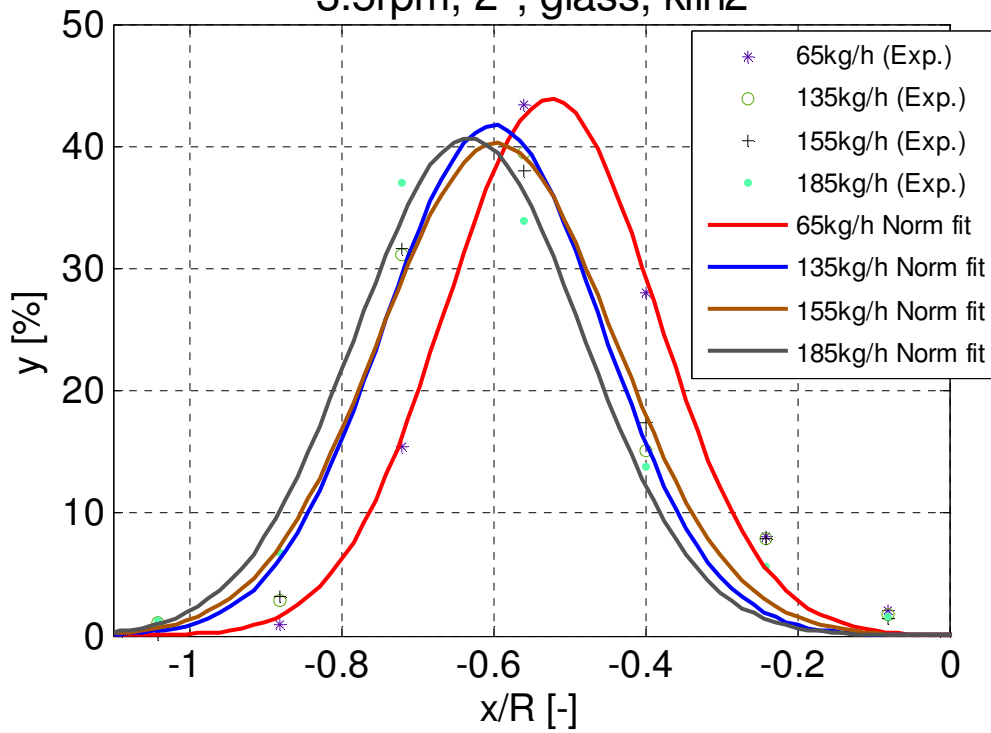




Axial outflow distribution
3.5rpm, 1°, glass, kiln2



Axial outflow distribution
3.5rpm, 2°, glass, kiln2



A 3.1 Experimental parameters and data (clinker)

Kiln inclination [°]	1	1	1	1	2	2	2	2	2	2	2	2
Mass flow [kg/h]	45	75	125	165	80	170	230	280	180	180	180	180
Rotational speed [rpm]	2.8	2.8	2.8	2.8	2.5	2.5	2.5	2.5	1.5	2	2.5	3.9
Angle of repose θ [°]	31	31	31	31	31	31	31	31	31	31	31	31
b1 (Radial) (Exp.) [-]	0.2835	0.3336	0.2927	0.3212	0.2592	0.2883	0.2963	0.2400	0.2039	0.2477	0.2634	0.3225
Scaled distance KBC [-] (KBC=R·sin(θ)/R)	0.52	0.52	0.52	0.52	0.52	0.52	0.52	0.52	0.52	0.52	0.52	0.52
L_{out} (Exp.)= KBC·b1 (Radial.) [-]	0.23	0.18	0.22	0.19	0.26	0.23	0.22	0.28	0.31	0.27	0.25	0.19
L_{out} (Exp.) [mm]	40.51	31.75	38.90	33.92	44.77	39.67	38.27	48.13	54.44	46.78	44.03	33.69
L_r=KBC·R·L_{out} (Exp.) [mm]	49.6125	58.38	51.2225	56.21	45.36	50.453	51.8525	42.0000	35.6825	43.3475	46.0950	56.4375
b1 (Axial) (Exp.) [-]	0.4391	0.3814	0.3669	0.3558	0.3929	0.40	0.46	0.51	0.42	0.43	0.41	-
Axial offset La(Exp.) =b1(Axial)·R [mm]	76.84	66.75	64.21	62.27	68.76	69.46	80.89	88.71	72.78	75.02	71.82	-

A 3.1 Experimental parameters and data (clinker)

Kiln inclination [°]	1	1	1	1	2	2	2	2	2	2	2	2
Mass flow [kg/h]	45	75	125	165	80	170	230	280	180	180	180	180
Rotational speed [rpm]	2.8	2.8	2.8	2.8	2.5	2.5	2.5	2.5	1.5	2	2.5	3.9
V_{sd} [m/s] (Exp.)	0.106	0.083	0.102	0.089	0.117	0.104	0.100	0.126	0.143	0.123	0.115	0.088
F₀ (Exp.) [%]	0.1250	0.1645	0.2118	0.2575	0.1718	0.2575	0.2982	0.3322	0.3559	0.2879	0.2575	0.2033
F₀ (Exp.) [-]	0.0012	0.0016	0.0021	0.0026	0.0017	0.0026	0.0030	0.0033	0.0036	0.0029	0.0026	0.0020
V_{sd}/(R·n^(2/3)·(g/d)^(1/6)) (Cal.)	1.298	1.014	1.245	1.084	1.548	1.370	1.320	1.666	2.655	1.878	1.522	0.863
V_{sa} [m/s]* (exp.)	0.1723	0.1493	0.1439	0.1393	0.1630	0.1557	0.1814	0.1995	0.1639	0.1685	0.1612	-
Bd [-]	0.0051	0.0085	0.0141	0.0186	0.0101	0.0215	0.0291	0.0354	0.0380	0.0285	0.0228	0.0146

Radial

y_{max}	19.760	21.730	31.180	31.140	31.510	30.550	34.420	35.070	36.130	34.460	34.330	27.600
c	0.313	0.282	0.194	0.192	0.194	0.200	0.178	0.176	0.165	0.175	0.179	0.220

Axial

y_{max}	34.330	31.520	35.710	33.720	41.250	34.640	34.140	30.110	33.280	34.000	33.180	-
c	0.180	0.199	0.179	0.188	0.153	0.186	0.190	0.213	0.193	0.188	0.193	-

A 3.1 Experimental parameters and data (clinker)

Kiln inclination [°]	3	3	3	3	3	3	3	3	3	3	3	3
Mass flow [kg/h]	100	150	150	200	200	200	250	250	250	250	250	300
Rotational speed [rpm]	2	2	3	2	3	5	1	2	3	5	7	3
Angle of repose θ [°]	31	31	31	31	31	31	31	31	31	31	31	31
b1 (Radial) (Exp.) [-]	0.2974	0.2938	0.3372	0.2399	0.287	0.2651	0.1763	0.1807	0.2171	0.2663	0.31	0.2509
Scaled distance KBC [-] ($KBC=R \cdot \sin(\theta)/R$)	0.52	0.52	0.52	0.52	0.52	0.52	0.52	0.52	0.52	0.52	0.52	0.52
L_{out} (Exp.)= KBC-b1 (Radial.) [-]	0.22	0.22	0.18	0.28	0.23	0.25	0.34	0.33	0.30	0.25	0.21	0.26
L_{out} (Exp.) [mm]	38.08	38.71	31.12	48.14	39.90	43.73	59.27	58.50	52.13	43.52	35.88	46.22
$L_r=KBC \cdot R-L_{out}$ (Exp.) [mm]	52.045	51.415	59.01	41.9825	50.225	46.393	30.853	31.6225	37.9925	46.6025	54.25	43.9075
b1 (Axial) (Exp.) [-]	0.3693	0.4246	0.4006	0.4699	0.3964	0.3735	0.4704	0.4471	0.332	0.3677	0.4292	0.4446
Axial offset L_a(Exp.) =b1(Axial)*R [mm]	64.63	74.31	70.11	82.23	69.37	65.36	82.32	78.24	58.10	64.35	75.11	77.81

A 3.1 Experimental parameters and data (clinker)

Kiln inclination [°]	3	3	3	3	3	3	3	3	3	3	3	3
Mass flow [kg/h]	100	150	150	200	200	200	250	250	250	250	250	300
Rotational speed [rpm]	2	2	3	2	3	5	1	2	3	5	7	3
V_{sd} [m/s](Exp.)	0.100	0.101	0.081	0.126	0.104	0.115	0.156	0.154	0.137	0.114	0.094	0.121
F₀ (Exp.) [%]	0.2384	0.2878	0.2384	0.3211	0.2573	0.2121	0.5312	0.3800	0.2878	0.2295	0.1869	0.3211
F₀ (Exp.) [-]	0.0024	0.0029	0.0024	0.0032	0.0026	0.0021	0.0053	0.0038	0.0029	0.0023	0.0019	0.0032
V_{sd}/(R·n^(2/3)·(g/d)^(1/6)) (Cal.)	1.525	1.551	0.949	1.934	1.220	0.952	3.793	2.358	1.600	0.948	0.623	1.416
V_{sa} [m/s]* (exp.)	0.1448	0.1665	0.1567	0.1848	0.1555	0.1467	0.1857	0.1764	0.1307	0.1444	0.1682	0.1748
Bd [-]	0.0158	0.0237	0.0158	0.0316	0.0211	0.0127	0.0791	0.0395	0.0264	0.0158	0.0113	0.0316

Radial

y_{max}	25.340	26.960	24.640	30.200	28.810	25.220	31.860	26.340	26.740	23.990	23.770	28.640
c	0.241	0.225	0.248	0.202	0.214	0.247	0.186	0.231	0.230	0.257	0.260	0.217

Axial

y_{max}	33.370	33.450	31.83	31.490	34.180	32.000	30.290	29.250	30.400	32.260	32.010	30.190
c	0.186	0.190	0.1988	0.203	0.186	0.410	0.214	0.239	0.210	0.197	0.202	0.216

A 3.1 Experimental parameters and data (clinker)

Kiln inclination [°]	4	4	4	4	5	5	5	5	5	5	5
Mass flow [kg/h]	400	400	400	400	120	150	190	250	260	370	440
Rotational speed [rpm]	1.7	2.4	3.4	4.4	1.5	1.5	1.5	1.5	1.5	1.5	1.5
Angle of repose θ [°]	31	31	31	31	31	31	31	31	31	31	31
b1 (Radial) (Exp.) [-]	0.1691	0.2125	0.2299	0.3133	0.2396	0.2272	0.2403	0.2208	0.1786	0.2029	0.1645
Scaled distance KBC [-] (KBC=R·sin(θ)/R)	0.52	0.52	0.52	0.52	0.52	0.52	0.52	0.52	0.52	0.52	0.52
L_{out} (Exp.)= KBC-b1 (Radial.) [-]	0.35	0.30	0.29	0.20	0.28	0.29	0.27	0.29	0.34	0.31	0.35
L_{out} (Exp.) [mm]	60.53	52.94	49.89	35.30	48.20	50.37	48.07	51.49	58.87	54.62	61.34
L_r=KBC*R-L_{out} (Exp.) [mm]	29.5925	37.1875	40.2325	54.8275	41.9300	39.7600	42.0525	38.6400	31.2550	35.5075	28.7875
b1 (Axial) (Exp.) [-]	0.5104	0.4644	0.4974	0.4794	0.3583	0.3504	0.3752	0.4162	0.3937	0.4704	0.4768
Axial offset L_a(Exp.) =b1(Axial)*R [mm]	89.32	81.27	87.05	83.90	62.70	61.32	65.66	72.84	68.90	82.32	83.44

A 3.1 Experimental parameters and data (clinker)

Kiln inclination [°]	4	4	4	4	5	5	5	5	5	5	5
Mass flow [kg/h]	400	400	400	400	120	150	190	250	260	370	440
Rotational speed [rpm]	1.7	2.4	3.4	4.4	1.5	1.5	1.5	1.5	1.5	1.5	1.5
V_{sd} [m/s] (Cal.)	0.179	0.156	0.147	0.103	0.147	0.153	0.146	0.157	0.180	0.167	0.188
F₀ (Exp.) [%]	0.4773	0.3682	0.3095	0.2775	0.2204	0.2385	0.2879	0.3322	0.3322	0.4203	0.4773
F₀ (Exp.) [-]	0.0048	0.0037	0.0031	0.0028	0.0022	0.0024	0.0029	0.0033	0.0033	0.0042	0.0048
V_{sd}/(R·n^(2/3)·(g/d)^(1/6) (Cal.)	3.056	2.117	1.580	0.936	2.722	2.847	2.715	2.912	3.340	3.093	3.483
V_{sa} [m/s]* (exp.)	0.2264	0.2054	0.2197	0.2106	0.1635	0.1601	0.1712	0.1902	0.1805	0.2153	0.2188
Bd [-]	0.0744	0.0527	0.0372	0.0288	0.0253	0.0316	0.0401	0.0527	0.0548	0.0780	0.0928

Radial

y_{max}	35.890	34.180	35.190	31.280	33.870	33.540	35.610	39.410	40.520	39.230	41.550
c	0.170	0.198	0.176	0.198	0.179	0.180	0.172	0.154	0.146	0.153	0.143

Axial

y_{max}	31.670	29.670	29.730	29.320	38.720	38.290	35.010	33.480	33.180	33.420	30.830
c	0.204	0.219	0.218	0.221	0.162	0.164	0.183	0.194	0.194	0.194	0.207

A 3.2 Experimental parameters and data (sand)

Kiln Inclination [°]	3	3	3	3	3	3	3	3	3	3
Mass flow [kg/h]	100	100	150	150	200	200	250	250	250	250
Rotational speed [rpm]	3	5	3	5	3	5	1	3	5	8
Angle of repose θ [°]	32	32	32	32	32	32	32	32	32	32
b1 (Radial) (Exp.) [-]	0.3583	0.3769	0.2757	0.3103	0.2202	0.2398	0.1052	0.1802	0.2034	0.2193
Scaled distance KBC [-] (KBC=R·sin(θ)/R)	0.53	0.53	0.53	0.53	0.53	0.53	0.53	0.53	0.53	0.53
L_{out}(Exp.)=KBC·b1 (Radial) [-]	0.17	0.15	0.25	0.22	0.31	0.29	0.42	0.35	0.33	0.31
L_{out} (Exp.) [mm]	30.05	26.79	44.50	38.45	54.22	50.79	74.34	61.22	57.16	54.37
L_r=KBC·R-L_{out} (Exp.) [mm]	62.70	65.96	48.25	54.30	38.54	41.97	18.41	31.54	35.60	38.38
b1 (Axial) (Exp.) [-]	0.3498	0.4236	0.3026	0.3663	0.3757	0.3865	-	-	-	-
Axial offset L_a (Exp.) =b1(Axial)·R [mm]	61.22	74.13	52.96	64.10	65.75	67.64	-	-	-	-

A 3.2 Experimental parameters and data (sand)

Kiln inclination [°]	3	3	3	3	3	3	3	3	3	3
Mass flow [kg/h]	100	100	150	150	200	200	250	250	250	250
Rotational speed [rpm]	3	5	3	5	3	5	1	3	5	8
V_{sd} [m/s] (Exp.)	0.0792	0.0706	0.1179	0.1016	0.1440	0.1348	0.1988	0.1630	0.1520	0.1445
F₀ (Exp.) [%]	0.1439	0.1244	0.2036	0.1642	0.2482	0.1952	0.4341	0.2673	0.1952	0.1571
F₀ (Exp.) [-]	0.0014	0.0012	0.0020	0.0016	0.0025	0.0020	0.0043	0.0027	0.0020	0.0016
V_{sd}/(R·n^(2/3)·(g/d)^(1/6)) (Cal.)	0.572	0.363	0.851	0.522	1.040	0.693	2.987	1.177	0.781	0.543
V_{sa} [m/s]* (exp.)	0.1369	0.1656	0.1190	0.1437	0.1481	0.1522	-	-	-	-
Bd [-]	0.0098	0.0059	0.0148	0.0089	0.0197	0.0118	0.0739	0.0246	0.0148	0.0092

Radial

y_{max}	40.000	33.78	41.090	30.540	44.080	32.770	44.240	36.620	34.040	26.070
c	0.160	0.1954	0.151	0.215	0.143	0.194	0.141	0.168	0.187	0.251

Axial

y_{max}	50.970	55.210	62.250	59.530	70.110	63.600	-	-	-	-
c	0.125	0.114	0.097	0.098	0.084	0.096	-	-	-	-

A 3.3 Experimental parameters and data (glass beads)

Kiln inclination [°]	1				3				4			5		
Mass flow [kg/h]	50	100	150	180	150	200	300	400	220	280	400	190	300	400
Rotational speed [rpm]	2	2	2	2	2	2	2	2	1.5	1.5	1.5	1.5	1.5	1.5
Angle of repose θ [°]	21	21	21	21	21	21	21	21	21	21	21	21	21	21
b1 (Radial) (Exp.) [-]	0.286	0.2382	0.2652	0.1916	0.21	0.1787	0.1285	0.08262	0.1244	0.1005	0.1197	0.1636	0.07928	0.1129
Scaled distance KBC [-] (KBC=R·sin(θ)/R)	0.36	0.36	0.36	0.36	0.36	0.36	0.36	0.36	0.36	0.36	0.36	0.36	0.36	0.36
L_{out} (Exp.)= KBC-b1 (Radial.) [-]	0.07	0.12	0.09	0.17	0.15	0.18	0.23	0.28	0.23	0.26	0.24	0.19	0.28	0.25
L_{out} (Exp.) [mm]	12.66	21.03	16.30	29.18	25.96	31.44	40.23	48.26	40.94	45.13	41.77	34.08	48.84	42.96
L_r=KBC*R-L_{out} (Exp.) [mm]	50.05	41.685	46.41	33.53	36.75	31.2725	22.4875	14.4585	21.7700	17.5875	20.9475	28.6300	13.8740	19.7575
b1 (Axial) (Exp.) [-]	0.4354	0.3899	0.4233	0.4465	0.3757	0.4736	0.4661	0.5622	0.4101	0.4313	0.4652	0.3658	0.4278	0.4675
Axial offset L_a(Exp.) =b1(Axial)*R [mm]	76.195	68.233	74.0775	78.1375	65.75	82.88	81.57	98.385	71.7675	75.4775	81.4100	64.0150	74.8650	81.8125

A 3.3 Experimental parameters and data (glass beads)

Kiln inclination [°]	1 (kiln2 D=250mm)				2 (kiln2 D=250mm)			
	Mass flow [kg/h]	25	50	75	90	65	135	155
Rotational speed [rpm]	3.5	3.5	3.5	3.5	3.5	3.5	3.5	3.5
Angle of repose θ [°]	28	28	28	28	28	28	28	28
b1 (Radial) (Exp.) [-]	0.1997	0.2504	0.1735	0.1402	0.2109	0.1013	0.1057	0.1402
Scaled distance KBC [-] ($KBC=R \cdot \sin(\theta)/R$)	0.47	0.47	0.47	0.47	0.47	0.47	0.47	0.47
L_{out} (Exp.)= $KBC-b1$ (Radial.) [-]	0.27	0.22	0.30	0.33	0.26	0.37	0.36	0.33
L_{out} (Exp.) [mm]	33.72	27.38	37.00	41.16	32.32	46.02	45.47	41.16
$L_r=KBC \cdot R-L_{out}$ (Exp.) [mm]	24.9625	31.3000	21.6875	17.5250	26.3625	12.6625	13.2125	17.5250
b1 (Axial) (Exp.) [-]	0.4421	0.4977	0.5349	0.5427	0.5238	0.5998	0.5949	0.6312
Axial offset L_a (Exp.) = $b1$ (Axial)* R [mm]	55.2625	62.2125	66.8625	67.8375	65.4750	74.9750	74.3625	78.9000

A 3.3 Experimental parameters and data (glass beads)

Kiln inclination [°]	1	1	1	1	3	3	3	3	4	4	4	5	5	5
Mass flow [kg/h]	50	100	150	180	150	200	300	400	220	280	400	190	300	400
Rotational speed [rpm]	2	2	2	2	2	2	2	2	1.5	1.5	1.5	1.5	1.5	1.5
V_{sd} [m/s] (Exp.)	0.0301	0.0501	0.0388	0.0696	0.0619	0.0750	0.0962	0.1156	0.1097	0.1210	0.1119	0.0942	0.1355	0.1190
F0 (Exp.) [%]	0.1025	0.1311	0.1871	0.2118	0.2033	0.2479	0.2879	0.3682	0.2674	0.3095	0.3808	0.2118	0.2879	0.3322
F0 (Exp.) [-]	0.0010	0.0013	0.0019	0.0021	0.0020	0.0025	0.0029	0.0037	0.0027	0.0031	0.0038	0.0021	0.0029	0.0033
V_{sd}/((R·n^(2/3)·(g/d)^(1/6)) (Cal.)	0.340	0.565	0.438	0.786	0.699	0.847	1.086	1.305	1.500	1.655	1.530	1.288	1.853	1.627
V_{sa} [m/s]* (exp.)	0.1692	0.1517	0.1646	0.1740	0.1463	0.1847	0.1821	0.2199	0.1795	0.1889	0.2036	0.1652	0.1939	0.2116
Bd [-]	0.0046	0.0091	0.0137	0.0164	0.0137	0.0183	0.0274	0.0365	0.0268	0.0341	0.0487	0.0231	0.0365	0.0487

Radial

y_{max}	56.130	49.370	44.540	45.670	56.430	50.460	44.310	45.280	44.840	49.420	46.690	46.870	46.100	44.870
c	0.113	0.130	0.146	0.137	0.112	0.123	0.143	0.138	0.139	0.125	0.137	0.134	0.139	0.140

Axial

y_{max}	43.650	37.600	36.980	36.150	46.960	42.240	40.530	44.540	40.790	42.700	43.770	45.900	43.470	47.390
c	0.147	0.170	0.172	0.173	0.127	0.147	0.154	0.135	0.153	0.148	0.140	0.136	0.148	0.127

A 3.3 Experimental parameters and data (glass beads)

Kiln inclination [°]	1 (kiln2 D=250mm)				2 (kiln2 D=250mm)			
	Mass flow [kg/h]	25	50	75	90	65	135	155
Rotational speed [rpm]	3.5	3.5	3.5	3.5	3.5	3.5	3.5	3.5
V_{sd} [m/s] (Exp.)	0.0876	0.0710	0.0962	0.1072	0.0853	0.1220	0.1205	0.1089
F_0 (Exp.) [%]	0.1090	0.1425	0.1935	0.2293	0.1718	0.2422	0.2837	0.3140
F_0 (Exp.) [-]	0.0011	0.0014	0.0019	0.0023	0.0017	0.0024	0.0028	0.0031
$V_{sd}/(R \cdot n^{(2/3)} \cdot (g/d)^{(1/6)})$ (Cal.)	0.954	0.773	1.047	1.167	0.929	1.328	1.311	1.186
V_{sa} [m/s]* (Exp.)	0.1268	0.1425	0.1535	0.1560	0.1526	0.1755	0.1740	0.1844
Bd [-]	0.0050	0.0099	0.0149	0.0179	0.0129	0.0268	0.0307	0.0367

Radial

y_{max}	41.540	42.770	44.870	48.850	47.670	48.310	49.530	48.850
c	0.202	0.201	0.194	0.172	0.187	0.182	0.175	0.172

Axial

y_{max}	41.680	40.690	43.500	42.120	43.680	41.700	40.220	40.640
c	0.216	0.214	0.194	0.202	0.197	0.204	0.218	0.212

Persönliche Daten

Name: Shi, YiChun
Geburtsdatum/Ort: 04.Juni 1980 / Nanjing, China
Familienstand: Verheiratet, 1 kind
Staatsangehörigkeit: Chinese



Studium/Ausbildung

2006-2009 **Doktorand in Otto-von-Guericke-Universität Magdeburg.**
Fakultät für Verfahrens- und Systemtechnik.
Institut für Strömungstechnik und Thermodynamik

2004-2005 **Otto-von-Guericke-Universität Magdeburg**
Studium: Quality, Safety and Environment (Chemisch)
Abschluss: Master of Science (M. Sc.)

1998-2002 **Nanjing Technik Universität (China)**
Studium: Safety Engineering
Abschluss: Bachelor of Engineering (B. Sc.)

Schulbildung

1995-1998 **Nanjing Renming Schule (High School) (China)**

1992-1995 **Nanjing zhonghua Schule (Primary School) (China)**

1986-1992 **Nanjing Fu Zi Miao Grundschule (Elementary School) (China)**

Berufliche Tätigkeit

2002-2004 **Nanjing Erji Machine Tools Co,Ltd. (China)**
Arbeitsstelle: Project Ingenieur